Tiago Miguel Nico Pereira

Licenciado em Engenharia Civil

Experimental Campaign Addressing Lap-Splices under Cyclic Loading

Dissertação para obtenção do Grau de Mestre em Engenharia Civil

Orientador: Professor Doutor João Pacheco de Almeida, Investigador Pós-Doutorado, EPFL

Co-orientador: Professor Doutor Corneliu Cismasiu, Professor Associado, FCT/UNL

Presidente: Prof. Doutor Carlos M. Chastre Rodrigues, Professor Auxiliar da Faculdade de Ciências e Tecnologia da Universidade Nova de Lisboa

Arguente: Prof. Doutor António M. P. Ramos, Professor Auxiliar da Faculdade de Ciências e Tecnologia da Universidade Nova de Lisboa

Vogal: Prof. Doutor Corneliu Cismasiu, Professor Associado da Faculdade de Ciências e Tecnologia da Universidade Nova de Lisboa

FACULDADE DE CIÊNCIAS E TECNOLOGIA
UNIVERSIDADE NOVA DE LISBOA

Setembro 2017

Acknowledgements

Em primeiro lugar um especial agradecimento para a minha família por todo o apoio que me deu ao longo de todo um percurso de cinco anos pela universidade.

For this dissertation, I want to express my deepest gratitude to all the EESD lab in EPFL in particular to my co-advisors Danilo Tarquini and João Pacheco de Almeida for the opportunity and for all the help along the former semester.

A special thanks to my advisor in FCT/UNL, Professor Corneliu Cismasiu for all the advices and guidance which allow me to complete this dissertation.

Abstract

Many existing bridges were built before modern seismic design guidelines were written. This means that particularly in countries with moderate seismicity where another type of loads such as gravity, wind or snow are more demanding, the seismic hazard may have been underestimated in the past years. Past experience shows that critical details, including lap-splices on the potential plastic hinge region above the foundation and low transverse reinforcements ratios, can lead to a small deformation capacity of the existing bridge piers and therefore to a possible major structural damage.

The performance of RC members featuring lap splices was extensively studied in the past. However, a large number of authors focused on the force capacity of lap splices while their deformation capacity was rather neglected. This topic has become a target of interest only recently.

This dissertation represents the first part of a research project developed at *École Polytechnique Fédérale de Lausanne* that has the final goal of presenting a constitutive law capable of predicting the lap splice behavior, in particular its deformation capacity. The dissertation presents an experimental campaign regarding the lap splice performance under cyclic loading.

This experimental campaign gives continuity to the experimental campaigns presented by Bimschas (2010) and Hannewald et al. (2013), where three large-scale piers featuring lap splices near the foundation were tested. Three specimens representing a boundary region of the previously specimens are presented in this dissertation.

The test specimens subjected to the same cyclic load history only differ regarding the transversal reinforcement. Particular attention is given to the slippage between the rebars and the steel strains in the lap splice zone.

These tests along with the results of future specimens intend to create a database that will allow to validate the future expression mentioned above.

Key-words:

Reinforced concrete

Lap-splices

Plastic hinge

Experimental Campaign

Cyclic Loading

Resumo

Grande parte das pontes existentes foram construídas antes dos atuais códigos de dimensionamento o que significa que particularmente em países onde seja admitida uma sismicidade moderada e onde outro tipo de cargas tais como as cargas gravíticas, do vento ou da neve assumem maior importância, o risco sísmico pode ter sido subestimado no passado. Experiências passadas mostram que detalhes construtivos como emendas em potenciais zonas de rotulas plásticas bem como baixos rácios de armadura transversal podem levar a uma pequena capacidade de deformação dos pilares existentes e como consequência levar grandes danos estruturais.

O desempenho de elementos de betão armado com emenda foi extensivamente estudado no passado. No entanto, a maior parte dos autores focaram-se na resistência das emendas enquanto que a sua capacidade de deformação foi desprezada sendo apenas foco de maior interesse mais recentemente.

A presente dissertação está integrada num projeto de investigação desenvolvido pela *École Polytechnique Fédérale de Lausanne* que tem o objetivo final de apresentar uma expressão que consiga prever o comportamento das emendas, em particular a capacidade de deformação em elementos de betão armado. Esta tese apresenta uma campanha experimental referente ao desempenho das emendas quando carregadas ciclicamente.

Esta campanha experimental dá continuidade as campanhas experimentais apresentadas por Bimschas (2010) e Hannewald et al. (2013), onde foram testados três pilares com emendas perto da fundação. Nesta dissertação vão ser apresentados três espécimes representativos do extremo dos pilares acima referidos.

Os espécimes sujeitos ao mesmo carregados cíclico apenas diferem na quantidade de armadura transversal. Particular atenção vai ser dada ao deslizamento e às extensões na armadura longitudinal na zona da emenda.

Estes testes, conjuntamente com os resultados de futuros espécimes, têm como principal objetivo criar uma base de dados que permita validar a futura expressão acima referida.

Palavras chaves:

Betão armado

Emendas

Rotula Plástica

Campanha experimental

Carregamento Cíclico

Contents

List of Figures

List of Tables

List of Symbols

A_b Single Spliced bar area

A_{st} Area of stirrups

A_{trx} Area stirrups in x

A_{try} Area stirrups in y

b Section width

c_b Clear cover between the longitudinal reinforcement and the bottom face

c_{si} Clear distance between longitudinal reinforcement

c_{so} Clear cover between longitudinal reinforcement bar and the side face

E_c Concrete Young's Modulus

E_s Steel Young's Modulus

$F_{splitting}$ Splitting force

$F_{stirrup}$ Force carried out by a stirrup

f_{ct} Concrete Tensile Strength

f_y Steel yield stress

f_u Steel ultimate Stress

$f_{u,ls}$ Equivalent ultimate stress in lap splices

$f_{y,ls}$ Equivalent yielding stress in lap splices

$f_{s,lp}$ Lap splice Stress

f'_c Concrete compressive strength

L_s Shear Span of RC member

l_s Lap splice length

N_{st} Number of stirrups within the splice length

N_l Number of stirrup legs

n Number of bars being developed in a splice

n_i Number of cycles per load step

s Spacing between stirrups

R Strain hardening parameter

γ_{cc} Concrete specific weight

γ_s Steel specific weight

ε_{cc} Concrete strain at peak compression stress

$\varepsilon_{y,ls}$ Equivalent yielding strain in lap splices

ε_y Steel yield strain

ε_u Steel ultimate strain

$\varepsilon_{u,ls}$ Equivalent ultimate strain in lap splices

η Number of load steps

η_{total} Total number of load steps

ρ_w Confining reinforcement ratio

ρ_x Confining reinforcement ratio in x

ρ_y Confining reinforcement in y

σ_{st} Stress in Stirrups

$\emptyset_L$ Longitudinal Reinforcement Diameter

$\emptyset$ Diameter

1 Introduction

1.1 Motivation

The occurrence of earthquakes is still an unpredictable phenomenon. Their occurrence cannot be predicted neither as regards to time, magnitude nor location. To overcome this randomness, it is assumed a certain return period, i.e., an average period of time between two seismic events in a given region. This leads to a distinction between regions in accordance with their return period. Thus, regions with high risk of a seismic event have a smaller return period. On the other hand, longer time without any significant seismic event means a low risk region.

Switzerland is considered a region with a low to moderate seismicity. But even if the earthquake damage in regions with moderate seismicity is not often associated to a life safety hazard, the economic and social damage can be very harmful. However, the low probabilities for seismic events in Switzerland led to a disregard of the importance of this hazard while others more frequent loads like for example wind had a greater importance on the design codes.

The first Swiss Code that included seismic provisions was released in the year of 1970, (SIA160, 1970). To define a seismic event, the code adopted a maximum peak ground acceleration between $0.02g$ and 0.05g, according to the importance of the structure. The maximum peak acceleration was increased in 1989 when a new generation of codes was established. Different peak ground-accelerations are distinguished using a map of different seismic zones.

The current code was adopted in 2003 (SIA.SIA261, 2003). As shown in the figure 1.1, Switzerland is divided in four seismic zones and the hazard in each zone is assumed to be a constant value. The value for the horizontal ground acceleration ranges from $0.06g$ to $0.16g$, considering a return period of 475 years.

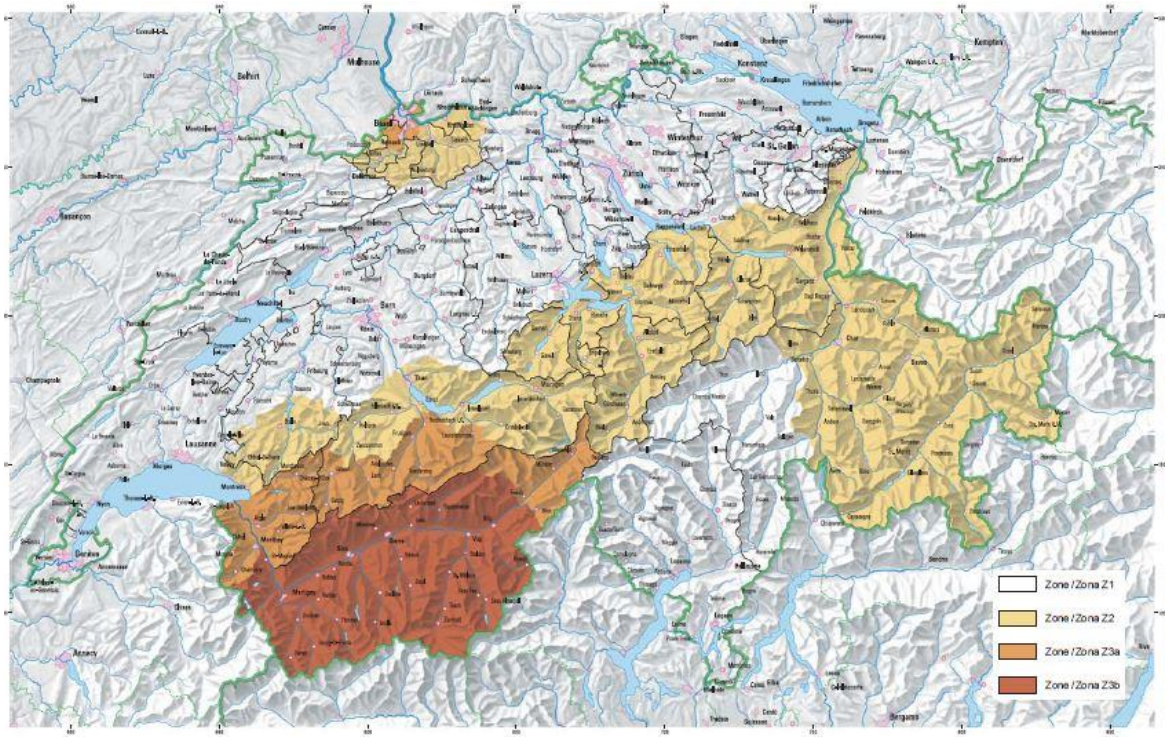

Figure 1.1: Seismic Risk Zones according to SIA 261 (SIA.SIA261, 2003)

According to Bimschas (2010) about 90 % of all bridges in Switzerland were constructed before 1990, half of those between 1970 and 1989 and the rest before that date. Therefore, it can be assumed that a large amount of the Swiss bridge population do not feature adequate seismic construction details and therefore it is not capable of sustain the modern codes demands.

Although in modern codes lap splices are no more accepted in the inelastic regions of RC members, there are a large number of published studies (Lowes, et al., 2012; Hardisty, et al., 2015; Sritharan, et al., 2014) showing that longitudinal rebars of many bridge piers are spliced at the base of the column, i.e., in the zone where a plastic hinge is expected to developed.

Experimental tests backed up by field reports shown that the presence of lap splices in RC members may lead to a poor behavior of the member and especially if located in the high deformation region and poorly detailed.

Most of the already published research focused mainly the strength capacity of lap splices while the deformation capacity of this construction detail was just addressed in a few of more recent papers. The information about the influence on the deformation capacity of members with lap splices, particularly on RC walls, is still scarce.

Trough experimental campaigns on RC walls, Bimschas (2010) and Hannewald et al. (2013), demonstrated that splicing the longitudinal reinforcement near the plastic hinge region leads to a significant reduction of

their displacement capacity. Furthermore, the authors claim that the transversal reinforcement, the splice length and the loading history have a significant importance in the response of the member.

While the transversal reinforcement was assumed as the most critical factor on the response of lap splices, a small splice length will not be able to effectively distribute the strength along its length and a cyclic loading have proved to be much more detrimental to lap splices than repeated loads.

More recently, Tarquini et al. (2017) proposed a model to predict the monotonic response of lap splices for RC walls where it considers the transversal reinforcement and splice length. However, this model was only validated against experimental data on experimentally tested RC walls piers and is only valid for monotonic load, not considering cyclic or reversing loading.

A constitutive model for the average behavior of lap splices, under cyclic loading, is still lacking in the literature. Experimental data are required to establish the cyclic behavior of lap splices, including the effects of the splice length and the transversal reinforcement.

1.2 Objectives of the Study

The main goal of this dissertation is to plan and carry out an experimental campaign to better understand the expected performance of RC members with lap splices when subjected to cyclic loading.

The specimens presented on this dissertation allow to study in more detail the expected behavior of lap splices in the event of an earthquake. In particular, the experimental campaign presented in the present dissertation was conducted in order to examine the influence of the transversal reinforcement ratio on the displacement capacity of lap splices.

Future tests regarding the former experimental campaign will allow to study the influence of another features that also effect the displacement capacity of this construction detail and they will allow to create an important database that is currently missing.

The data gathered during all the experimental campaign will be used for calibration of a future constitutive model concerning the lap splice behavior.

1.3 Outline of the Dissertation

Before starting addressing the experimental campaign is important to understand the behavior of lap splices. The chapter 2 present a literature review about this construction detail.

First, in section 2.1, a theoretical introduction of the lap splice strength is presented, explaining its force transfer mechanism, and its failure modes.

Afterwards, in section 2.2, Post-Earthquake field observations are presented. This section presents different problems seen in RC members after recent seismic activities where lap splice played an important role.

As the present dissertation addresses an experimental campaign, the section 2.3 will present the past experimental campaigns that focused on the same subject. This summarizes the different obtained results from the past experiences in beams, columns and walls and can be useful to have an idea of the past studies and the work that is still missing regarding the lap splice displacement.

The following section 2.4, presents a summary of the factors that most significantly influence lap splices and the correlation that the formers have with each other. The chapter 2 is finished with a sub-section where the past simplified constitutive models for lap splice strength and displacement are presented.

After that the experimental campaign will be introduced. The sections 3.1, 3.2 address the background of the campaign and the characteristics of the test specimens respectively. The following sections, 3.3, 3.4 and 3.5, respectively, indicate the material proprieties, the load history and to give more detailed information about the test setup and instrumentation.

In the sections 3.6 and 3.7 test observations and the test results of each specimen of this experimental campaign are represented. Lastly, in section 3.8 a summary of the results of the test specimens is presented.

On the final chapter 4, the author concludes about the information obtained through the experimental campaign and suggest further studies concerning the results achieved.

2 Literature Review

2.1 General Introduction

The most convenient location, for constructive reasons, for a lapped spliced in a column is immediately above the foundation or above the floors in the case of a multi-story building. This location coincides with the maximum moment along the height of the column. For wind loading the existing codes rules can guarantee a satisfactory splice performance since no large inelastic demands will be reached. However, in case of severe ground shaking, the resulting moments can differ significantly from the ones obtained from the standard elastic analysis established in the codes for lateral seismic loading.

Although the force transfer mechanism between concrete and rebars have been extensively studied in the past years the experiments were mostly centered on monotonic loads while bond cyclic loads received minor attention. These cyclic loads can be divided into two categories, low cycle, and high cycle. The former, concerning both earthquakes and wind loadings, has few cycles at a bigger intensity while the latter, has more cycles at a low bond intensity (e.g. fatigue load).

Similarly, bond behavior can be further subdivided according to the type of stress applied. One is unidirectional loading, which implies that the bar stress does not reverse from tension to compression during a load cycle and the other is regarding when the rebar is alternatively subjected to tension and compression and it is defined as reversed/cyclic loading. Earthquake loading is typically a cyclic loading. (ACI-ASCE, 2012)

Since concrete is a non-homogeneous material neither is expected to be free of internal cracks it can be assumed different levels of strength at the top, bottom or side of the lap splice zone. Additionally, past experimental research have shown that local stresses can be four or five times higher than the average stresses along the bond. However, the currently required development lengths are based on a uniformly distributed bond stress assumption over the entire length of the rebar.

In general, the stress between the bars and the concrete is transferred to the concrete by an inclined force that can be decomposed into two components, (i) a component parallel to the rebar axis and (ii) a radial one. The longitudinal force is associated with the irregularities along the surface of the steel (lugs) while the forces orientated perpendicular to the bars can arise as the bar is loaded and induce tensile stresses in the surrounding concrete that can lead to the splitting of the concrete cover. (See figure 2.1)

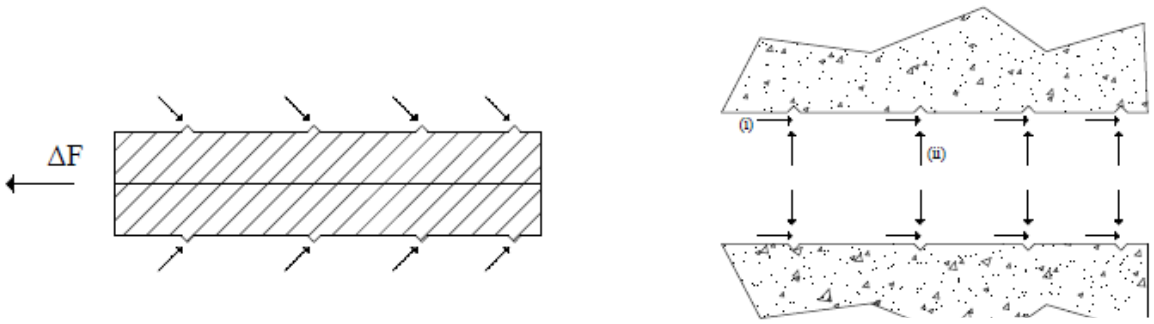

(a) (b)

Figure 2.1-Representation of the transfer of forces; (a) bond force on bar and (b) components on concrete

These forces can be related directly to the different types of bond failures. The first, pull out failure, occurs due to the shearing of the concrete between the ribs and it is likely to happen when the concrete cover and the transverse reinforcement prevent the splitting. The resistance depends firstly on the concrete strength and in the pattern and geometry of the rebar while the size and spacing of the transverse reinforcement also plays an important role by keeping the slitting cracks small. (See figure 2.2 (a))

However, after the slip of the longitudinal reinforcement some resistance is still maintained due to friction and the interface shear.

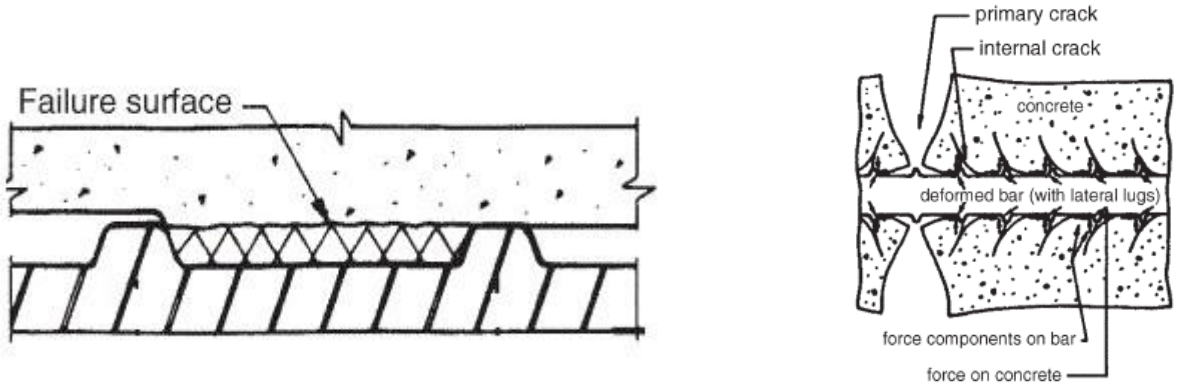

(a) (b)

Figure 2.2: Failures Modes; (a) pullout failure and (b) splitting failure (ACI-ASCE, 2012)

The second type of bond failure is the splitting failure and is depicted in figure 2.2 (b). This type of failure takes place when concrete cover or confinement is insufficient to attain the entire pull out strength. As said above, this type of failure is due to radial stresses which induce tension stresses to the surrounding concrete and hence, small lateral cracks appear.

This type of failure generally manifest for bars with three or less diameters of concrete cover and thus it's most likely to happen for usual RC structures than the pull-out failure.

The number and configuration of the bars will establish the orientation of the splitting cracks. For members featuring bars with a concrete cover less than half the bar spacing splitting cracks will occur parallel to the bar and correspondently perpendicular to the surface (face-splitting). For bars in which the concrete cover is higher than twice the bar spacing, splitting cracks tend to appear in the plane of the reinforcement (side-splitting). (ACI-ASCE, 2012)

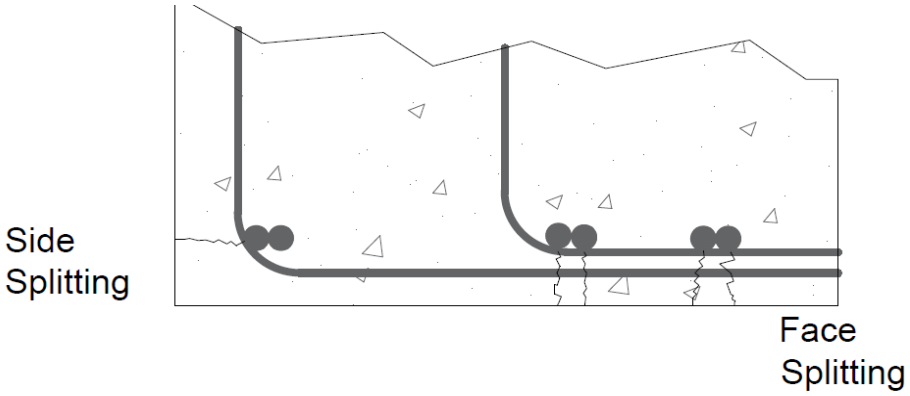

Figure 2.3: Physical Model of splitting failures

2.2 Post-Earthquake Field Observations

This section discusses the damage mainly caused by lap splices on RC members seen in several post-field observations. The section will be divided into two sub-sections, the first addresses the visible damage caused by the presence of lap splices into columns while the second treats the damage on lap splice regions of RC walls.

2.2.1 Columns

In this sub-section damage in the lap splice region observed in the earthquakes of Northridge, 1994 and Turkey 1999 is summarized. (Melek, et al., 2003; Sezen, et al., 2002)

Consequent of the Northridge earthquake shear and spliced failures in reinforced concrete columns could be seen in particular in older buildings. In figure 2.4 (a) is presented an exterior column of a one story parking structure with a 450 mm square cross section and $20\emptyset_L$ splice length.

The post-earthquake reports state that the cross section of the interior columns was posteriorly increased in accordance with the initial project, however, no apparent changes were made on the exterior columns. Damage in the column indicated that slip occurred along the splice together with the spalling of the concrete.

(a) (b)

Figure 2.4: Poor performance of columns during the Northridge Earthquake 1994 (Melek, et al., 2003)

Following this seismic event, it also was found more damaged columns in an eight-story parking structure represented in figure 2.4 (b). In this case splice damage was limited due to the use of shear walls which limited the lateral drift imposed on the columns (Melek, et al., 2003).

Another example of an extensive damage on reinforced concrete columns occurred during the 7.4 magnitude earthquake that struck northwestern Turkey on August 17, 1999.

Post-field observations shown that the behavior of splices may have played a role on the collapse of buildings in 1999, Turkey. Figure 2.5 (b) shows a typical beam-column connection for a six-floor building and the failure surface indicates that longitudinal bars of the column were inadequately anchored and probably they were pulled out at relative low load levels. (Melek, et al., 2003)

The reports made after the fields observation show that the Turkish earthquake code provisions were not followed in detailing reinforced concrete columns, especially in potential plastic hinge zones at the end of the columns. As shown by figure 2.5 (a) lap splices were typically made at the column bottom (floor or foundation interface) without the needed confinement to perform in a ductile way. The reports have also showed that the buildings that featured shear walls as structural elements generally didn't manifest much damage under the seismic event. (Sezen, et al., 2002)

In summary, column damage linked with the poor behavior of splices have been often observed in recent earthquakes with the damage ranging from minor cracking to collapse.

(a) (b)

Figure 2.5: Field Observations after Turkey Earthquake in 1999 (Melek, et al., 2003; Sezen, et al., 2002)

2.2.2 Walls

In the reports by Birely (2012), Song et al. (2012) and Sritharan et al. (2014) is possible to find an extensive database including the damages presented on RC walls associated with lap splices that occurred during the past years. The authors observed that the majority of the damage was located near the interface between floors where the splices of the longitudinal reinforcement were made.

Focusing on the most recent events, damage to more than one hundred high-rise RC walls buildings resulting from lap splice failures was recorded in the Chile earthquake of February 2010.

Song et al. (2012) observed lap splice failures on a collapsed building. Song et al. (2012) claims that even if the cause that led to a collapse of an entire building can be always debatable, longitudinal bars were cut off in the lap splice zone which indicates a clear lap splice failure.

Also the 2010 Canterbury earthquake revealed problems in the lap splice zone. Sritharan et al. (2014) reported a concentrate damage above the lap splice region in RC walls of a seven-story building. Although the lap splice wasn't located in the plastic hinge region the damage can be explained by the poorly detailed transversal reinforcement and the scarcity of stirrups between the two layers of web reinforcement.

Lap splices also contributed to the failure of a chimney. During the Niigata-ken Chuetsu-Oki earthquake in Japan a chimney with 58 m height failed. Figure 2.7 shows the damage on the chimney at the lap splice zone at approximately 17.5 m from the ground level.

The chimney featuring a splice length of $40\emptyset_L$, presented a relevant strength discontinuity in the zone where the damage concentrated. In the lap splice zone half of the longitudinal reinforcement was dismissed, two layers of longitudinal reinforcement were changed to a single layer, and double transverse hoops were changed to a single transverse hoop at the same height (see figure 2.6). The sudden changes on the longitudinal and transversal reinforcement at the lap splice region most likely triggered the failure of this RC chimney. (Kim, et al., 2012)

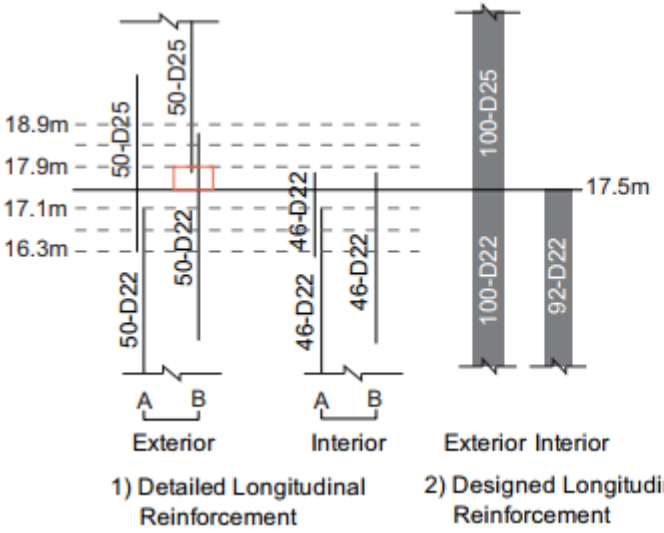

Table 3. Reinforcements at around 17.5m

Height, m	Longitudinal bars		P_g, %
	Exterior	Interior	
18.9	100-D25		0.965
18.4	75-D25, 25-D22		0.904
17.9	50-D25 50-D22		0.843
17.5	50-D25 50-D22	46-D22	1.175
17.1	50-D25 50-D22	92-D22	1.500
16.7	100-D22	92-D22	1.450

Figure 2.6: Reinforcement Detail at around 17.5 m height (Kim, et al., 2012)

(a) (b)

Figure 2.7: Lap splice damage on a chimney during Niigata-ken Chuetsu-Oki earthquake (Kim, et al., 2012)

2.3 Review of Past Experimental Campaigns

On this sub-section will be presented the recent experimental studies that address the behavior of lap splices, under monotonic and cyclic loading, on beams, columns and walls.

The goal of this sub-section is to report the characteristics of the past experimental tests as well as the obtained results, compiling a data which can describe the member behavior and how this one is modified by the presence of lap splices.

2.3.1 Beams and Columns

Experimental tests on beams and columns have been extensively carried out along of the past years. The first extensive campaign regarding the influence of lap splice in RC beams was at the end of the 1970s at Cornell University. (Sivakumar, et al., 1982; Gergely, et al., 1980)

The former campaign was particularly important because the influence of lap splices under repeated and reversed loading was approach for the first time and it was also the first one which state the importance of the stirrups along the splice. The study showed that it is possible to design lapped splices to sustain repeated loading beyond yield if closely spaced stirrups are used and if the splice length has an appropriate length. The location of the stirrups along the splice length was also studied and the results revealed differences between monotonic and cyclic loading. (See sub-section 2.4.3)

Based on the results from this campaign some authors proposed design procedures and expressions to determine the amount of transversal reinforcement needed to resist to a larger number of reversed cyclic loads. These recommendations were corroborated by the observations of Sparling and Rezansoff (1986) where the authors affirmed that the provisions for the seismic application increased considerably the ductility of the specimens.

The first experimental tests on columns with deficient lap splices was just reported later. (Chai, et al., 1991; Aboutaha, et al., 1995)

Both, Chai et al. (1991) and Aboutaha et al. (1995), proposed the reinforcement of RC concrete columns with inadequate lap splices and poor transversal reinforcement through steel jackets (see figure 2.8). Theirs experimental campaigns were important because columns were tested for the first time under cyclic lateral loads.

The results showed mainly a splitting failure, with vertical splitting cracks along the splice, after the yielding of the longitudinal reinforcement for the non-retrofitted columns, while in the columns confined by the steel jacketing was observed an increasing in both strength and strain and no bond failure occurred.

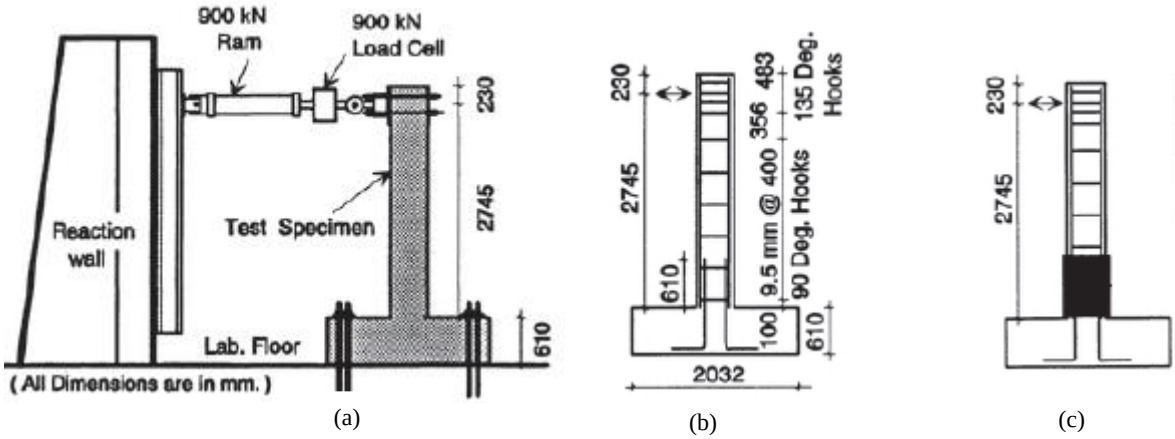

Figure 2.8: (a) Test Setup, (b) Unretrofitted Columns and (c) Strengthened Column (Aboutaha, et al., 1995)

More recently, Pam et al. (2010), studied the differences of the locations of lap splices on the flexural strength and ductility of RC columns. The experimental campaign concluded that although the specimens that feature lap splices in the critical region had a largest strength than the ones with a continuous longitudinal reinforcement, their ductility capacity decreased. These results will be further discussed in sub-section 2.4.

2.3.2 Walls

Experimental tests of lap splices on the longitudinal reinforcement of walls were only recently reported. The main characteristics of all the tested walls presented in this sub-section are listed in table 2.1.

The first experimental campaign regarding the behavior of RC walls with lap splices was just reported in 2003, by Paterson and Mitchell. Two non-retrofitted RC walls were tested, one with lap splices in the critical region while the other had the lap splice outside the critical region (W1 and W2).

The test specimen that featured the lap splice near the foundation exhibit a poor ductility failing soon after the yielding of the rebars. The lap splice failure was evident by the vertical splitting cracks along the length of the splice. The other specimen, that had the lap splice outside of the critical zone, showed a ductility response three times bigger than the specimen with the longitudinal reinforcement spliced near the critical zone. A large amount of cracking appeared at the base of the wall damaging this area and leading to a brittle tensile failure of one lap splice, resulting in a large drop in the capacity of the specimen.

At 2008 in McMaster University, Canada, Elnady (2008) carried out an experimental campaign where two RC walls with lap splices where tested (CW2 and CW3)

Both walls were identical but they were subjected to different horizontal loads that imposed different moments along the member. The horizontal actuators were controlled so that the moment to shear ratio (M/VL) was held constant at 5 and 2.25 for each specimen.

The first test specimen, subjected to horizontal forces, showed flexural cracks at the bottom of the wall at the very first loading cycle, as the horizontal loads continue to increase the cracks on the bottom spread to near mid-height and a new horizontal crack developed at the top end of the splice. Finally, the wall failed prematurely due to bond slip of the lap splice. The yielding of the longitudinal reinforcement was not achieved. The second wall showed a higher deformation capacity, the first cracks just developed at a value of drift five times bigger than the drift achieved at failure in the former wall. While loading the cracks, inclined at 45°, opened up and extended from corner-to-corner of the wall in both diagonal directions. The wall finally failed due to bond slip of the lap splice.

After, Bimschas (2010) tested one other RC wall with lap splices at the base (VK2). The damage in the wall began with side splitting cracks in the tensile edge of the wall and after by the development of a large bond crack with the same length as the splice which cause a drop in the flexural strength of the member. With the increasing of the load the bond failure of the splices occurred causing a progressive degradation of the cyclic strength of the member.

Following the former experimental campaign of Bimschas, more two specimens featuring lap splices were made by Hannewald (2013). A reversed cyclic loading was applied to the test specimens. The first specimen (VK4) signs of damage revealed by the first specimen were compression cracks at the wall edge, when reversed the horizontal loading a splice failure occurred followed by a sensible drop of the wall strength, reversing again the horizontal loading more splices failed again at tension side of the pier. The second RC wall (VK5) showed first vertical side splitting cracks along the splice length and a horizontal crack at the top end of the splice. After, splice failure occurred leading to a decrease of the wall lateral strength. The carachteristics of the specimens' tested by Bimschas (2010) and Hannewald (2013) are presented in table

The next experimental campaign addressing lap splices in RC walls was presented by Layssi et al. (2012). The campaign counted with two specimens that feature lap splices near the plastic hinge zone (W1* and W2*). Both specimens revealed a non-ductile response due to a brittle side splitting of the external lap splice prior to yielding that led to a significant drop in the strength capacity. Furthermore, neither of the specimens achieved the predicted flexural capacity.

Birely (2012) reported the following experimental campaign focused on RC walls. One specimen with lap splice at its base was studied (PW2) and revealed a behavior similar to the formers specimens already mentioned on this sub-section. Cover spalling appeared above the splice region at an early stage of the test followed by the exposition of the longitudinal reinforcement which led to the buckling of the rebars. Increasing the applied forces, the concrete crushed where buckling occurred and the damage extended to the web of the wall propagating afterwards to the top of the web splices.

A paper presented by Aaleti et al. (2013) reported another experimental campaign regarding structural RC walls featuring lap splices near the base. Only one specimen with this construction detail was tested (RWS). The damage on the specimen was mainly visible by the cracks above the lap splice region and in the wall base, a strength degradation appeared probably due to slipping in the splice region. With the demand, bond degradation progressed increasingly.

More recently, four large scale RC walls were tested by Villalobos and Pujol (2014) (W-60-C, W-40-C, W-60-N and W-60-N2). The specimens intended to represent the configuration of structural walls featuring lap splices that have failed in the Earthquake of Chile, 2010. The behavior of the four specimens was substantially identical. First, side splitting cracks appear near the splice ends being widest near the base. The loss of strength due to the bond degradation was clear by the force displacement response of the member. At the final imposed displacement, one specimen showed vertical cracks along the length of the splice.

The last experimental campaign known by the author was reported by Almeida et al. (2017) at École Polythechnique Fédérale de Lausanne. The experimental test only featured one RC wall with lap splices at the plastic hinge region (TW3). The behavior of the specimen was governed by signs of damage in the lap splice region. At an earlier loading stage, a first face splitting vertical crack appear, with the increasing of the imposed displacement, some side splitting cracks showed up extending throughout the entire lap splice length. Later, wide horizontal cracks above and below the splice developed. In the end of the test, it was clear that the damage concentrates essentially in the lap splice region while the remaining part of the member remained intact.

In resume, the response of all the tested specimens was associated with the failure of the lap splices.

Table 2.1: Resume of the main characteristics of experimental tested walls with lap splices

Test Specimen	Reference	Scale	l_s (mm)	$\emptyset_L$ (mm)	Number of splices	L_s (mm)	Wall Length (mm)
W1	(Paterson, et al., 2003)	1:1	900	25	2	3250	1200
W2		1:1	900	25	2	3750	1200
CW2	(Elnady, 2008)	1:3	360	16	2	5000	1000
CW3		1:3	360	16	2	2250	1000
VK2	(Bimschas, 2010)	1:2	600	14	4	3300	1500
VK4	(Hannewald, 2013)	1:2	600	14	4	3300	1500
VK5		1:2	600	14	4	4500	1500
W1*	(Layssi, et al., 2012)	1:1	600	20	2	3250	1200
W2*		1:1	600	20	2	3250	1200
PW2	(Birely, 2012)	1:3	609	13	2	6710	3048
RWS	(Aaleti, et al., 2013)	1:2	19 29	2 2	2	6096	2286
W-60-C	(Villalobos, et al., 2014)	1:1	1520	25	2	3660	1520
W-40-C		1:1	1020	25	2	3660	1520
W-60-N		1:1	1520	25	2	3660	1520
W-60-N2		1:1	1520	25	2	3660	1520
TW3	(Almeida, et al., 2017)	2:3	215	6	2	3150	2700

2.4 Factors Affecting Strength and Deformation Capacity of Lap Splices

The prediction of the behavior expected by RC members with lap splices is always a difficult task since both the lap splice strength and strain depend largely on the correct identification of its governing factors. On the following sub-section, a summary of the factors that most affect the strength and strain of lap splices will be presented.

2.4.1 Splice Length and Bar Diameter

As seen in sub-section 2.1, the transfer of forces between the rebars is made along the entire splice length. Thus, the influence of a small splice length can be easily understood. The smaller the splice length, the higher is the value of the stresses along its length. Consequently, a small length of the splice can lead to peak stresses that in turn can lead to an important reduction of the ductility and member strength.

However, a constant increasing of the splice length would not inherently increase the splice strength. In fact, as the length of the splice increases, the effectiveness of the splice length decreases, the assumption of a uniform distribution of stresses is properly accurate if the lap splice is short but with the increasing of the splice length this idea becomes less valid. (Chinn, et al., 1955; Fergunson, et al., 1971; Canbay, et al., 2005).

Figure 2.9 represents the stress distribution along the splice length. The ineffectiveness into increasing the splice length can be explained by the tendency of bond stresses to concentrate near the region of the end of the splice instead of an approximately constant distribution. (Canbay, et al., 2005)

Furthermore, in a poorly confined member adding splice length is of little value. Paulay (1982) reported that in long splices not well confined longitudinal splitting cracks will propagate along the splice length, reducing progressively the length over which the force from one bar can be effectively transmitted to the other.

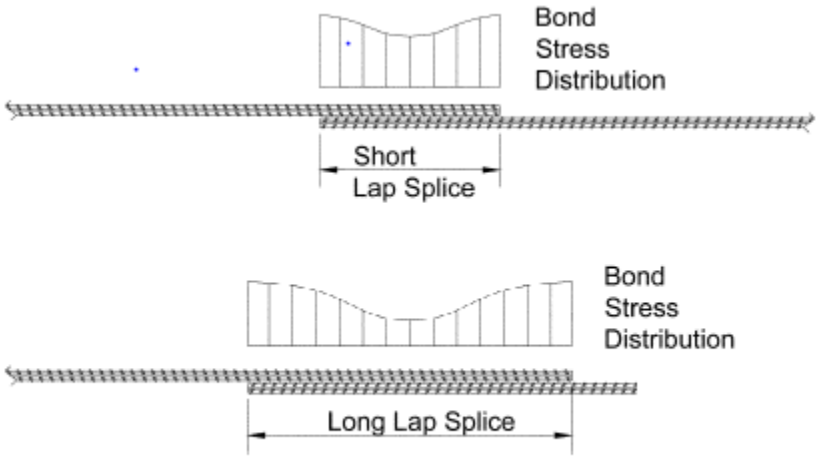

Figure 2.9: Stress distribution along the splice length

The effectiveness of the splice length is also strongly dependent on the bar size. Almeida et al. (2017) pointed out that bond stress concentration is more pronounced for smaller diameters and hence a ratio between the splice length and the bar diameter should be taken into consideration. However, several researches showed that increasing the diameter of the bar will not increase the splice strength and can lead to a decrease of the deformation capacity of the splice. (ACI-ASCE, 2012)

Therefore, the splice length is relative and must be adapted to the bar diameter. For this reason, a given splice can be considered long for a given bar diameter while the same length can be considered short for bars with larger values of bar diameters.

2.4.2 Concrete cover

As addressed previously one of the failure modes for RC members with lap splices is related with the development of splitting cracks. Although the concrete cover can be directly linked to the formation of cracks it is still not clear the influence of this on the deformation capacity of the member.

The concrete cover can largely influence the failure mode. When the concrete cover is smaller than 2.5 bar diameters, a splitting tensile failure is likely to happen at a shorter anchorage length than the one needed for sustain pull out failure. (ACI-ASCE, 2012)

The abovementioned report also claim that the influence of the concrete cover is even more important for cyclic loads since more severe cracking will likely occur.

2.4.3 Transversal Reinforcement

The effect of transversal reinforcement have been highly studied in the past years and its influence both on strength and strain capacity of lap splices is particularly important. The importance of the transversal reinforcement is even more highlighted by the current codes that only allow lap splices in the plastic hinge region if a minimum amount of transverse reinforcement is provided.

The transversal reinforcement is particularly important after splitting cracks taken place. As seen in sub-section 2.1, tensile stresses will be applied to the surrounding concrete leading to transversal cracks and hence, posteriorly to splitting, the tensile stresses will be sustained by the transversal reinforcement.

Several researches showed that a well confined splice can achieve a displacement ductility at least two times higher than the displacement achieved by specimens with less transversal reinforcement ratio when subjected to many cycles of repeated load. (Gergely, et al., 1982; Sparling, et al., 1986; Lukose, et al., 1982).

Although well detailed lap splices can increase the flexural strength of the member, an excessive amount of transversal reinforcement can decrease significantly its ductility performance. A large amount of transversal reinforcement can lead to a failure mechanism that relocates the plastic hinge on the top of the splice and concentrating the damage on that zone. (Pam, et al., 2010; Lowes, et al., 2012).

Furthermore, with a big amount of transversal reinforcement the plastic hinge length may reduce significantly. Thus, the curvature ductility required to a certain imposed lateral displacement will therefore

increasing resulting in large steel strains which can lead to a possible fracture of the longitudinal reinforcement. (Almeida, et al., 2017; Paulay, 1982)

Past researchers reported that also the layout of the transversal reinforcement plays a role in the strength and strain of lap splices. While in the past Gergely et al. (1982) stated that multiple stirrups at splice ends are more effective for monotonic loads, for cyclic loads, yield penetrate in the splice and it will progress at an accelerated rate if internal confinement along the splice length is poor. (ACI-ASCE, 2012)

2.4.4 Loading History

The difference between monotonic, repeated and reversed load has been a case of study for the past years. Many experimental campaigns have proved that reversed cycle loads are more detrimental to splice performance than are repeated loads. This comparison is made by the amount of cycles that the same test specimens need to reach failure in the both loading protocols.

Gergely (1982) showed through experimental tests in beams that repeated loading and the number of load cycles do not have a pronounced effect on the performance of lap splices if the load level is below 75% of the monotonic capacity of the member.

According to Sparling at al. (1986), cyclic loading will origin an increase of stiffness deterioration, mainly due to cracking and crushing of the concrete, bar slip and softening of the reinforcement, which will reduce the deformation capacity of the RC member when compared to monotonic and repeated tests.

Although the failure modes for both loading cases are essentially the same, both authors agreed that the number of cycles to failures is much less when in the presence of reversed load cycles.

2.4.5 Moment Gradient

The moment gradient in relation with lap splices was not extensively studied in the past. When the effect of moment gradient was firstly addressed, some authors claimed that the effect of the former did not have relevance enough to justify its inclusion on the developed expression for the bond strength. (Orangun, et al., 1977)

The influence of the moment gradient just became clear on the experimental campaign at Cornel University by Lukose et al. (1982). Reported by the authors the test results clearly demonstrate the increasing of the performance of the test specimens in the presence of shear in comparison with the specimens loaded with a constant moment along the splice. With a uniform moment, the damage progresses from both ends of the splice and hence, enhancing its detrimental interaction. Adding shear forces on the splice, the failure will begin at the extremity with the highest moment and the interaction between the two splices is reduced.

However, the same authors claim that the shear forces aggravate the damage on the region of the splice where is present the high moment. Extensive transversal cracking take place due to i) the change in the stiffness beyond the splice end; ii) stress concentrations at the bar ends; and iii) due to flexural shear cracks.

A recent experimental campaign by Villalobos et al. (2016) addressed the effect of the moment gradient of lap splices in structural walls. The campaign tested RC walls with lap splices similar to the ones tested in

beams in the experimental campaigns of Richter (2012) and Hardisty et al. (2015). The authors claimed that the results showed that the beams tested under constant moment had splice failures while in the structural walls tested by Villalobos et al. (2016) no splice failures occurred. It was therefore concluded by the authors that the response of the splices can differ with respect to the scale of the test specimens.

2.5 Simplified constitutive models for Lap-Splices

Modelling the lap splice behavior is a challenging task since this regard the accurate modelling of the non-linear behavior on the interface between the two rebars. As have been mentioned previously, to model the behavior of lap splices two different methods can be used, i) a force approach, which is interested in estimating the lap splice strength and ii) a displacement approach, is used to predict the displacement capacity of lap splices.

Although the strength of a lap splice has an important part on the assessment of RC members, its deformation capacity cannot be neglected. Furthermore, while the force capacity of lap splices has been rather studied in the past years, for predicting their displacement capacity just few models are available that can accurately represent their deformation ductility.

The following sub-section intends to present the most relevant models to estimate both the lap splice strength as the lap splice displacement available.

2.5.1 Lap-Splice Strength

In the author opinion, the model currently available that predict more accurately the lap splice strength is the model proposed by Canbay and Frosch (2005). The model was chosen among the available formulations because is the only model that accounts for the different lap splice failures, side-splitting and face-splitting (see sub-section 2.1) and it was verified through the results from 203 unconfined and 278 confined beam tests subjected to monotonic loading.

According with Canbay and Frosch (2005) the maximum bar stress can be evaluated:

$$f_{s,lp} = \frac{F_{splitting} + F_{stirrup}}{nA_b \tan(\beta)} \qquad (2.1)$$

Where

$\beta = 20\ degres$

$A_b = single\ spliced\ bar\ area$

$n = number\ of\ bars\ being\ develop\ or\ spliced$

To calculate of the splitting force ($F_{splitting}$) geometrical relations are provided for effective concrete cover c and splice length l_s.

$$c_{b,eff} = c_b \frac{0.77}{\sqrt{\frac{c_b}{\emptyset_L}}} \leq c_b \quad (2.2)$$

$$c_{so,eff} = c_{so} \frac{0.77}{\sqrt{\frac{c_{so}}{\emptyset_L}}} \leq c_{so} \quad (2.3)$$

$$c_{si,eff} = c_{si} \frac{0.77}{\sqrt{\frac{c_{si}}{\emptyset_L}}} \leq c_{si} \quad (2.4)$$

$$l_{s,eff} = l_s \frac{53.48}{\sqrt{\frac{l_s}{\emptyset_L} \times \sqrt[4]{f'_c}}} \leq l_s \quad (2.7)$$

Where c_b is the clear cover between the longitudinal reinforcement and the bottom face; c_{si} the clear distance between longitudinal reinforcement bars and c_{so} the clear cover between the longitudinal reinforcement bar and the side face.

With the expressions of the effective cover and effective splice length is possible to model the splitting force depending on the type of failure expected

For side-splitting failure

$$F_{splitting} = l_{s,eff}\left[2c_{so,eff} + (n-1)2c_{si,eff}\right]6\sqrt{f'_c} \quad (2.5)$$

And for face-splitting failure

$$F_{splitting} = l_{s,eff}\left[2c_{b,eff} + 0.1\left(\frac{c_{so,eff}}{c_{b,eff}} + 0.9\right) + 2c_{b,eff}(n-1)\left(\frac{c_{si,eff}}{c_{b,eff}} + 0.9\right)\right]6\sqrt{f'_c} \quad (2.6)$$

Where

$$0.1\left(\frac{c_{si,eff}; c_{so,eff}}{c_{b,eff}} + 0.9\right) \geq 1.0 \quad (2.7)$$

For the side-splitting case, the additional force on the failure plane created by stirrups can be formulated as

$$F_{stirrup} = N_{st}N_l A_{st}\sigma_{st} \quad (2.8)$$

Where N_{st} represents the number of stirrups within the splice length; N_l number of stirrup legs; A_{st} area of stirrups and σ_{st} stress of stirrups.

By opposite, and admitting orthogonal cracks for face splitting the force developed by the stirrups can be formulated as

$$F_{stirrup} = N_{st}nA_{st}\sigma_{st} \quad (2.9)$$

However, the presented model has some important limitations. First does not account for the cyclic loading, since the splice strength was obtained by the evaluation of splices under monotonic loading and the beneficial effect of the moment gradient in the lap splice strength is not consider.

2.5.2 Lap-Splice Displacement

Currently few proposals are available to determine the ultimate strain limit of lap splices in RC walls. Furthermore, the existing ones, are used in conjunction with plastic hinge models where are proposed moment-curvature relations to account for the presence of lap splices.

Plastic hinge models can be resumed as a method that assumes that the inelastic curvatures are concentrated in a limited region, within they are linearly distributed and outside of this zone the deformations of the member are accepted as elastic. Thereafter, the global force-displacement response of a structure can be achieved by the moment-curvature relation determined for the section at which the maximum moment occurs.

The first author addressing this subject was Priestley et al. (1996). The method consists in checking if the equivalent tension stress in the rebars is less than the yield stress. If so, a reduced moment capacity is

calculated after which a decreasing of the flexural resistance of the member begins. If the yield stress is higher than the maximum equivalent tension, the nominal moment capacity is kept constant up to a curvature corresponding to a compression strain limit of $\varepsilon_c = 0.002$ followed by the failure of the RC member.

The idea of adopting compression strain limits is linked with the formation of longitudinal splitting cracks that reduce the concrete resistance in compression and tension. The author claims that after reached the ultimate strain level, a residual moment can be admitted for the member. The former that can be defined by a residual strength that the lap splices can sustain without falling for large slip values.

Following the displacement approach started by Priestley, Biskinis and Fardis (2007) developed simple rules for the calculation of the flexural resistance of RC members that feature lap splices in the plastic hinge region. The authors suggested an expression obtained from experimental tests on beams and columns. The expression was based on tensile strains limits that were defined as corresponding at 20% of the drop of lateral force of the specimens.

Finally, Hannewald (2013) based on compression strains limits in the context of plastic hinge analyses of three RC walls reported that the strain limit proposed by Priestley et al. (1996) was quite conservative while the strain at peak stress proposed by Mander (1988) provided better results.

Both, Hannewald (2007) and Biskinis and Fardis (2013), do not provide any values for residual forces after exceeding the strain limits proposed.

A qualitative representation of the moment-curvature for all the above-mentioned plastic hinge is depicted in figure 2.10. All the authors suggested further experimental campaigns addressing the displacement capacity of lap splices to increase the available database.

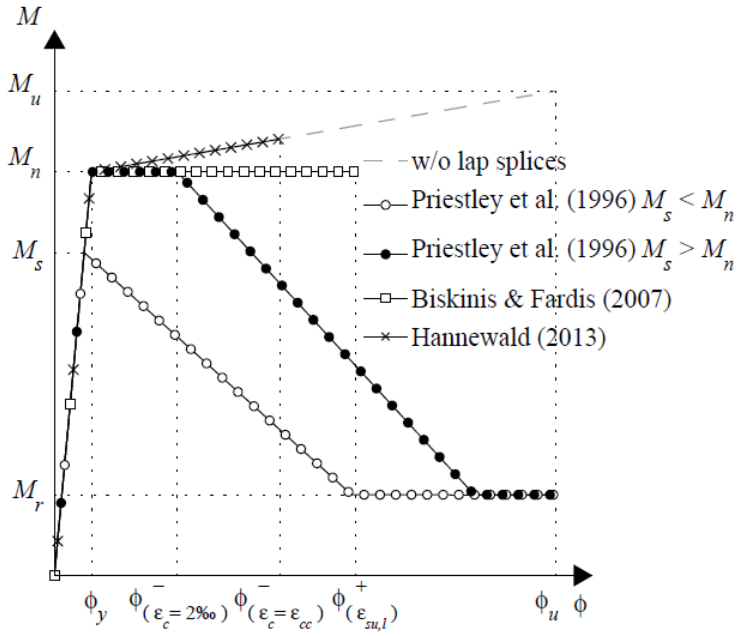

Figure 2.10: Qualitative representation of the moment-curvature relation for all the above-mentioned plastic hinge models (Tarquini, et al., 2017)

Recently, in *École Polytechnique Fédérale de Lausanne (EPFL)*, supported by a campaign in which were tested RC walls featuring lap splices, was introduced a simple equivalent uniaxial stress-strain model that claims to be capable of representing the behavior of the steel reinforcement and the bond slip mechanism present in the lap splice easily in a common finite element software. (Tarquini, et al., 2017)

Is important to note that although this model does not concern reversed loading, being only applicable for monotonic load, the former was calibrated from data on cyclic tests and so, the effect of the cyclic loading is indirectly included.

The stress-strain curve proposed can be divided in two components, first an elastic branch until the equivalent yielding point $(\varepsilon_{y,ls}, f_{y,ls})$ follow by a post-yield behavior up to an ultimate point $(\varepsilon_{u,ls}, f_{u,ls})$. The equivalent yield strain of the former $(\varepsilon_{y,ls})$ can be simply define dividing the equivalent yield stress by the Young's modulus E_s of the reinforcement steel. The equivalent yield stress $(f_{y,ls})$ is characterized by minimum value between the steel yield stress f_y and the lap splice strength f_s. The model chosen by the authors to compute the splice strength was the model from Canbay and Frosch (2005) (see sub-section 2.5.1).

The expression to identify the ultimate strain limit is

$$\varepsilon_{u,ls} = \varepsilon_{y,ls} + 0.65 \times \rho_w + 0.03 \times \frac{l_s}{L_s} \quad (2.10)$$

Where $\varepsilon_{y,ls}$ represents the equivalent yield strain, l_s the length of the outermost lap splice in tension, L_s the shear span of the member and ρ_w the confining reinforcement ratio that is defined as

$$\rho_w = \rho_x + \rho_y \quad (2.11)$$

$$\rho_x = A_{trx} \times \frac{N_l}{s_x \times b} \quad (2.12)$$

$$\rho_y = \frac{A_{try}}{s_y \times (\emptyset_L + c_{bo})} \quad (2.13)$$

Where ρ_x and ρ_y represent the reinforcement ratios in the different planes of bending, A_{trx} and A_{try} the area of the stirrups, s the spacing between them, n_{legs} the number of stirrup legs, d_{bl} the diameter of the longitudinal bars, b the section width and c_{bo} the clear face concrete cover.

Attained the value of the ultimate strain limit the authors propose to predict the equivalent ultimate stress $f_{u,ls}$ as follows:

i) If the steel yield stress f_y is bigger than the lap splice strength f_s it is assumed that the splice maintains a constant strength up to the ultimate strain limit and thus $f_{u,ls} = f_{y,ls} = f_s$;
ii) If the equivalent yield stress is governed by the value of the steel yield stress ($f_{y,ls} = f_y$) then the stress strain curve is assumed to be equal to the one of the reinforcing steel until the strain limit $\varepsilon_{u,ls}$.

It must be considered that the model does not give any information about a possible residual strength on the splices. Hence, after the strain limit $\varepsilon_{u,ls}$ the strength of the splices should be assumed as zero.

3 Experimental Test Campaign

3.1 Background

To calibrate a constitutive law that can predict the lap splice behavior, experimental data about the factors governing the lap splices performance is required.

Since building a specimen in real scale of a bridge pier is an expensive and time-consuming task it was necessary to find a solution that could allow the authors to test a relevant amount of specimens in a feasible time.

The test program was built follow up the campaign of Angeli et. al. (2013). Following the experimental campaign of Bimschas (2010) and Hannewald et al. (2013) which tested RC walls with lap splices at the bottom, Angeli et al. (2013) carried out an experimental campaign to study the behavior of lap splices under cyclic loading.

The suggested test specimen, depicted in figure 3.1, reproduces the behavior of a small corner region which will roughly correspond to the "influence zone" of a single lap splice and it will provide information about the factors controlling its behavior.

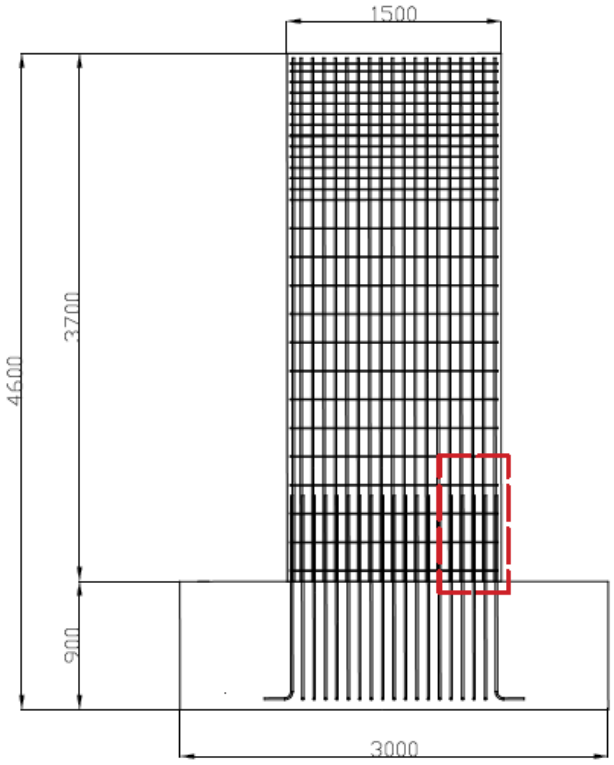

Figure 3.1: Typical wall tested by Bimschas (2010) and Hannewald et al. (2013) and representation of suggested specimen

The results of this preliminary test shown the general viability of such experimental approach but they were strongly influenced by the chosen boundary conditions. Thereby, the shape of the test specimen was adjusted, introducing RC blocks on the top and bottom of the column creating an I-shaped figure (see figure 3.2).

Furthermore, the instrumentation used on the test of Angeli et al. (2013) was also updated, increasing the number of optical measurements in a way to achieve a better understanding of the average strains on the reinforcement bars and on the concrete cover.

The main tested parameters were chosen based on the literature review on chapter 2. Naturally different parameters can play a role and therefore the casting of the test specimens will be scheduled according with the test results. Thus, after the results of the first test series the configuration of new specimens will be chosen in order to study in more detail different parameters, such as splice length and smooth rebars.

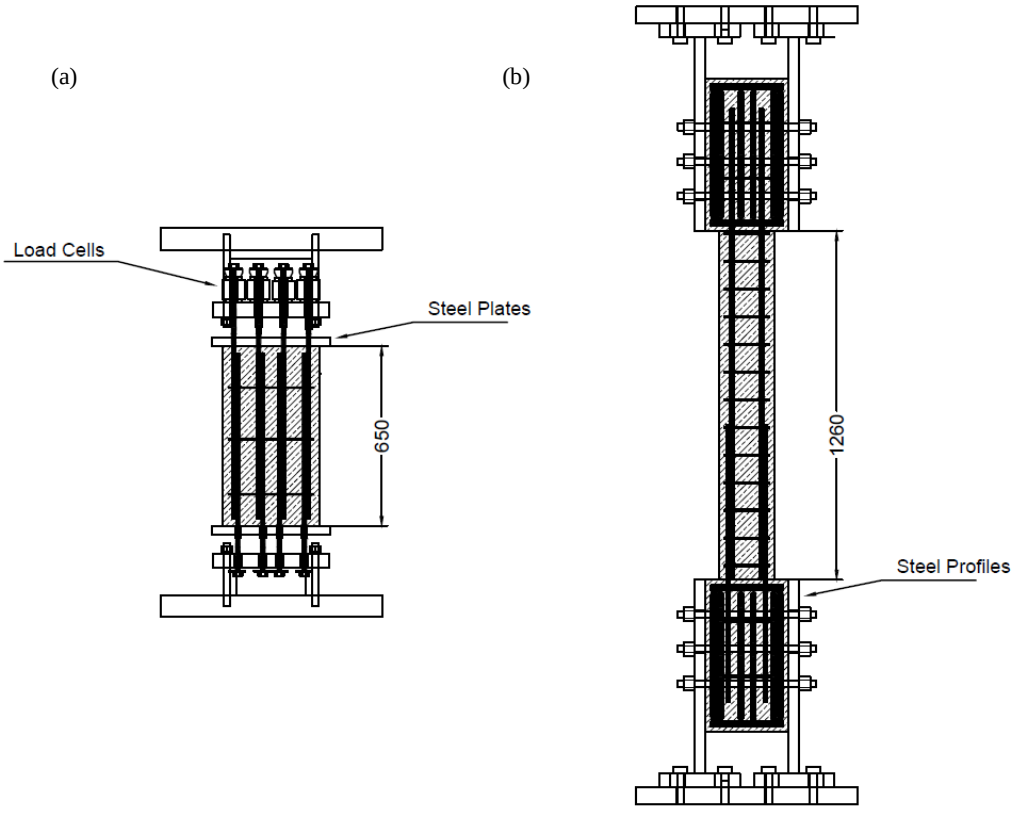

Figure 3.2: Comparison between (a) Test Setup Angeli et al. (2013) and (b) Test Setup of the author

3.2 Characteristics of the test specimens

The characteristics of each column are presented on table 3.1. The specimens' share the same dimensions, a cross section with $200 \times 200\ mm^2$and a total height of $1260\ mm$ (see figure 3.3).

For the first phase three specimens were tested. Each specimen feature two stiff RC blocks at the foundation and in the head which intend to simulate a fixed-fixed boundary conditions and this way be better representative of the real conditions on the wall. These rigid blocks have a rectangular cross section $550 \times 300mm^2$ and a total height of $550mm$.

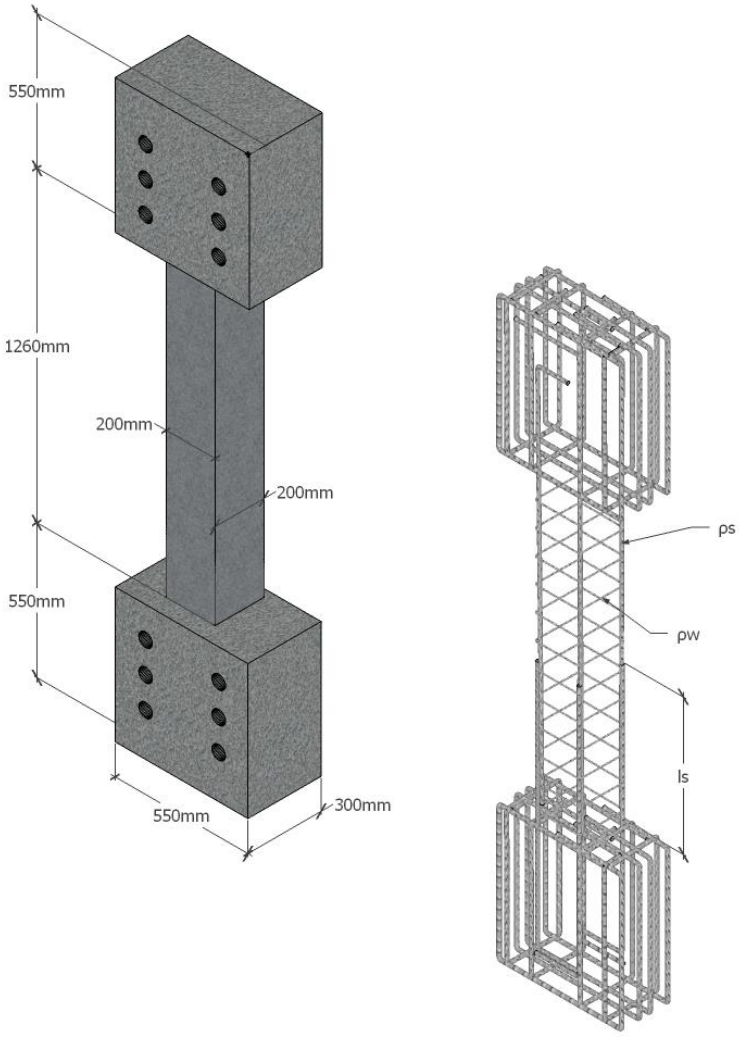

Figure 3.3: Test specimen model and its reinforcement

The first specimens were mainly focus in the influence of the transversal reinforcement. Thus, the specimens just differ with respect to the transverse reinforcement which consists on stirrups of $6mm$ diameter. Three different layouts were chosen, stirrups with $10cm$ spacing for LAP-P1, stirrups with $20cm$ and for LAP-P3 and finally $30cm$ between the stirrups on the specimen LAP-P2. This amount to a respective transversal reinforcement ratio of 0.283% 0.141% and 0.094%.

Considering the old Swiss design codes, that allowed a minimum splice length of $40\phi_L$, a splice length of $560mm$ was chosen for the longitudinal reinforcement of the test specimens LAP-P1, LAP-P2 and LAP-P3.

Table 3.1: Characteristics of Test Specimens of first test series

	LAP-P1	**LAP-P3**	**LAP-P2**
Section $(mm \times mm)$	200×200	200×200	200×200
Height (mm)	1260	1260	1260
Longitudinal Reinforcement Layout (ρ_s)	$4 \times \emptyset 14mm$	$4 \times \emptyset 14mm$	$4 \times \emptyset 14mm$
Longitudinal Reinforcement Ratio (%)	1.53	1.53	1.53
Transversal Reinforcement Layout (ρ_w)	$\emptyset 6mm//10cm$	$\emptyset 6mm//20cm$	$\emptyset 6mm//30cm$
Transversal Reinforcement Ratio (%)	0.283	0.141	0.094
Splice Length (l_s) (mm)	560	560	560

3.3 Material Proprieties

3.3.1 Concrete

A number of three concrete compression tests were carried out in cylinders specimens to determine the compression strength for the concrete used in the tested piers. Table 3.2 presents the results obtained from three cylinders with 200 cm^2 section and a height of 31.5 cm.

Table 3.2: Concrete proprieties

Material Properties	
Concrete	f'_c $[MPa]$ (First Test Series)
	31.7

3.3.2 Steel

Two different types of reinforcement were used in the tested specimens.

To determine the proprieties of the 14 mm and 6 mm diameter reinforcement six and eight different steel bars, respectively, were tested. With these tests the modulus of elasticity, the yield and ultimate strength and the yield and ultimate strain were obtained. The results are presented in table 3.3

Table 3.3: Steel proprieties

Material Properties					
Steel	f_y $[MPa]$	$f_u[MPa]$	E_s $[MPa]$	$\varepsilon_y[\%]$	$\varepsilon_u[\%]$
$\emptyset$6mm	475.0	625.0	183313	-	9.8
$\emptyset$14mm	511.3	635.4	201766.7	0.33	9.3

3.4 Load History

The existing load protocols are based in recordings from regions of high seismicity. Since the goal of this experimental campaign is to be representative of Swiss bridge population and the Swiss seismicity is assumed as moderate this can lead to overestimate damage demands.

A correct assumption of the loading history, for regions with low to moderate seismicity, will inherently result in less strength and deformation demands and hence in less expensive retrofit measures. (Mergos, et al., 2014). Therefore, this experimental campaign will consider the proposed loading protocols by Mergos et al. (2014) that limit the amount of load steps in function of seismicity, period and the number of cycles per step.

The total amount of loads step is typically

$$\eta_{total} = \eta \times n_i \qquad (3.1)$$

Where η represent the number of load steps and η_i represents the number of cycles per step.

This adaption of the loading protocol will increase the approximation of the test results with the real behavior of bridge piers in Switzerland when subjected to seismic action and hence lead to more accurate results.

To anticipate the behavior of the specimens was made a simple numerical model with the commercial software SeismoStruct. The model, with continuous reinforcement along its height, was loaded with incremental displacement until failure. The results represented in figure 3.4 were considered in the loading protocol.

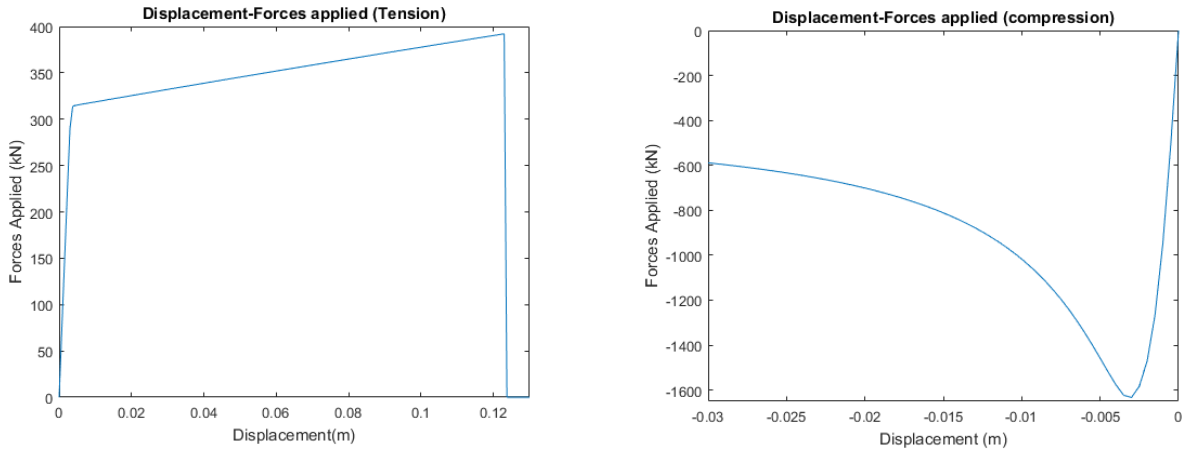

(a) (b)

Figure 3.4: Force-displacement (a) tension and (b) compression

The loading protocol consisted in two alternate cycles, compression and tension, at the same value of displacement. When two cycles in tension and two cycles in compression were completed the applied displacement increased.

The applied displacement was increased progressively along the test for both compression and tension. The levels of displacement were based on strains measured near the base for the walls tested by Bimschas (2010) and Hannewald et al. (2013).

Since the horizontal load in the abovementioned specimens led to different levels of compression and tension strains at the base of the walls a compression-tension proportion is required to define the displacement applied levels of the proposed test.

The proportion compression-tension chosen was constant throughout all cycles being the compression displacement 10% of the displacement applied in tension. This proportion value was taken from the relation between the compressive and tensile strains near the base at failure of the abovementioned walls.

In figure 3.5 is presented the loading history graph. The quasi-static test began with a cycle to 1 mm and 0.1 mm in tension and compression respectively and it was increased to 2 mm-0.2 mm and then to 3 mm-0.3 mm. After the displacement was increased 3 mm at the time.

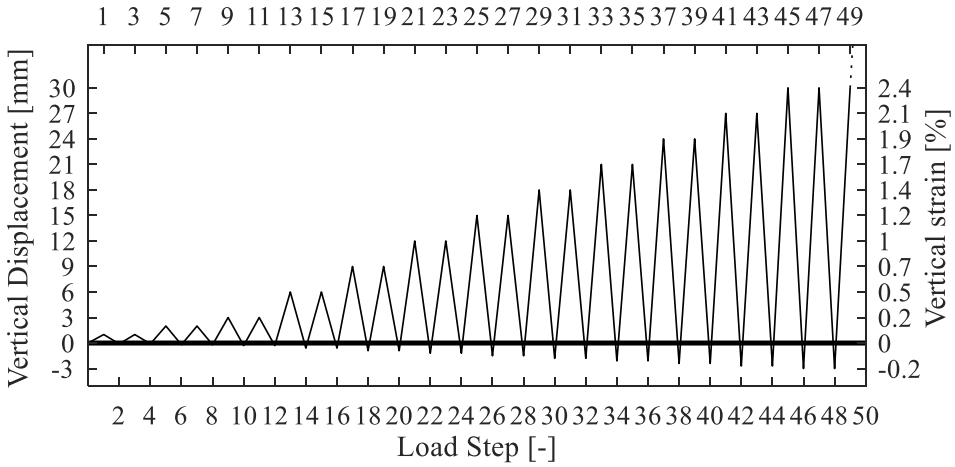

Figure 3.5: Loading history Graph

3.5 Test Setup and Instrumentation

In figure 3.6 is shown the test setup used on this experimental campaign. Before placing the specimens in the machine each specimen was painted and instrumented.

Since one of the aims of this campaign is to describe the progressive increasing of the cracks and the evolution of their widths the correct painting of the specimens has a particular importance.

When the load is low, the cracks will in correspondence have a smaller width and size. This means that, due to the elastic behavior of commercial paints, the former can cover the concrete and hide the small cracks of the specimen. Therefore, a white paint that does not feature this type of performance it was adopted.

To have the correct boundary conditions the RC blocks in the head and in the foundation of each specimen needed to be attached to the actuator and to the bottom of the engine respectively. To make this connection were chosen four T-shaped steel profiles that were clamped at each specimen and which in turn were connected to the press.

At first, the steel profiles were connected to the actuator. Knowing that the specimen will be subjected only to axial load the perpendicularity of the steel profiles had a particular importance since these would affect directly the perpendicularity of the tested piers. An imperfection in the verticality of the specimens can origin moments which could lead to an unrealistic response of the pier. To measure the verticality of the steel profiles vertical lasers and manual inclinometers were used.

When guaranteed the verticality, the steel profiles were connected to the actuator on the top and to the bottom through 8 bolts per each profile which makes up a total of 32 bolts. The bolts used in this link had all the same proprieties, a property class of 10.9 and a diameter of $24\ mm$. Each bolt was pre-stressed posteriorly to $350\ Nm$.

Completed the preparation works, the specimens were erected and placed between the two steel plates on the top and on the foundation. In order to guarantee a correct perpendicularity, the piers were aligned through stiff steel plates under the foundation. These allows ensuring a support on the bottom which is particularly important before the final pre-stress between the steel plates and the test experiment be applied.

The final phase for the test setup was the correct linkage between the steel plates and the RC blocs on the specimen. As observed on the figure 3.6, 12 horizontal openings per pier were left to allow the pathway of the same amount of pre-stressed bars to facilitate the link between the steel profiles.

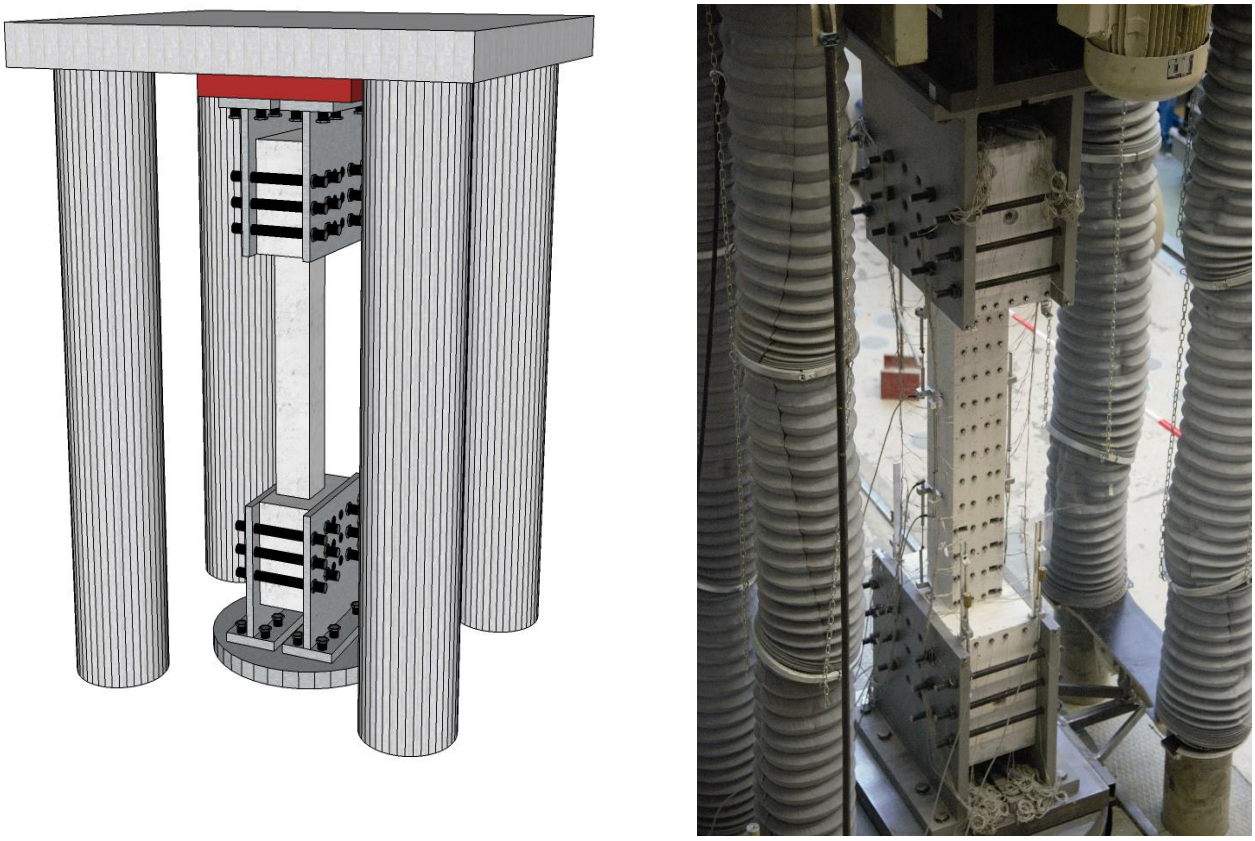

Figure 3.6: Test setup 3D view

Before the application of the pre-stress it was important to establish a correct surface to transfer the forces. The steel profiles should have a correct bond to the concrete blocks in order to avoid any peak stresses resulting from the pre-stressed forces. Therefore, small steel plates were used on the interface between the steel plate and the concrete to ensure a more uniform transfer of the stresses between the two elements. At last, the pre-stress of $937\ Nm$ was applied throughout twelve $d24$ rods and the steel plates under the foundation were removed.

The vertical loading was applied in deformation control. A hydraulic actuator with $\pm 2000\ kN$ capacity force was used. The actuator features four load cells that were used to measure the actives forces in the test specimen during the test.

Although the vertical actuator was equipped with a displacement transducer, to double check the displacement rate four LVDT's were used tho measure the displacement between the RC block on the head and the block on the foundation. The displacement applied to the specimen was given by the average of the four gages.

The instrumentation of the specimens is presented in figure 3.7. During the test, the data relatively to the displacements in the column was collected through strain gages, LVDTs and light emitting diodes (LEDs).

76 LEDs were used in each side of the column which corresponds to a total of 152 per specimen. The LEDs were glued along a regular pattern on the concrete of 13 rows and 4 columns per side.

In the tested specimens, small holes were left on the concrete. LEDs were glued directly in each longitudinal bar which will allow to measure the slip between the two rebars.

Furthermore, additional LEDs were placed in the two RC blocks, top and bottom, and on the four steel profiles of the test setup.

To measure the strains in different regions on the concrete surface three LVDTs in each side of the specimen were used. The LVDTs were located along the entire height of the column and its position was chosen according with the expected behavior of the test specimen.

Since the strain gages are glued directly in the concrete, the formation of cracks can damage the measure system. Therefore, the LVDTs were placed where cracks are less likely to develop, i.e., between the transversal reinforcement and distant from the top of the spliced zone.

Moreover, as the zone were largest strains are expected is located near the spliced length, two gages were placed in this zone to have a better understanding of its displacement. Thus, the LVDTs were set at a distance of $200\ mm, 660\ mm\ and\ 1260\ mm$ corresponding to L1, L2 and L3 respectively.

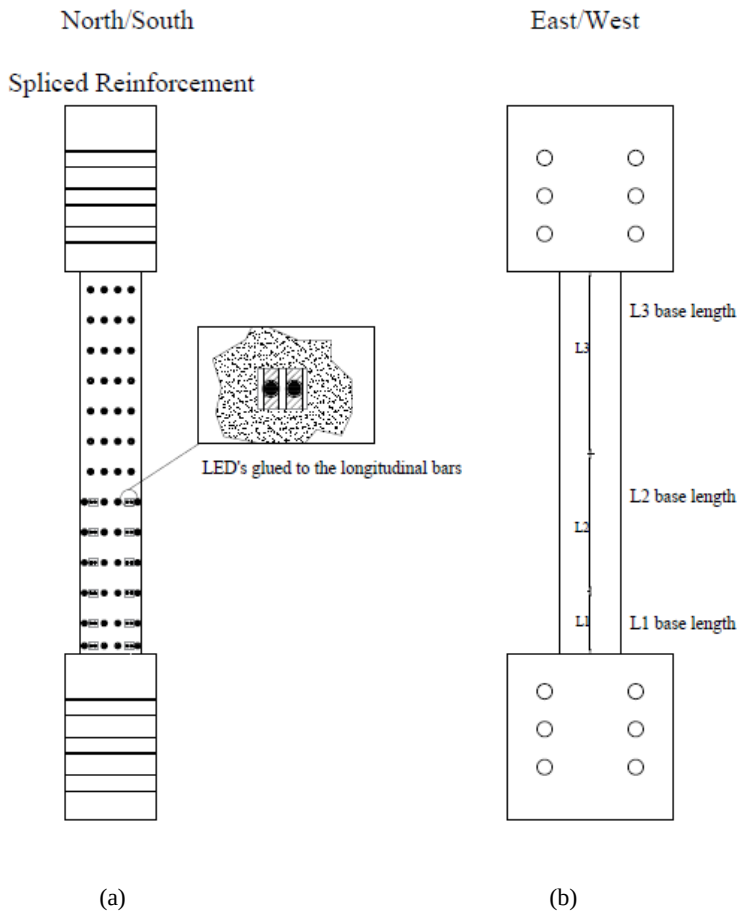

Figure 3.7: Instrumentation, (a) LEDs pattern and (b) LVDTs base length

3.6 Test Observations

3.6.1 LAP-P1

The specimen LAP-P1 features a lap splice length of 560 mm and stirrups spaced of 10 cm.

At the first tension cycle the first cracks appear. The formers mainly appear with a placement similar to stirrups, every 10 cm. The formation of the cracks was regular and equivalent on the four sides of the test specimens but its development was not complete. The maximum crack width had a value of 0.1 mm and it was concentrated on the end of the splice.

On the next loading cycle, at 3 mm, a change in the crack pattern occurred. Until this cycle the crack with the more pronounced width was the one on the south side at the end of the lap splice but after the applied displacement the crack on the bottom of the column also reached the same width than the one on the end of the splice. Both the cracks had a width of 0.5 mm. At the second load step, the crack maintain the same width but the crack on the bottom propagate up to the holes made on the concrete to glue the LED's in the longitudinal reinforcement.

During the cycle to 6 mm the yielding of the rebars was reached. It should be notice that at the end of the cycle some small vertical splitting cracks were now visible on the North and South sides between the bottom two holes. Although no relevant new horizontal cracks were formed, the smaller cracks on the past cycle had a relevant expansion of their width. However, the biggest cracks were still found at the end of the splice and on the bottom of the specimen in the south side with a width of 0.9 mm. The north side has a clear difference on the width of the cracks being the biggest one the one on the splice end but with only 0.6 mm width. (See figure 3.9 (a))

Reaching the displacement of 9 mm it was clear the changings on the behavior of the specimen. First the cracks outside the lap splice zone were opened almost uniformly, i.e., with approximately the same width of 0.8/0.9 mm for all, while the cracks within the splice were almost closed with a narrow value in the order of 0.1 mm. Then the crack at the end of the splice at the south side wasn't clearly the biggest anymore, but instead this crack can be comparable with the other cracks above it. Finally, the East Side reveal the biggest crack of the specimen, the former is located at its bottom and had a width value of 1.4 mm.

At the second step of tension at the same cycle of loading a new vertical splitting crack have developed. The former is located at the south side between the two holes close to the end of the splice. Furthermore, the base crack opened more achieving a width of 1.4 mm.

Addressing now the first cycle at 12 mm in tension. Cracks widened and a few vertical splitting cracks appeared joining the holes. However, the crack at the base is still the biggest one with 2.5 mm the one at the splice end region has now an important value of 2 mm. At the remaining step loads at this cycle no measurable new damage take place.

The formation of vertical splitting cracks was evident on the end of the first load cycle at 15 mm tension. They are now appearing on the East side where no holes are presented and with affluence in the region of the splice end at the south part. The width of the biggest cracks looks not have changed much ranging from

2.5 at the splice top and 3/3.5 mm at the base. At the second step of the same tension cyclic it was possible to see a propagation of the splitting cracks to the North part on the East Side.

The following cycle, 18 mm, shown an important increase of the width of the crack at the splice end region. Although the biggest crack is still the one at the base with 4 mm width, particularly on the southeast corner, the horizontal crack located at the splice end open significantly to a value of 3.5 mm. Some cracks above the splice length also reveal an expansion following different paths while the cracks at the lap splice zone are still smaller and with a little importance relatively to the other remaining cracks.

During the remaining compression and tension steps at the same cycle, the splitting cracks increased and became even more evident especially at the southeast part with the formation of new cracks and with the increasing of the old ones.

On the next cycle, the specimen demonstrate clear signs of damage. When reached the displacement of 21 mm in tension the specimen shown vertical cracks going all the way through the lap splice length in the east side and the crack width at the end of the splice reached an impressive value of 4 mm while on the base the column a bigger width of 5 mm is visible. The test specimen when loaded in compression have decreased its compression resistance and thus its compression stiffness. (Figure 3.9 (b))

Through the increasing of the displacement to 24 mm in tension the specimen has unequivocally gave signs of imminent failure. The first cycle to tension shown an evident slip of the bars on the southeast edge and an increasing of the crack width on the region at the end of the splice to a value of 5 mm. Slipping was also evident on the longitudinal reinforcement in the Northeast region. (Figure 3.9 (c))

Proceeding with the compression displacement, the slip on the rebars of the Southeast part were even more evident on the end of this cycle. The slip between the two rebars were clearly visible by eye from the position of the LED's in the order of a few millimeters. It was also possible to see the plateau of the vertical force, i.e., clear increase of the displacement while the force applied maintain its value.

When subjected to the second cycle of tension at 24 mm the specimen failed without even reaching the maximum tension point revealing a huge crack on the top of the splice end.

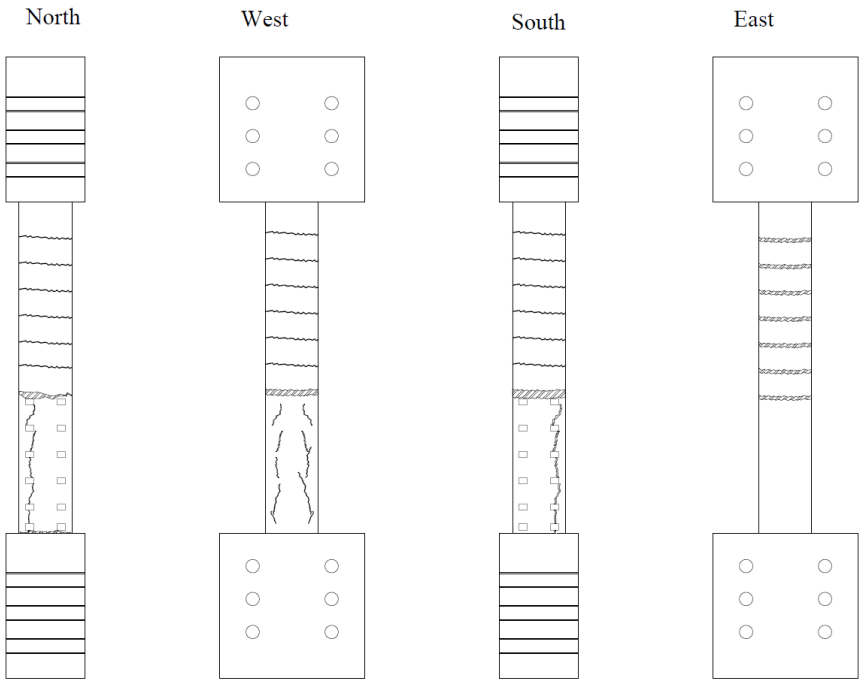

Figure 3.8: Sketches of Lap-P1 after failure

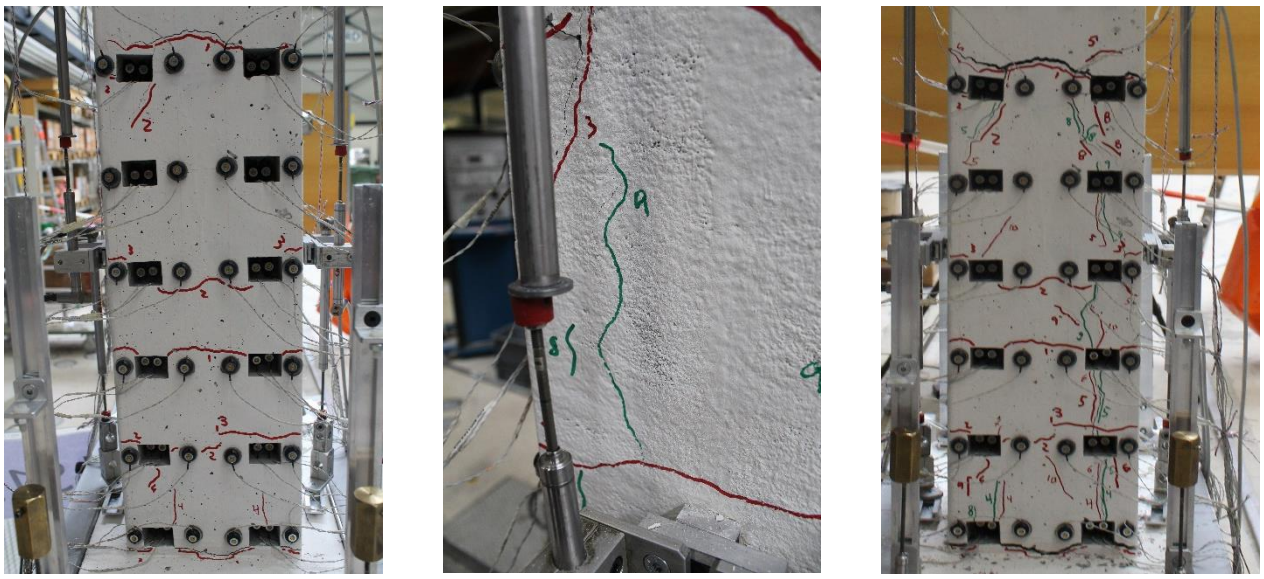

(a) (b) (c)

Figure 3.9: Pictures at different load levels Lap-P1; (a) Vertical splitting cracks that appear when achieved the yielding of rebars; (b) Splitting cracks along the length of the splice; (c) Last cycle before failure

3.6.2 LAP-P3

This specimen contains the medium transversal reinforcement ratio from the amount of specimens tested. After the first cycle to 1 mm in tension 5 cracks opened along the specimen length and one more at the base. The spacing of the cracks is not uniform along the entire specimen, above the splice is clear the formation of cracks spaced of 20 cm but then is possible to see another crack at the splice end that breaks the regularity of the spacing. Within the lap splice zone there was only a small crack. Apart from the cracks inside the lap splice region, the remaining cracks feature approximately the same width, 0.1 mm. When loaded again to the same cycle value of displacement a few new cracks appear and the existing ones developed and opened to a value of 0.15 mm.

Increasing the imposed displacement to 2 mm, several new cracks develop and in Southeast region some vertical splitting cracks were visible at the top and bottom of the spliced region. It was also possible to see a growth of the width of the old cracks to 0.2 mm on lap splice end and to 0.3 mm to the bottom. (figure 3.11 (a))

At the first cycle to 3 mm a few new horizontal cracks were seen. The specimen shown also some vertical splitting cracks in the north side close to the top and bottom of the splice extremities. Regarding to the cracks width this seemed to be equal outside of the splice region with 0.3/0.35 mm.

At the cycle to 6 mm the yielding force of the rebars was attained. New splitting cracks were visible along the entire length of the lap splice. The cracks at the splice end was clearly the biggest with w = 1.2 mm while above the splice the cracks had w = 0.9 mm.

During the first cycle to the new load step of 9 mm the first drop of force about 10 % was seen. A significant splitting crack developed in the Northeast side and a manifest slippage between the two longitudinal bars was visible see figure 3.11 (b). The crack at the end of the splice increased vertiginously to the value of 5 mm while. The damage caused by the horizontal cracks were not uniformly distributed along the specimen, at the West side and above the splice zone it was possible to see 5 cracks with a width of 1.2 mm while in the East side, side where the rebars slip, were only 4 cracks above the lap splice. At the second cycle in tension at the same amplitude of displacement no drop of force was registered and it was only seen the widened of the horizontal cracks.

When increased the displacement to 12 mm in tension two more lap splices failed with the same behavior, splitting cracks along the entire height. (See figure 3.11 (c))

Following this, the specimen was loaded in tension until the failure of the remaining lap splice. The last lap splice just failed by slippage around 19 mm of displacement in tension.

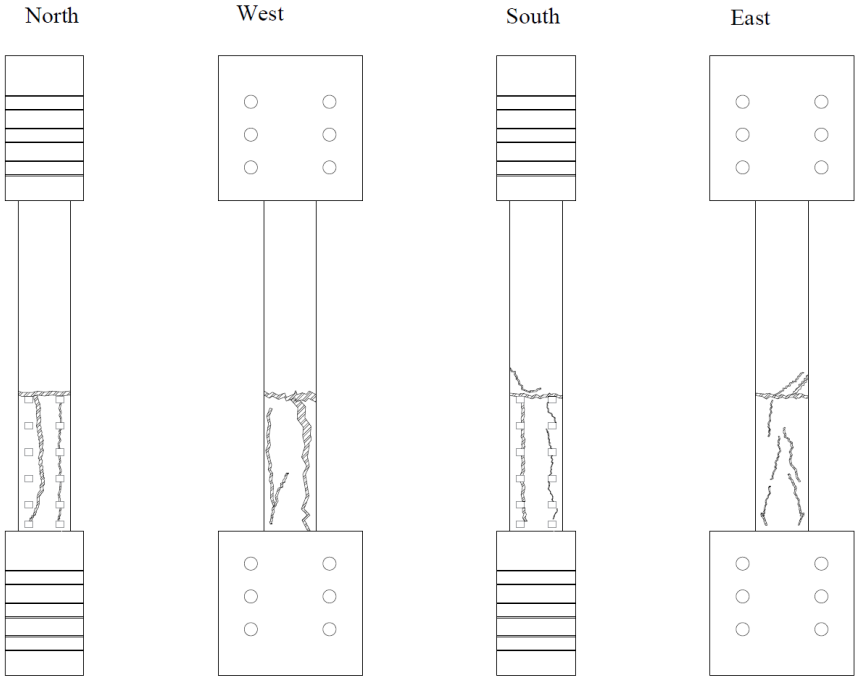

Figure 3.10: Sketches of Lap-P3 after failure

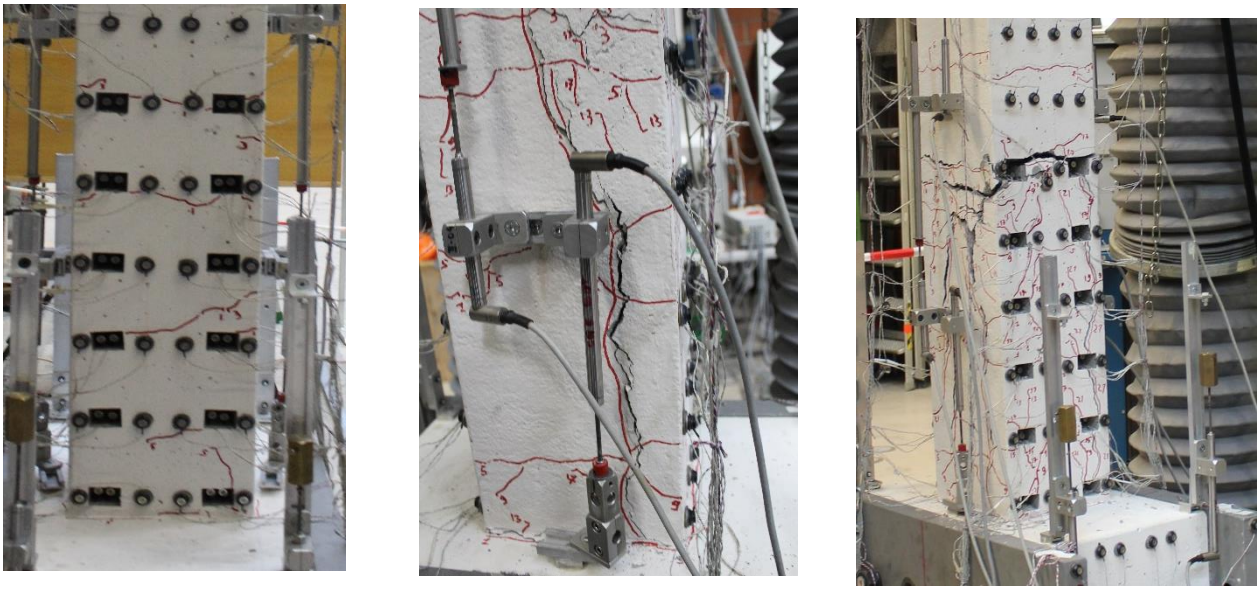

(a) (b) (c)

Figure 3.11: Pictures at different load steps Lap-P2; (a) Small vertical splitting at 2 mm of displacement; (b) Splitting cracks at the Northeast side; (c) Picture at the end of the cycle to 12 mm of displacement

3.6.3 LAP-P2

Taken into account that this specimen is the one with the lowest transversal reinforcement ratio it is expected a quicker and more sudden failure. Similarly with the previously specimen, by the end of the first tension cycle at 1 mm cracks open at the pattern similar to the one adopted for the colocation of the stirrups along the column height. Thus, a total of 6 to 7 cracks per side were formed spaced of 20/30 cm. The biggest crack was located above the splice and it had a width of 0.1 mm. At the second step of the same load cycle a few small new cracks were formed.

The first cycle in tension to 3 mm a number of new cracks opened, by this time the spacing was quite uniform and around 20 cm. Differently from the first specimen, this specimen had the particularly that its biggest cracks developed above the splice end with a width of 0.25 while the crack at the splice end has a value of 0.15 mm. In the region inside the splice the cracks are still considerably smaller (w=0.05 mm). On this cycle, it was even possible to see a tiny vertical crack at the south side on the top of the splice.

When loaded again to tension at the same amplitude of displacement it was possible to see a development of the existing horizontal cracks being still the biggest the ones above the splice end with w = 0.35 mm. By the end of the second tension step it was clear the increasing of the splitting vertical crack both in length and in width. (See figure 3.13 (a))

During the first cycle to 6 mm and reaching the yielding of the rebars the force started to decrease suddenly, a evident slippage of the longitudinal bars on the west side, mainly on the south, which lead to a decrease of force around 30/35 %. Unexpected vertical splitting cracks appear on the west side with a substantial width value of at least 3 mm. The biggest horizontal cracks are now unequivocally located on the end of the splice and at its base with a width of 1.5 mm. (Figure 3.13 (b))

Moving on to the comprehensive first step of this cycle the failure was evident with the clear opening of the splitting cracks apart from decreasing of the width of the horizontal ones. Finally, the specimen was load in tension until failure of the remaining spliced bars. (Figure 3.13 (c))

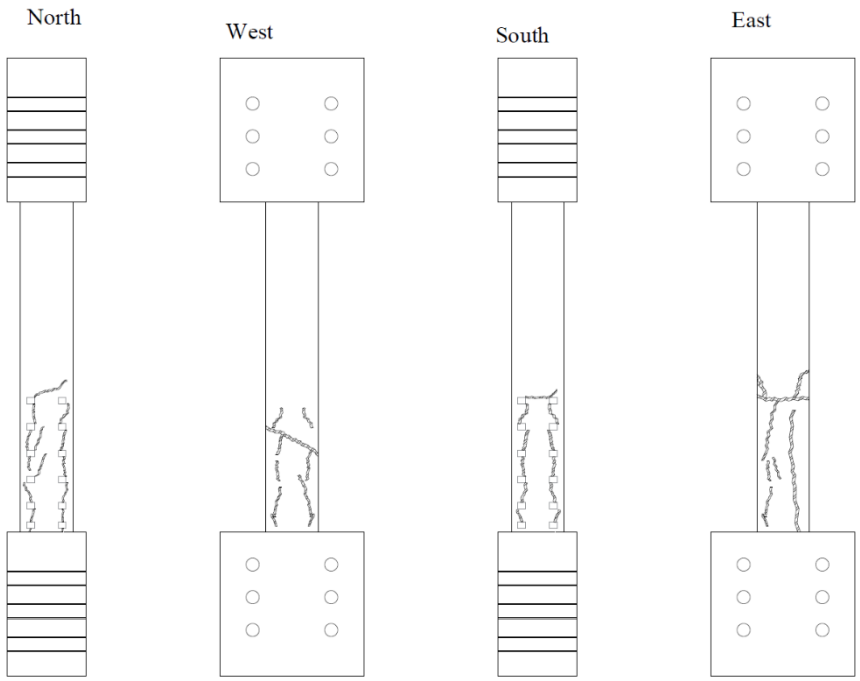

Figure 3.12: Sketches of LAP-P2 after failure

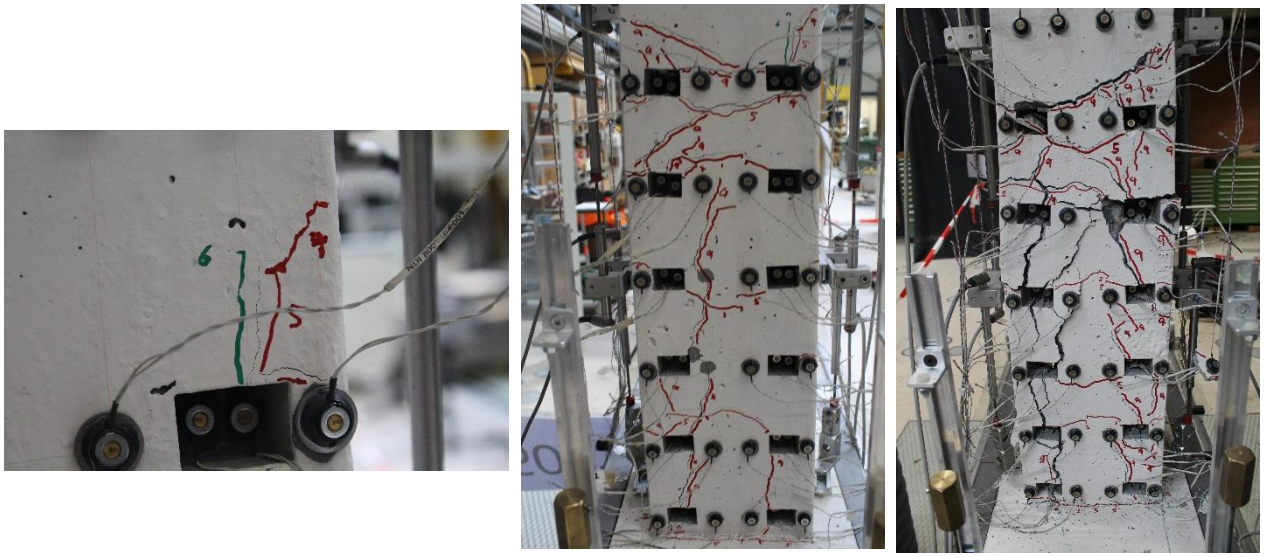

(a) (b) (c)

Figure 3.13: Pictures at different load levels Lap-P3; (a) Vertical Splitting cracks near top splice; (b) Failure of the first lap splice at the first cycle to 6 mm; (c) Failure of the remaining lap splices trough vertical splitting cracks

3.7 Test Results

In the following sub-section are presented the results from the tested specimens. The results focus mainly on the strains and displacements of the specimen along the different load steps.

The force-displacement relation of the three specimens as well as the comparison between each specimen are presented in figure 3.14. In figure 3.14 (d) are present two different types of markers for each specimen, the green square marker represents the maximum tensile strength while the blue circular marker highlights the maximum compressive force applied to each specimen.

As expected, both strength and strain increase with the increasing of the transversal reinforcement. While the specimens LAP P2 and LAP P3 failed soon after yielding, corresponding to tensile strengths slightly superiors than $320\ kN$, the specimen with the biggest amount of transversal reinforcement reached a tensile force around $360\ kN$ before failing. All the specimens' failed at values of strength below the ultimate tensile force of the steel. (See figure 3.15(a))

More evident than the influence of stirrups in the ultimate strength of the specimen is the impact in its ductility. LAP P1 reached a vertical displacement five times bigger than the specimen with half of its transversal reinforcement (LAP P3) at the peak strength. However, the displacement capacity does not increase linearly with the increasing of the transversal reinforcement. The vertical displacement for LAP P3, which had stirrups every 20 cm, was just 50% bigger than LAP P2 which had stirrups spaced of 30 cm.

Figure 3.15 (b) represent the average ultimate strain for each specimen in the lap splice zone.

Although all specimens featured failure related to lap splices, the strains at that zone at the peak tensile strength are rather different for each specimen. While LAP P2 didn't reach $0.4\ \%$ of strain in the splice region and LAP P3 just 0.5%, LAP P1 was able to sustain an average strain in the lap splice region of 1.4%.

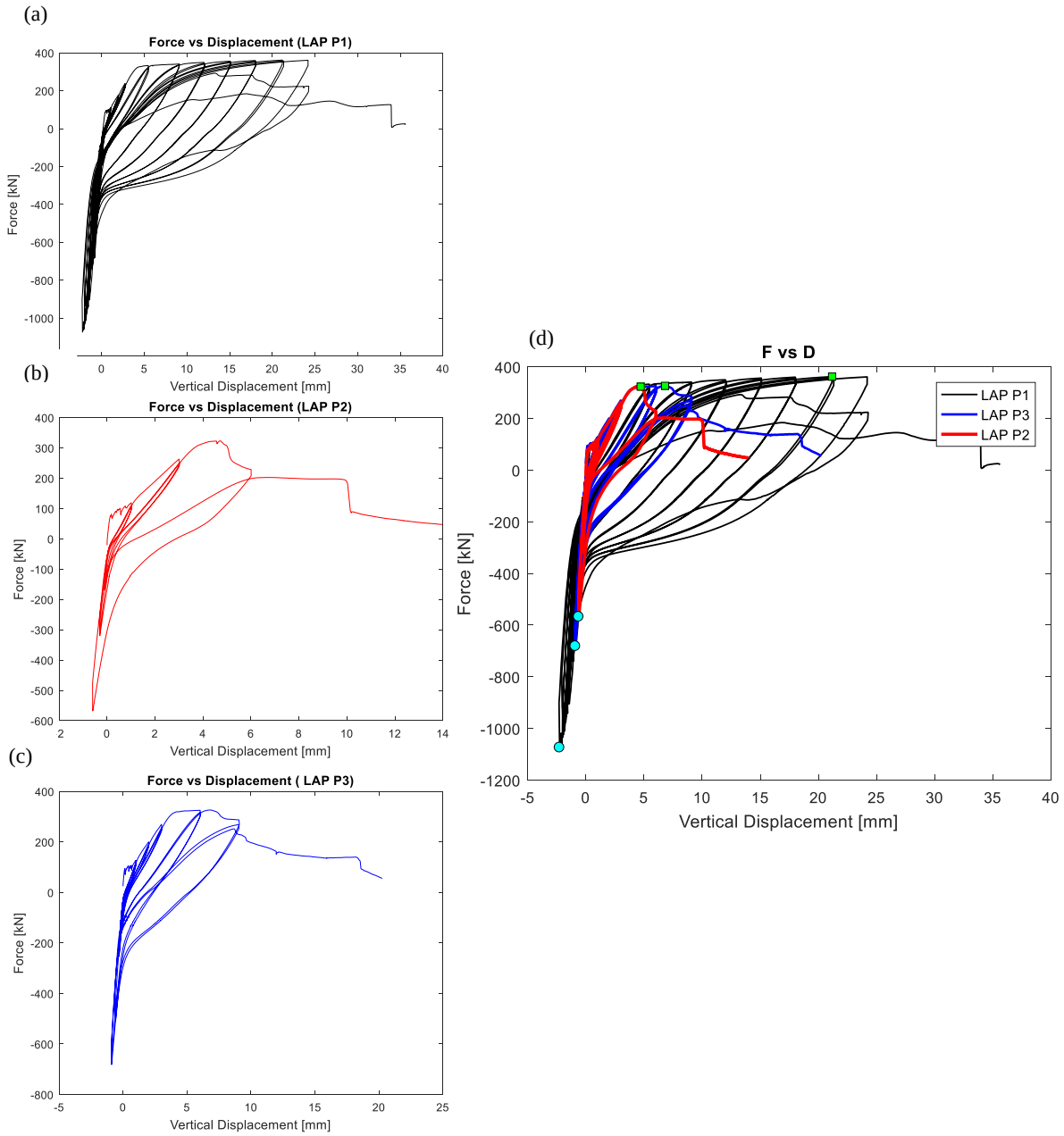

Figure 3.14: Force Displacement Relation in (a) LAP P1, (b) LAP P2, (c) LAP P3 and (d) comparison between the three

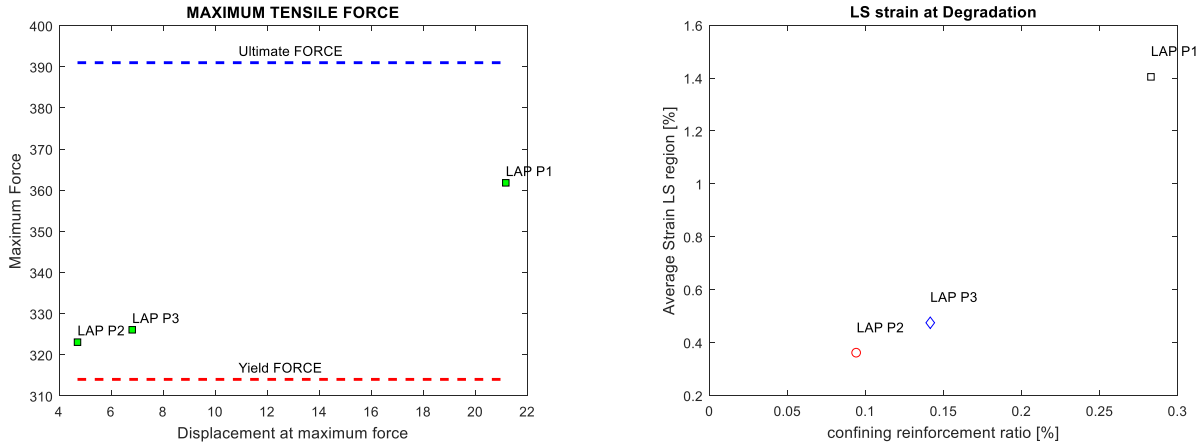

(a) (b)

Figure 3.15: Maximum values of (a) Strength and (b) Strain for each specimen

To compare the behavior between the different test specimens the results at the same load steps for each will be presented. To first load step presented will be the displacement until 3 mm in tension. This intend to show the similarities and differences between the three specimens at a beginning level of displacement.

After, the results at the load step after yielding are showed for the three specimens. Additionally, and since the specimen with less transversal reinforcement (LAP P2) failed at this load step, the results immediately before the failing will be presented, i.e., the results at the peak strength of the specimen.

Similarly, the same procedure will be applied at the next load step. The specimen LAP P3 failed at the first cycle to 9 mm. Hence, and like in the case abovementioned, will be presented the results at the peak strength for this specimen and the results for LAP P1 and LAP P3 at the end of the cycle.

Finally, the results at failure of the specimen with more transversal reinforcement will be presented. The specimen exhibited the peak strength in the end of the first cycle to 21 mm. The strength of the specimen decreased progressively been the failure presented just during the second cycle to 24 mm. Thus, the results when the specimen presented a 0.80% of the peak strength will be presented.

3.7.1 Load Step to $\Delta = 3$ mm

LAP P1

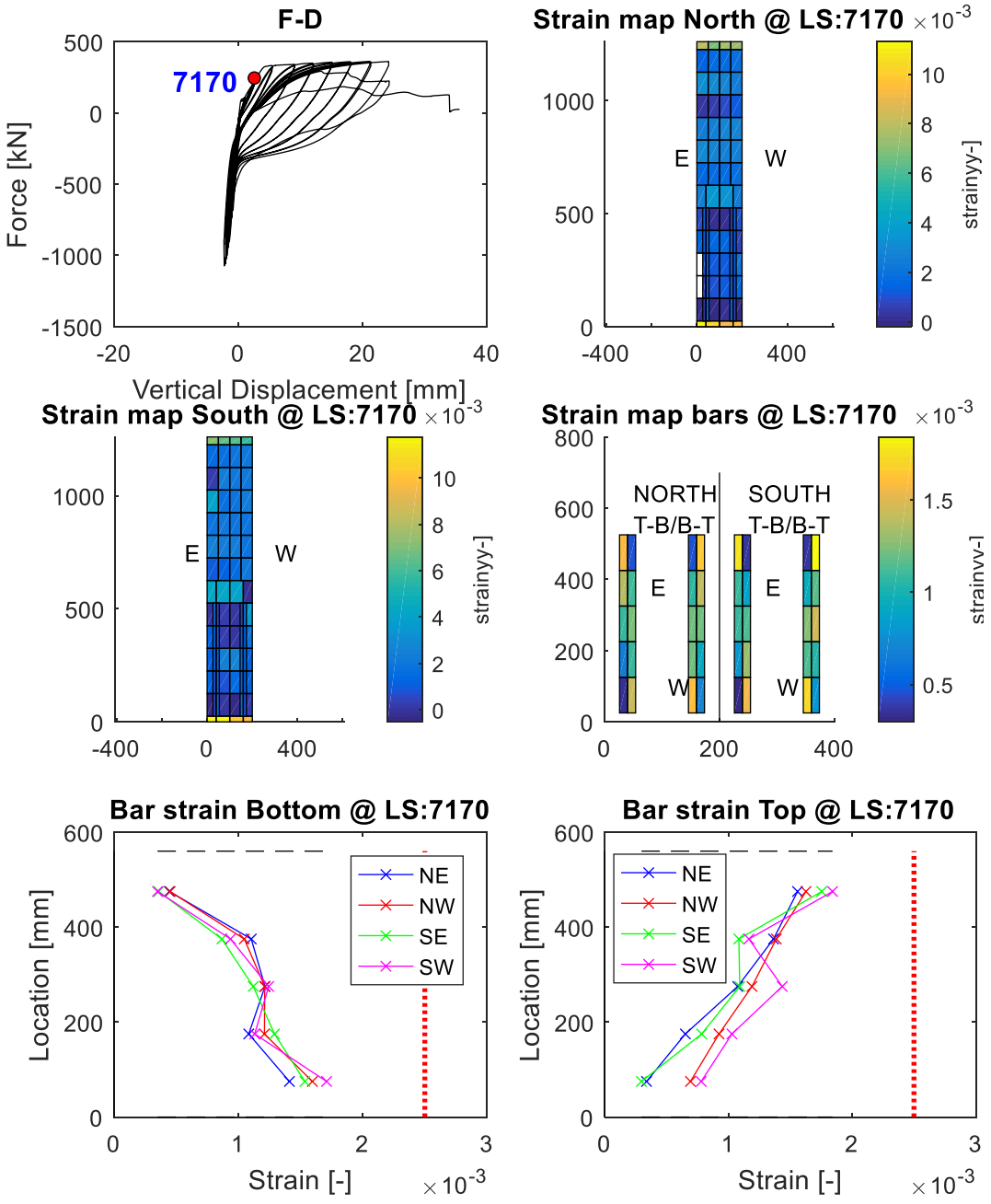

Figure 3.16: Strains of Lap P1 after load step to 3 mm

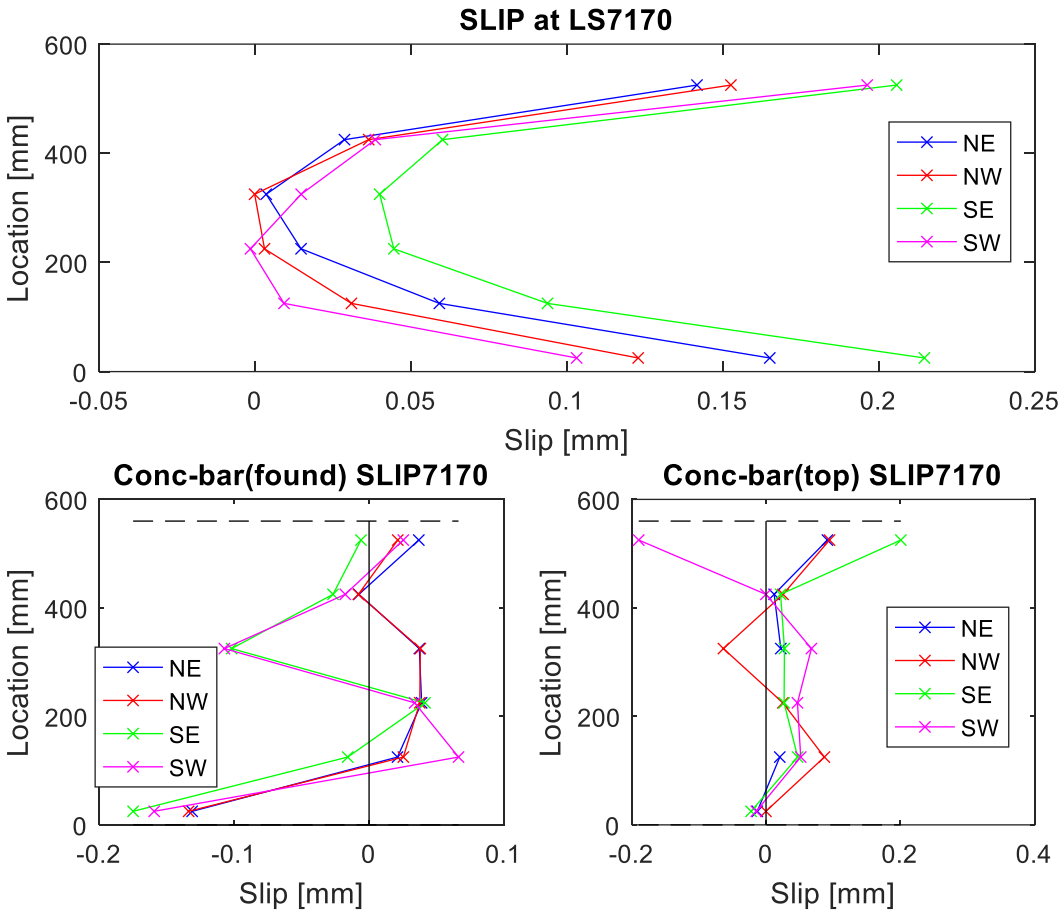

Figure 3.17: Slip LAP P1 after load step to 3 mm

LAP P2

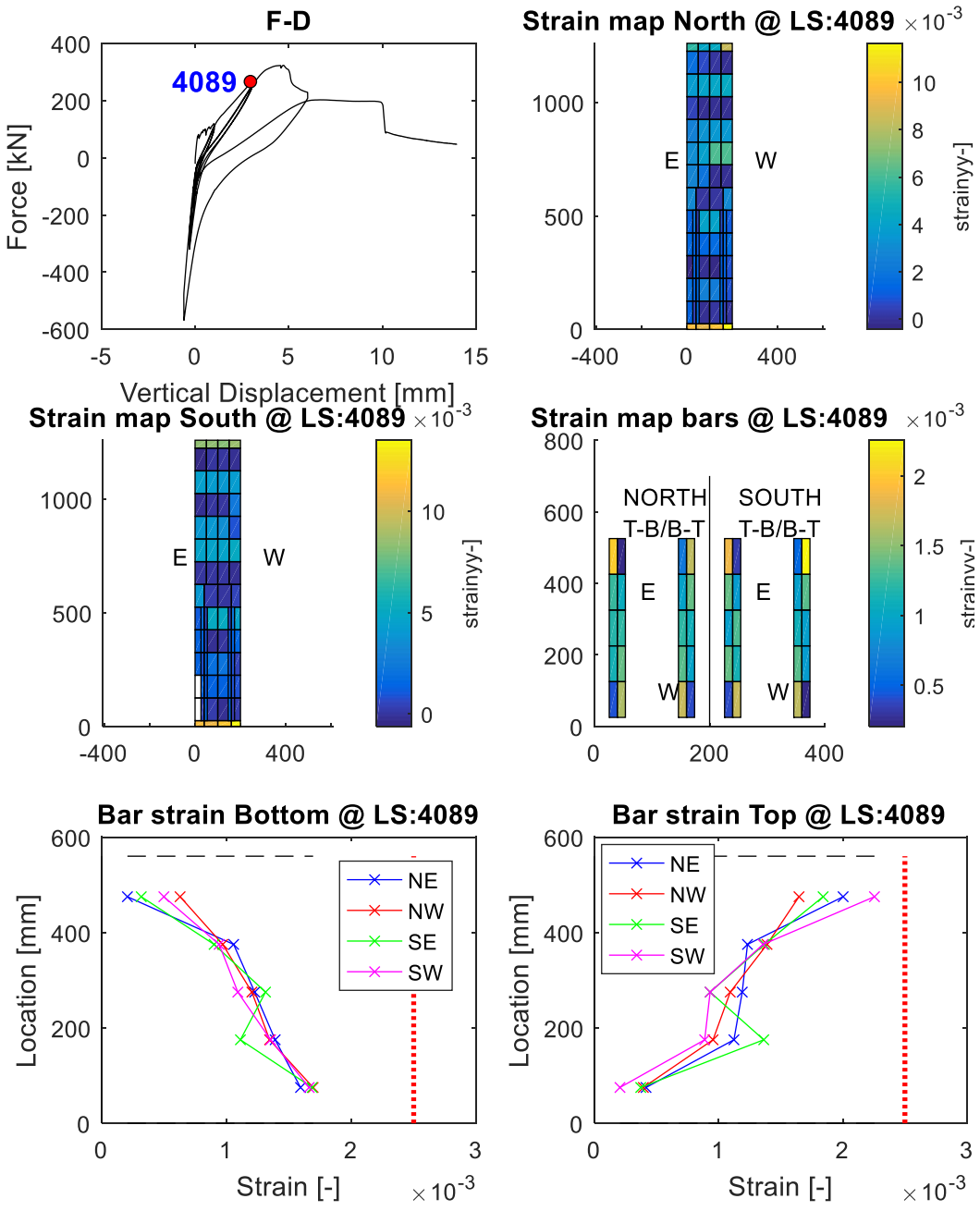

Figure 3.18: Strains LAP P2 after load step to 3 mm

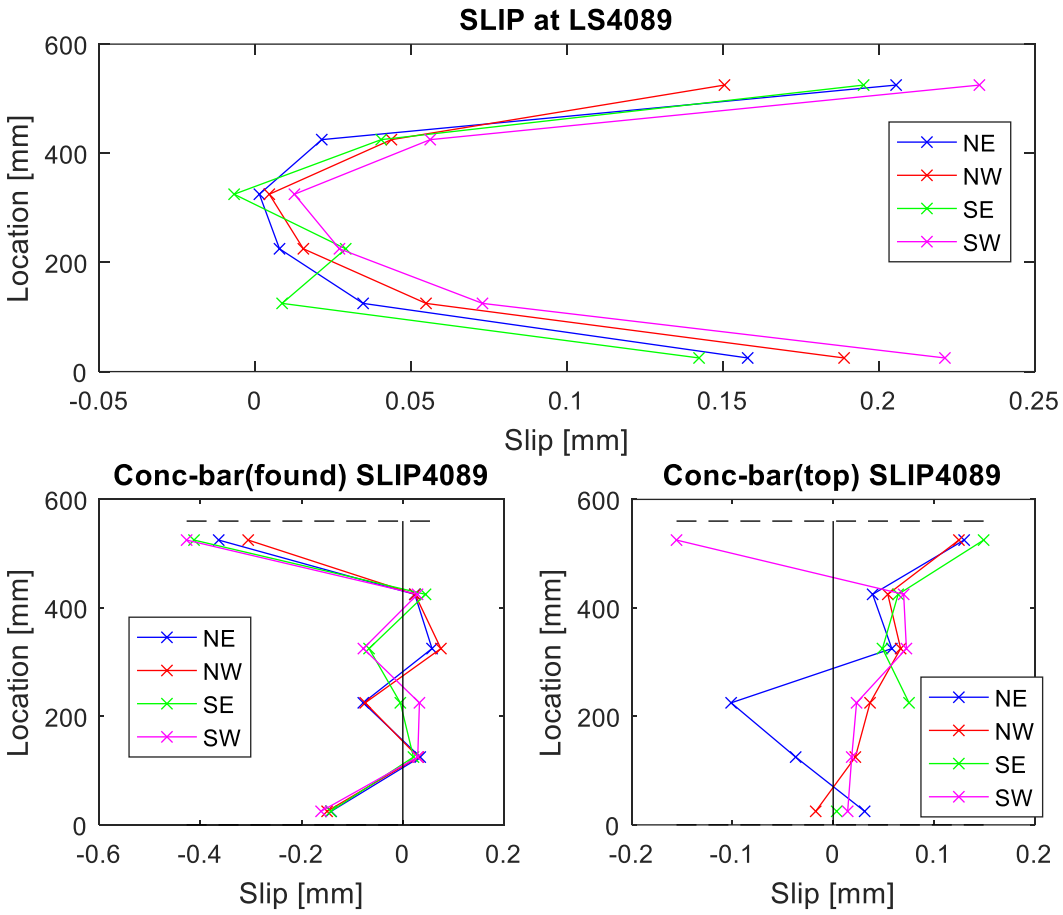

Figure 3.19: Slip LAP P2 after load step to 3 mm

LAP P3

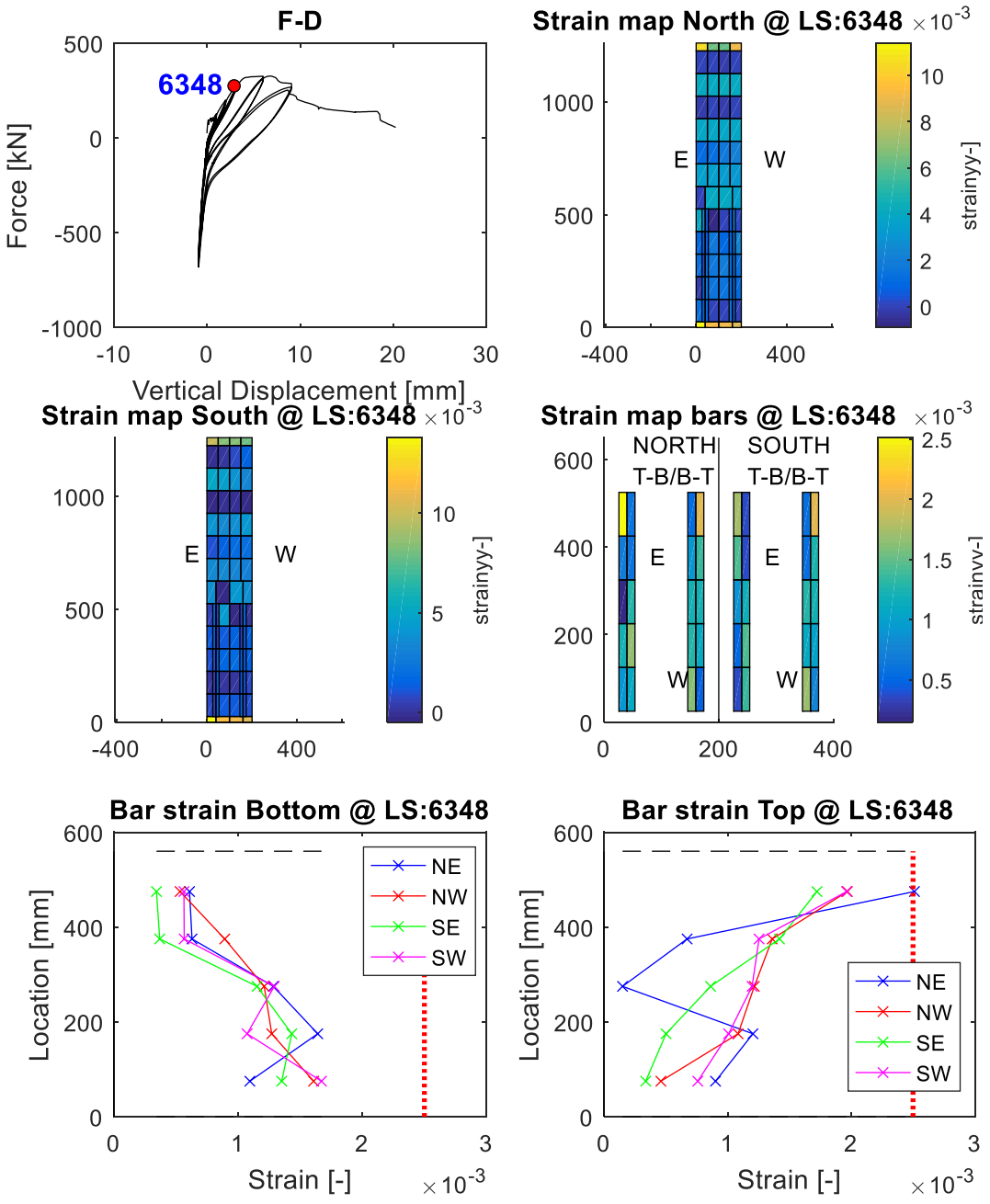

Figure 3.20: Strains LAP P3 after load step to 3 mm

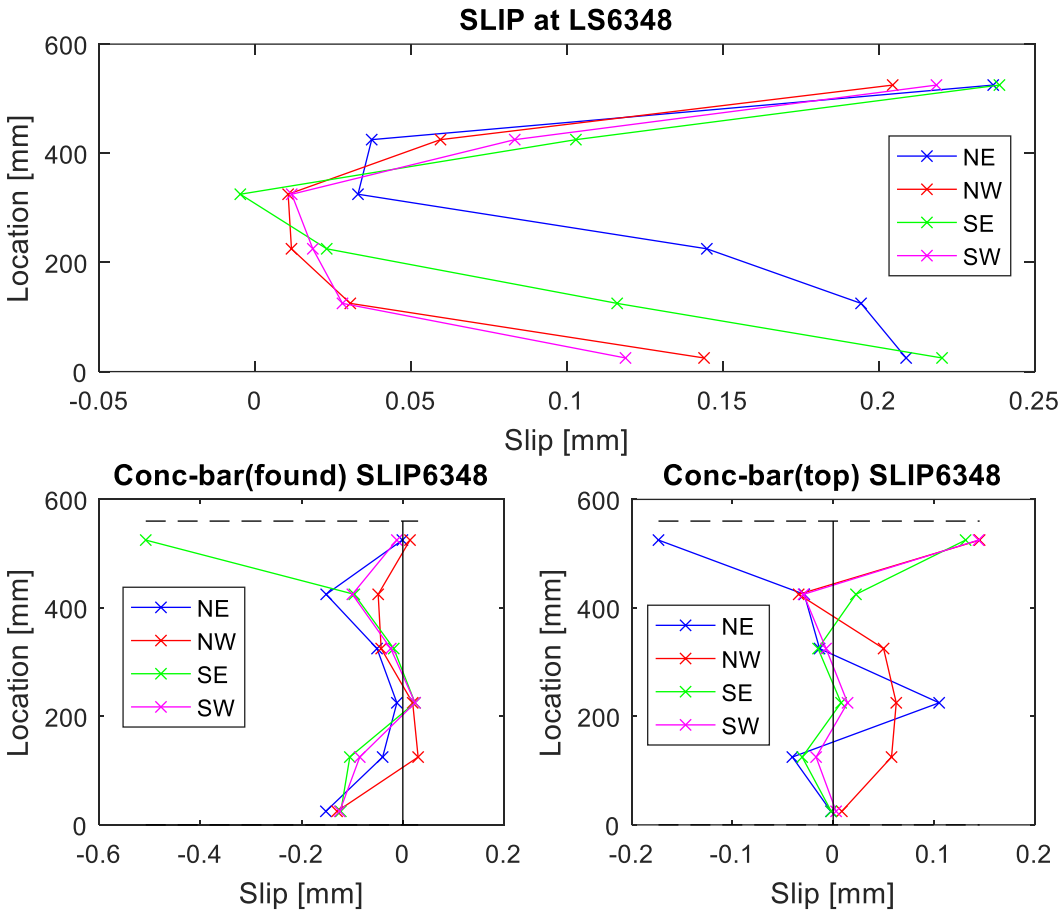

Figure 3.21: Slip LAP P3 after load step to 3 mm

In figure 3.16 is possible to see the map of strains in the specimen, the map of strains in the longitudinal reinforcement in the lap splice region and the average strain measured along the total length of the splice for LAP P1.

Looking at the strains at the first cycle to 3 mm the difference between the strains in and out of the splice zone is clear. In addition with the bigger strains outside of the splice region is also possible to see that the bigger strains along the specimen are concentrated at the top and bottom of the specimen. A different color layer, representative of bigger strains, can also be seen at the top of the splice.

When considering the strains directly in the rebars the differences of the strains in the extremities and in the middle of the splices are evident. Although all rebars have different values of strains two particularities can be seen:

i) The smallest strains are always in the end of the bar, i.e., for the bar anchored on the top the smallest strains are at the bottom part of the reinforcement while for the bar anchored on the bottom the smallest are in the top part of the rebar.

ii) On the contrary, the highest strains in the reinforcement are located in the opposite part of the rebar, i.e., for the bar anchored on the top the biggest strains are in the top of the splice while for the bar anchored on the bottom the biggest are in the bottom part of the splice.

In fact, a constant increasing of the strains can be seen along the splice length. The relation strain-bar length for LAP P1 is present in the last line of figure 3.16. In the present graphs is possible to see a progressive increasing of the strains along the bar length. While the strains of the bar anchored on the bottom increase progressively until the bottom part of the splice, the strains of the bar anchored on the top have the opposite behavior increasing progressively until the top part of the splice.

Additionally, the increasing of the strains is uniform for bottom and top anchored bar. In other words, the values of strains are similar in the opposite parts of both bars, i.e., the strains in the bottom part of the splice of the bar anchored in the bottom are similar with the values in the top part of the splice of the bar anchored on the top. This relation between the strains of the two rebars means that an average strain can be assumed along the entire splice.

The slipping between the longitudinal bars and the concrete of LAP P1 is presented in figure 3.17. Although small differences in the extremities, at the displacement to 3 mm, the splicing between the rebars was rather similar for all the splices. The biggest slips were on the top and bottom of the splices, in accordance with the biggest strains, while the slipping at the middle of the splices was close to zero.

Addressing the slip between the concrete and the longitudinal reinforcement is possible to see a similar behavior between the slip and the strains in the rebars. As reported by Shima et al. (1987) the slip is dependent on the strains along the reinforcement and so, especially before yielding, biggest strains along the rebar will correspond to biggest values of slip.

However, a particular behavior is present in the slip between the concrete and the bar anchored to the top. The splice at SW of LAP P1 showed a slip in the top of the splice different than the expected. This decrease in the slip can be explained in figure 3.22.

Firstly, it should be noted that the slip is a relation between the displacement of the LED glued into the bar and the LED glued into the concrete cover. Considering that the bar anchored to the top is in the exterior of the splice its displacement will be correlated with the displacement of the exterior LED glued into the concrete.

As seen in figure 3.22 a small crack above the LED, glued into the concrete, developed at the end of this cycle. The formation of this crack is assumed as the reason for the unexpected slip on the top of the SW splice of LAP P1. This assumption is supported by the strains maps of the specimen (see figure 3.16). Near to the top of the SW splice is possible to see a color gradient between the longitudinal bar and the exterior concrete cover. Due to the unrealistic behavior presented in figure 4.1, similar values of the slip between the concrete and the longitudinal bars will be disregarded in the results of further displacement.

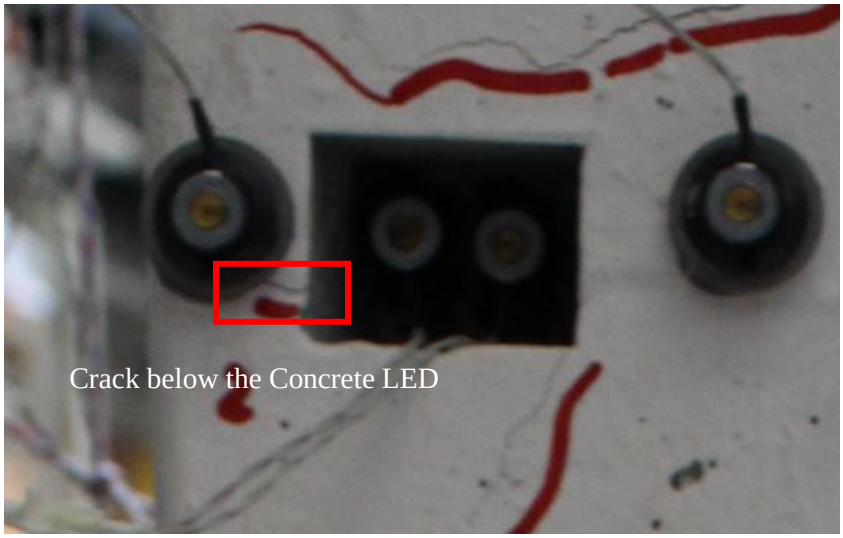

Figure 3.22: Picture of the crack on the top of the splice region at the end of load step to 3 mm

The response of the remaining specimens was rather similar at the end of this cycle.

Regarding the map of strains in the specimen, different color layer outside of the lap splice region are visible in LAP P2 and LAP P3. Particularly for LAP P2, in which the transversal reinforcement had a spacing of 30 cm which in turn was similar with the spacing of the horizontal cracks above the splice region. (See sub-section 3.6)

The two horizontal color layers above the splice zone presented in the Map of strains in figure 3.18 represent the horizontal cracks abovementioned.

Another particularity that should be considered is the differences in the strains of the longitudinal bars. While in LAP P1 the strains at the bar anchored at the top do not reach 0.2 %, for the specimen with the medium reinforcement (LAP P3) the splice in NE reached the yielding strain.

Regarding to the slip on the tested specimens, although the test is still in a beginning phase some differences in the slip of the rebars can be seen for LAP P1 and LAP P3. (See figure 3.17 and 3.21) The extremities of the splice show a bigger slip for the splices in NE and SE of both specimens.

3.7.2 Load Step to $\Delta = 6$ mm

LAP P1

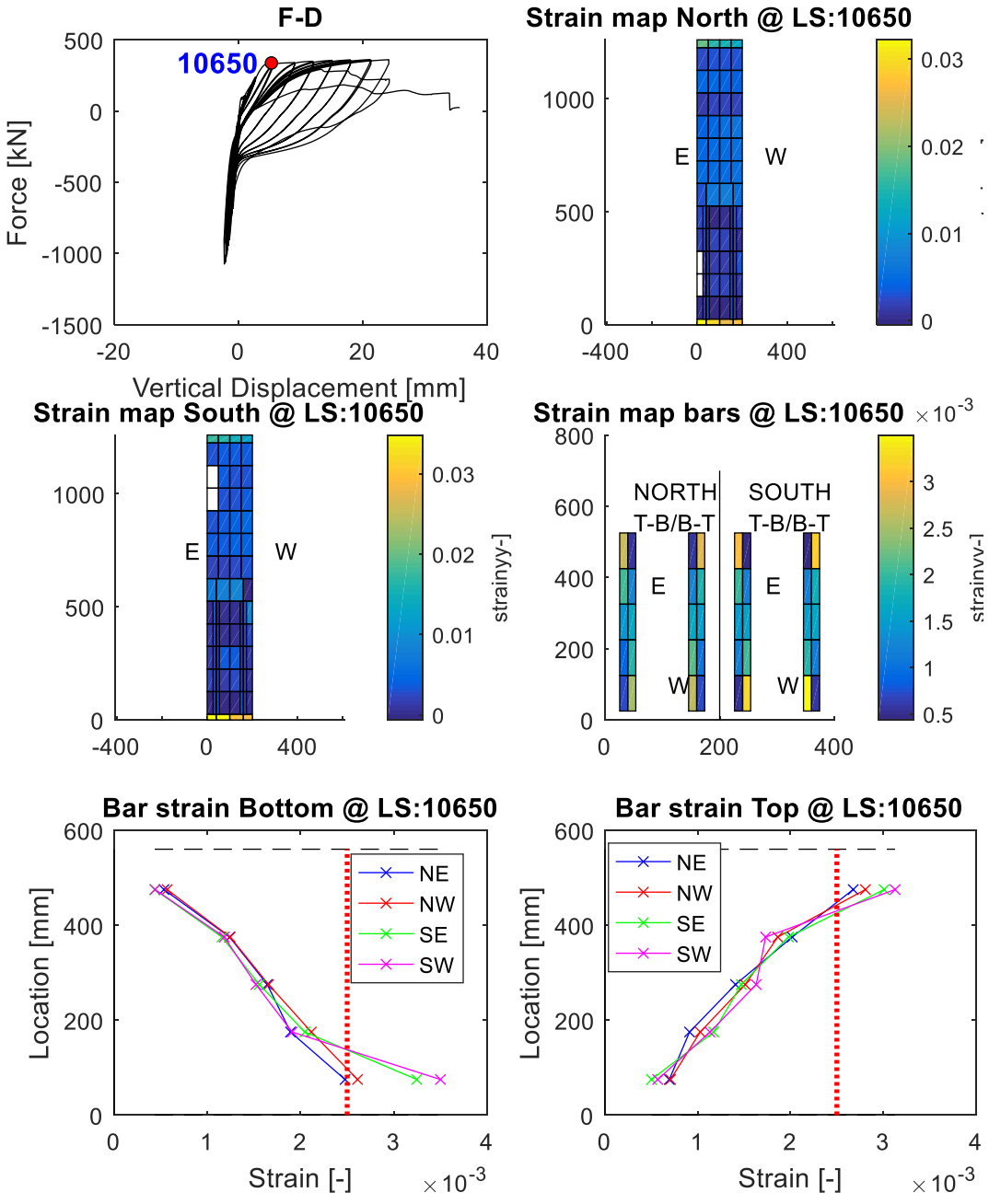

Figure 3.23: Strains of Lap P1 after load step to 6 mm

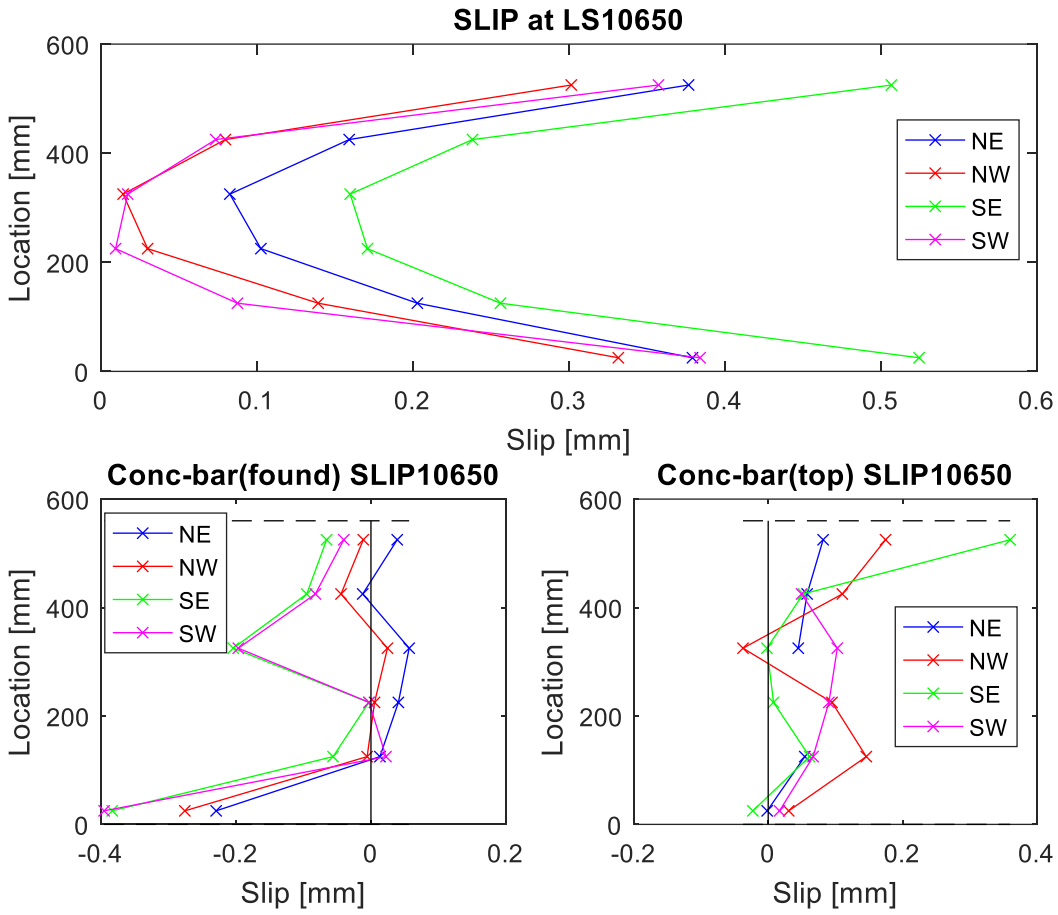

Figure 3.24: Slip LAP P1 after load step to 6 mm

LAP P2

i) peak force

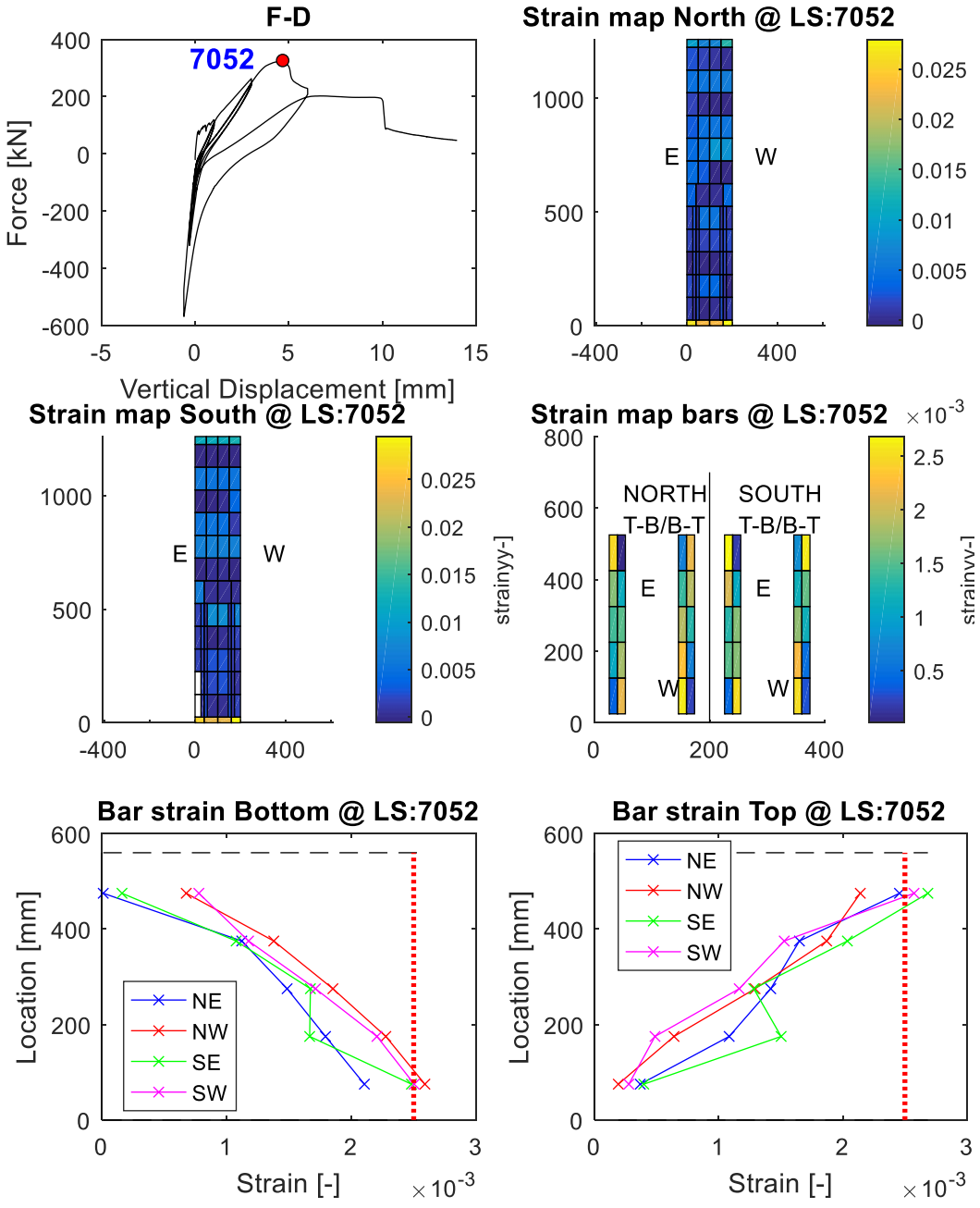

Figure 3.25: Strains of Lap P2 during load step to 6 mm at peak strength

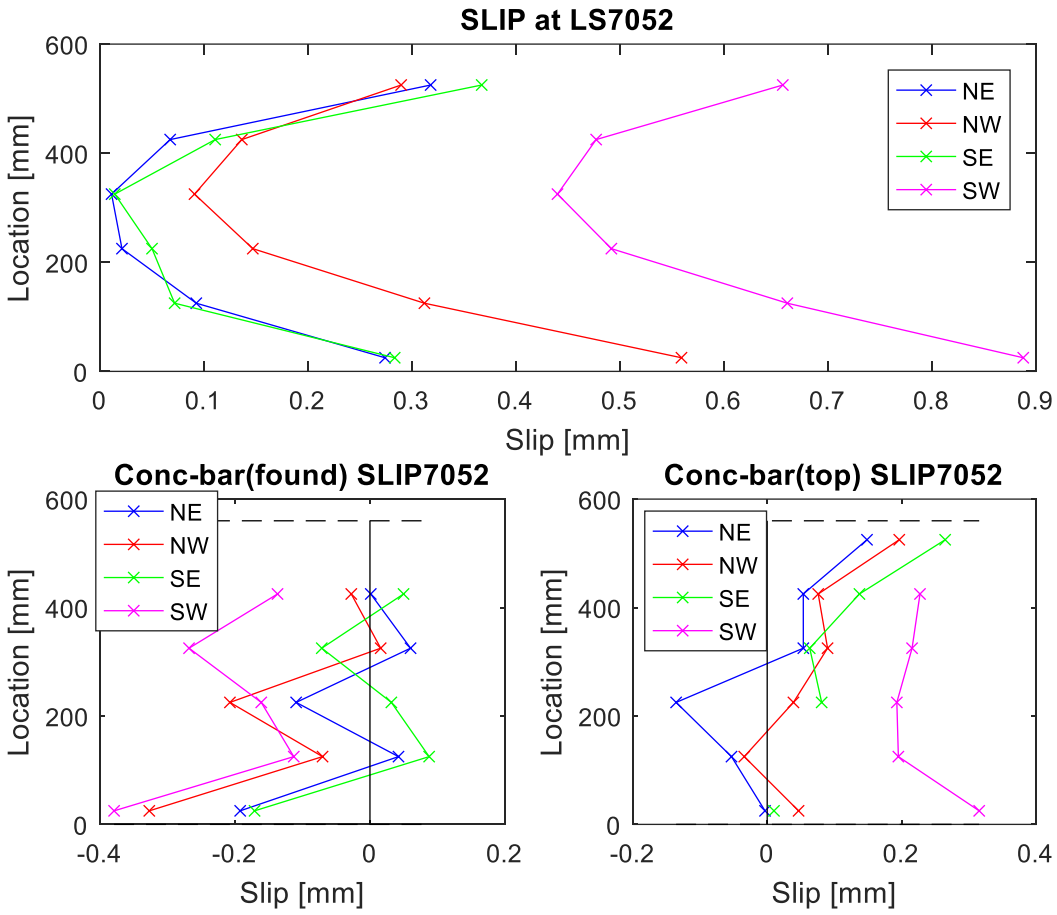

Figure 3.26: Slip LAP P2 during load step to 6 mm at peak strength

ii) *end of load step*

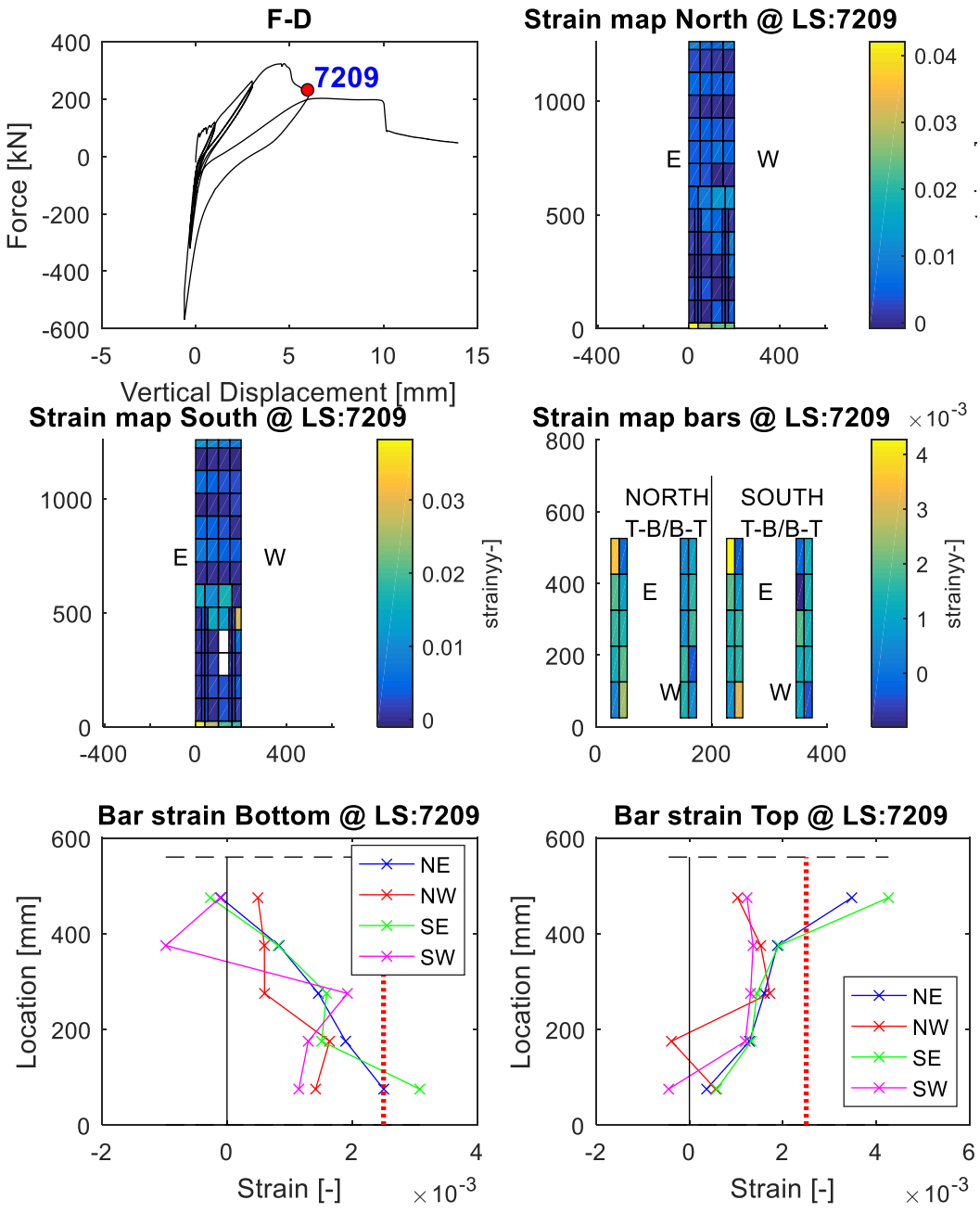

Figure 3.27: Strains of Lap P2 after load step to 6 mm

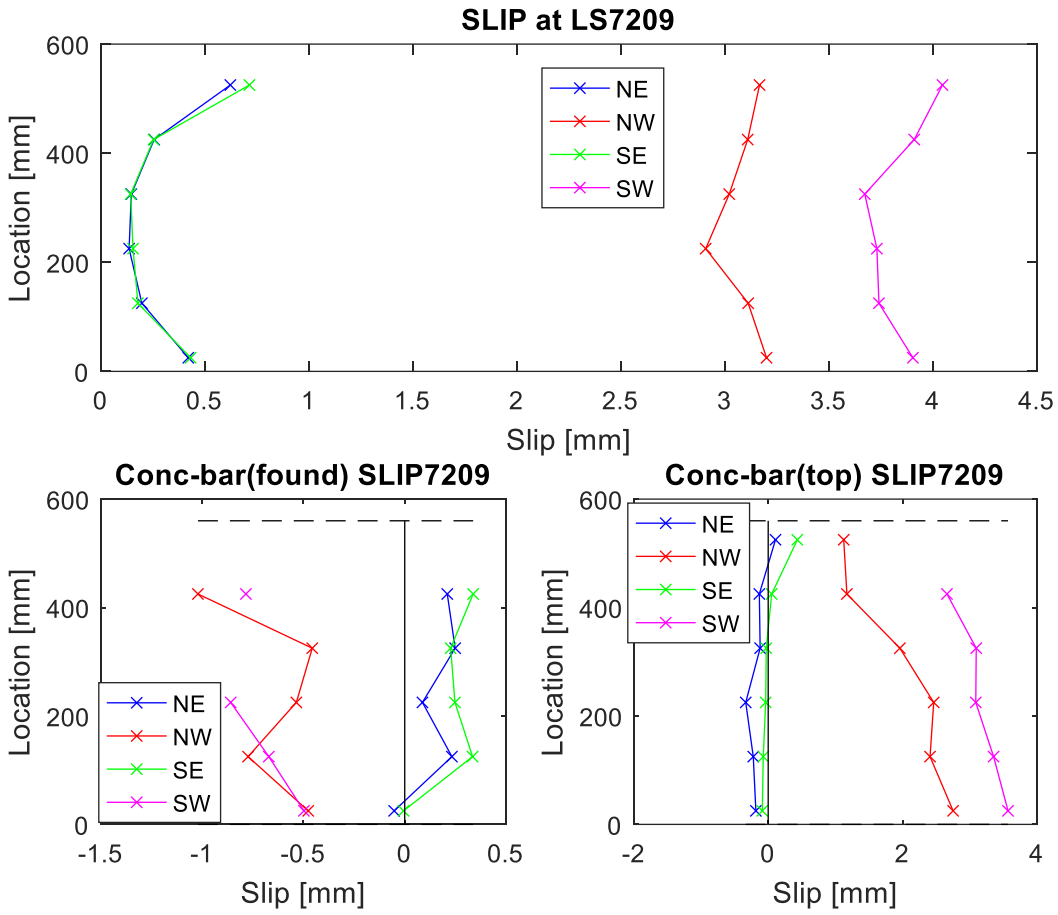

Figure 3.28: Slip LAP P2 after load step to 6 mm

LAP P3

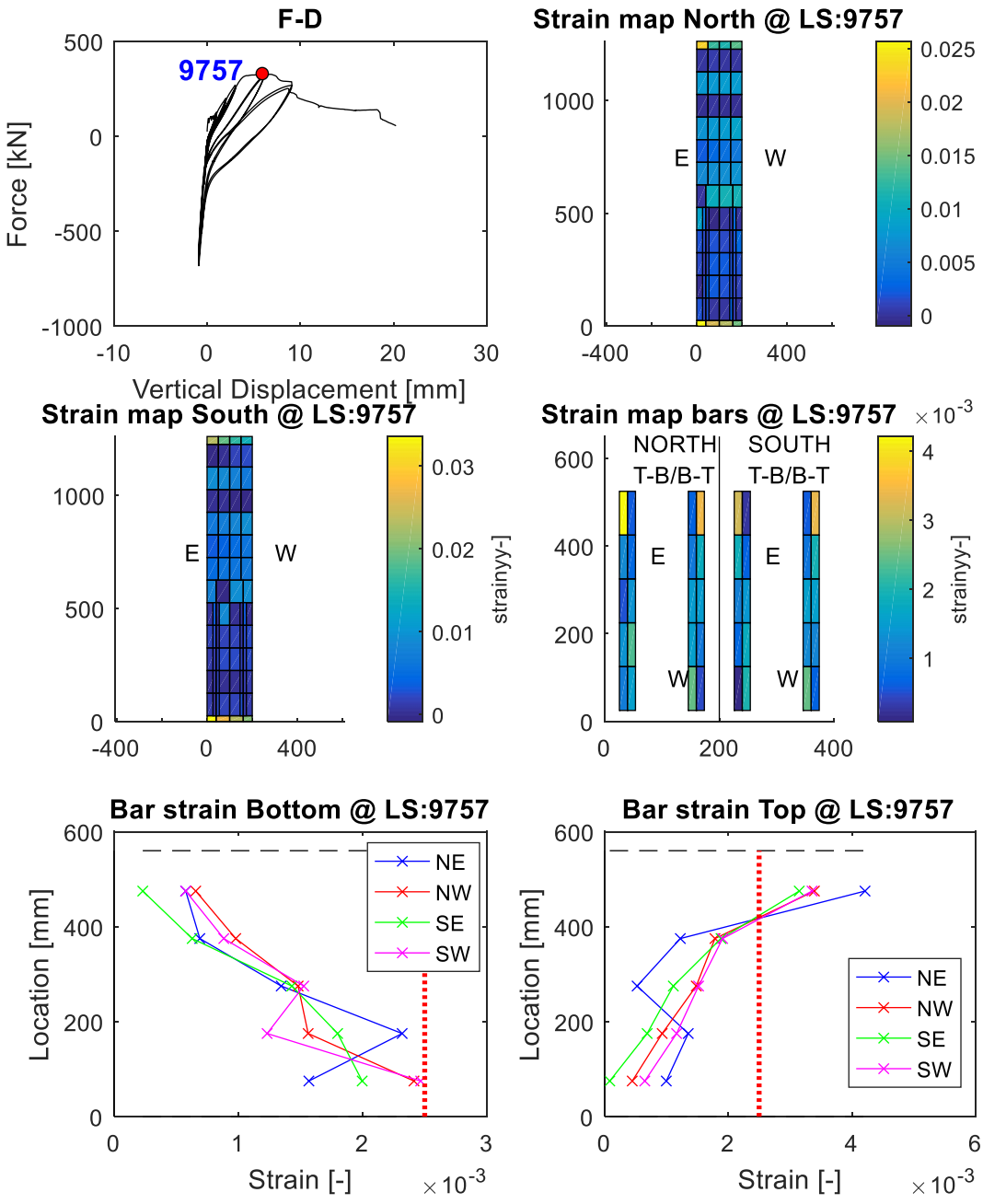

Figure 3.29: Strains of Lap P3 after load step to 6 mm

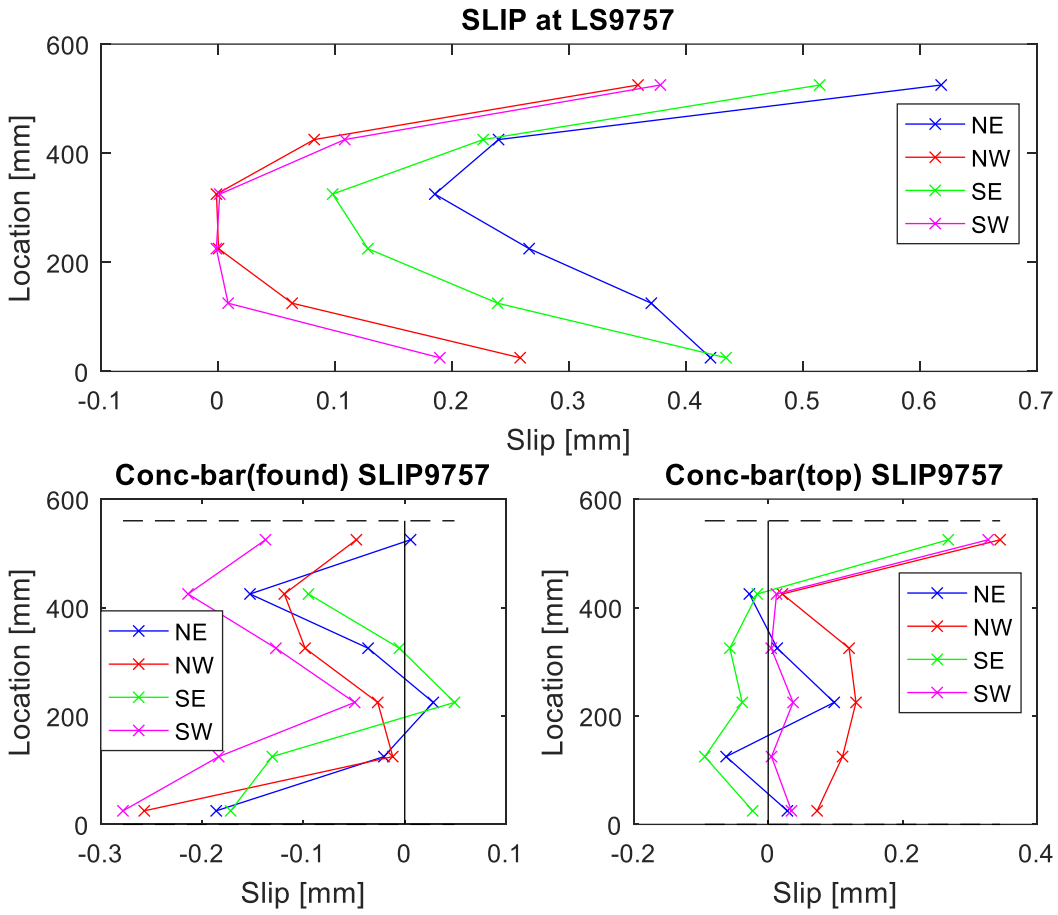

Figure 3.30: Slip LAP P3 after load step to 6 mm

During this cycle the yielding of the longitudinal reinforcement was achieved in all the three specimens. Further, the specimen LAP P2 failed at the end of this cycle.

The response of LAP P1, the specimen with most transversal reinforcement, remained similar after the yielding. Although an increase of the strains, the higher strains are still visible at the top of the splice and the strains inside the splice region have still minor values when compared with the strains along the specimen.

In figure 3.25 and 3.26 are presented the strains and slip at the peak force of LAP P2. Regarding the strains in the specimen no unexpected values are presented before failure. The higher strains are still present at the bottom of the specimen while the strains at the top of the splice are still not relevant. Major damage is seen in figure 3.26. The two bars at the SW splice revealed an important slip particularly in the bottom part.

Concerning the slip of the bar with respect to the concrete, some differences also highlight the slip of the bars at the SW splice. Although more evident for the bar anchored at the top, the slip of the bar anchored in the bottom was two times bigger than the slip of the bar at the east side (NE and SE).

The strains and slips at the end of the load step are present in figures 3.27 and 3.28. The strains in the specimen are now concentrated at the top of the splice, which can particularly be seen in the strain map South. The strains at the bars in the splice region at the West side, SW and NW, are now uniform along its length while the splices at the East side still present peak major strains at the extremities of the bars.

Concerning the strains, it should also be noted that the yielding in the splice region penetrated faster for the rebars anchored to the top than for the bars anchored to the bottom. While for the two longitudinal bars in the south anchored at the top (NE and SE) the yielding penetrates 200 mm for the bar at SE anchored at the bottom of the specimen the yield just penetrate half of that value.

After the failure, the slipping of the bars at the West side is even more evident with uniform values of slip along the bars around 3.5 mm and the slip between the top bar and the concrete is around 3 mm. By opposite, the bars at the East side show no important values of slip.

Finally, LAP P3 shown a response similar with LAP P1 at the end of this cycle. The strains in the specimen are mainly concentrated at the splice end. The strains at the bar anchored at the top reached higher values than in specimen LAP P1 achieving a value around 0.4 % while the strains at the bars anchored to the bottom didn’t reach the yielding strain. (See figure 3.29).

No significant slip occurred, neither between the two bars nor concrete and longitudinal reinforcement.

3.7.3 Load Step to $\Delta = 9$ mm

LAP P1

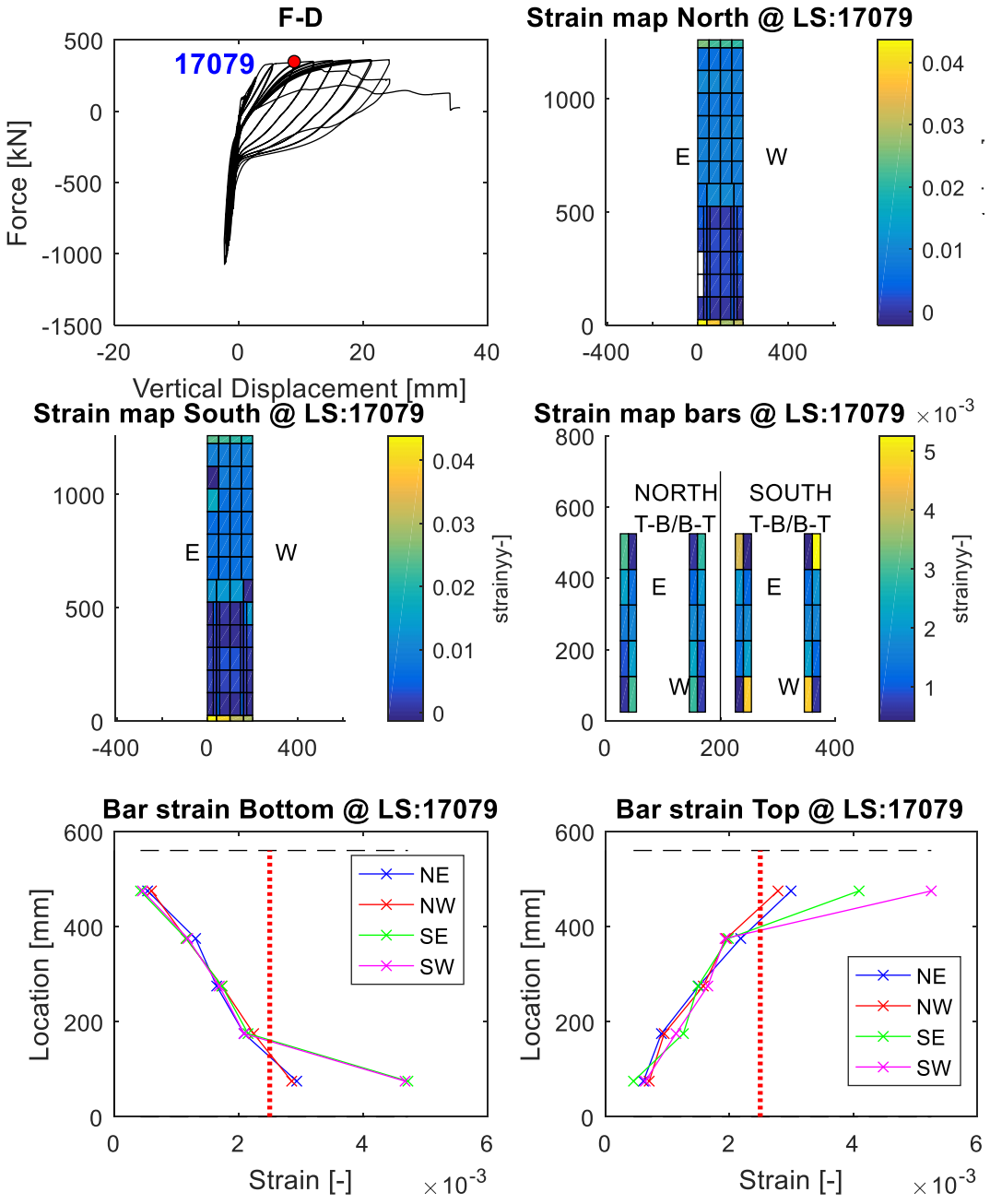

Figure 3.31: Strains of Lap P1 after load step to 9 mm

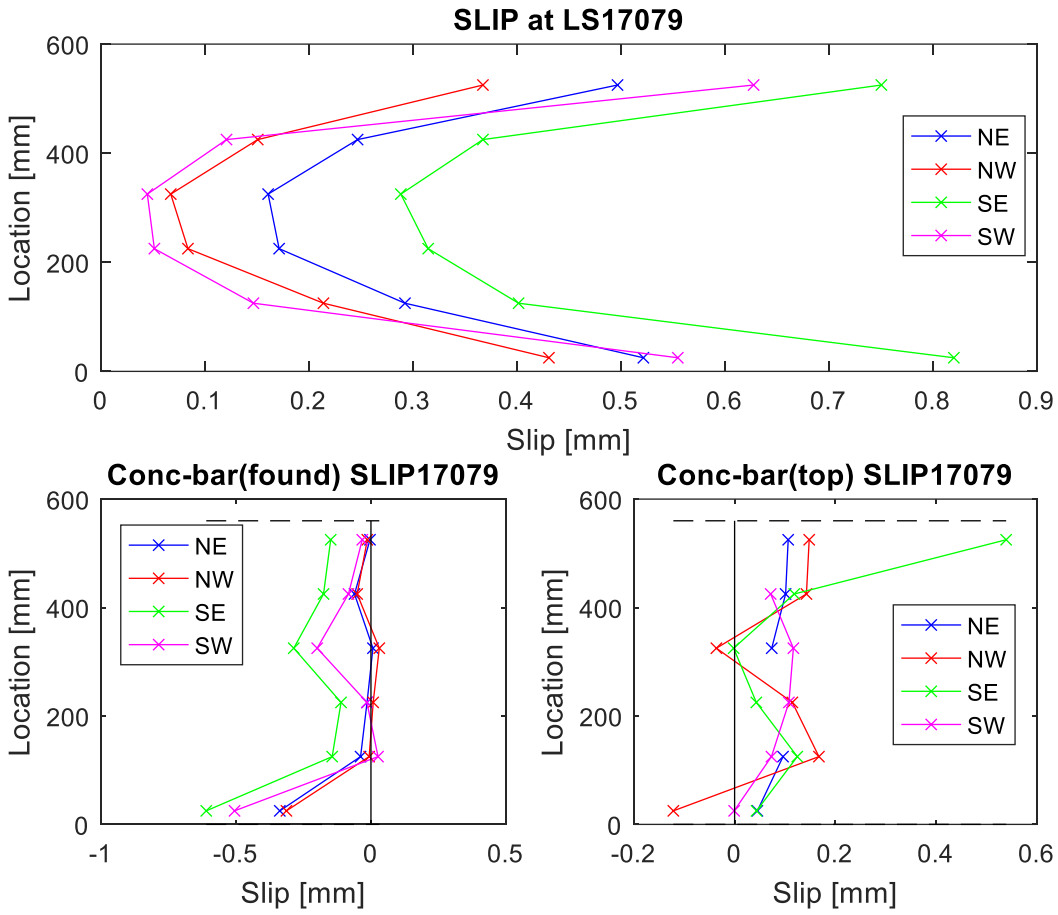

Figure 3.32: Slip LAP P1 after load step to 9 mm

LAP P3

i) Peak force

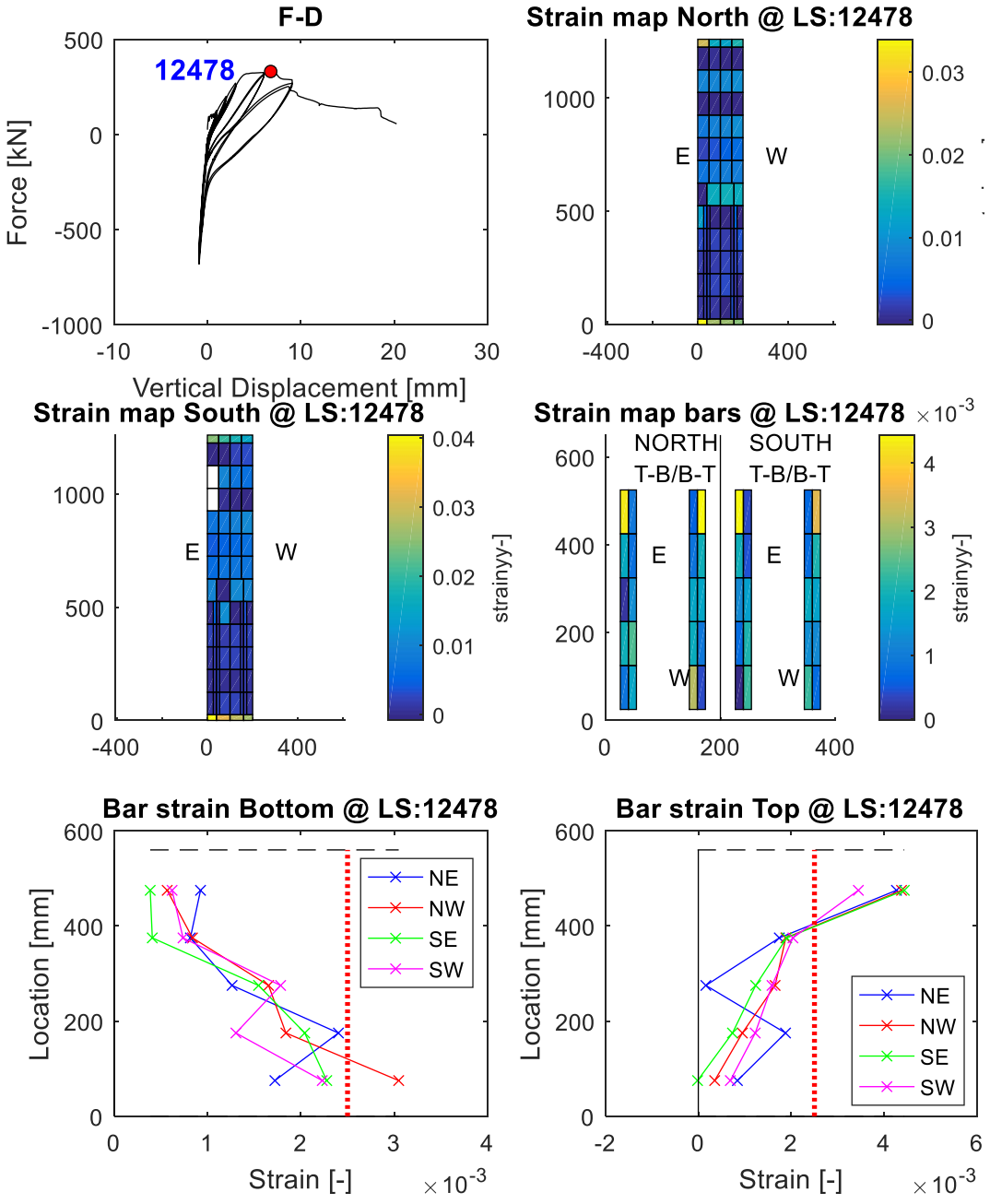

Figure 3.33: Strains of Lap P3 during load step to 9 mm at peak strength

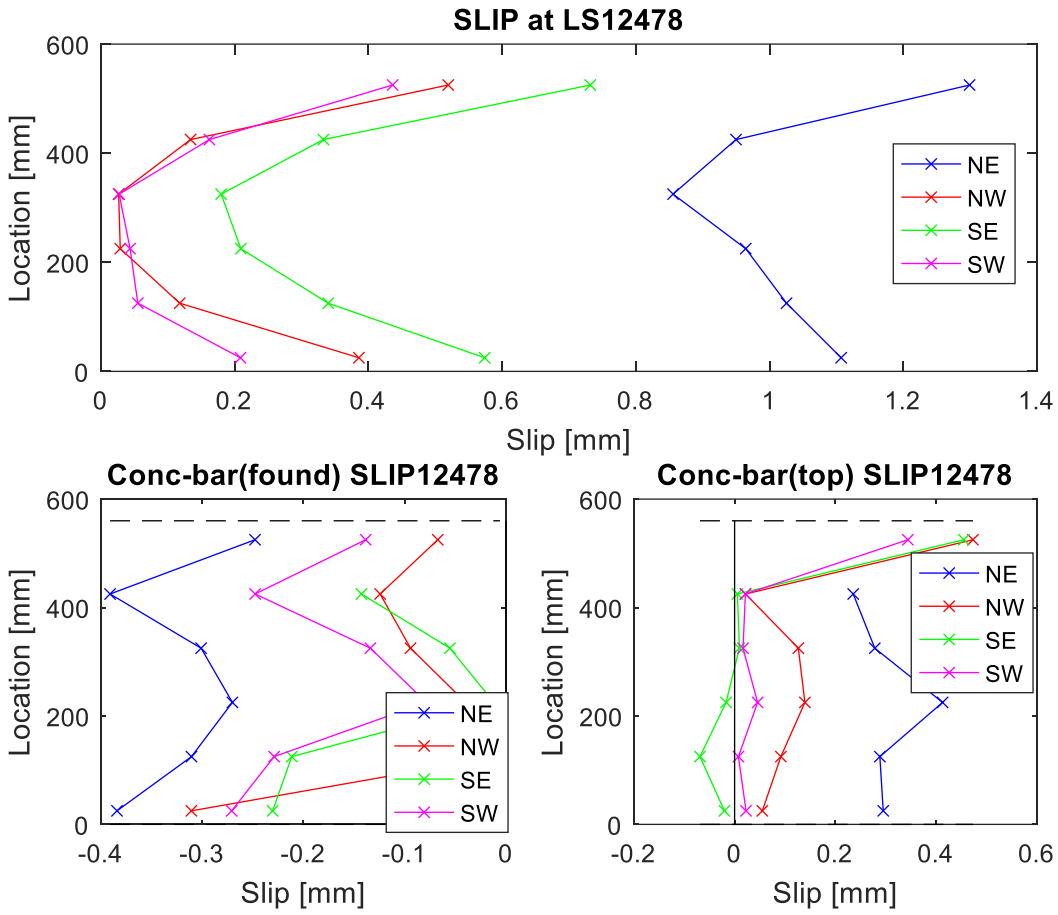

Figure 3.34: Slip LAP P3 during load step to 9 mm at peak strength

ii) End of the load step

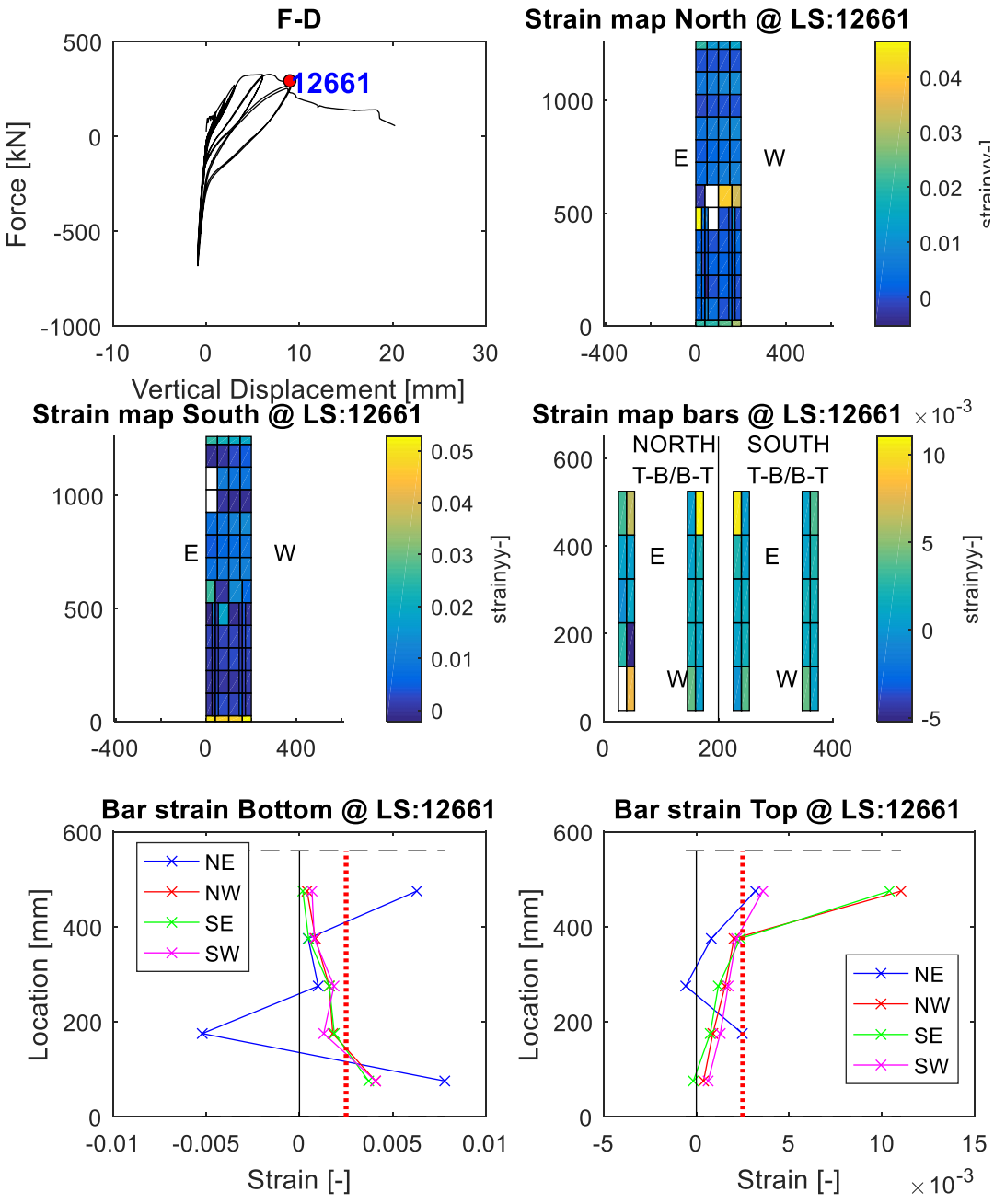

Figure 3.35: Strains of Lap P3 after load step to 9 mm

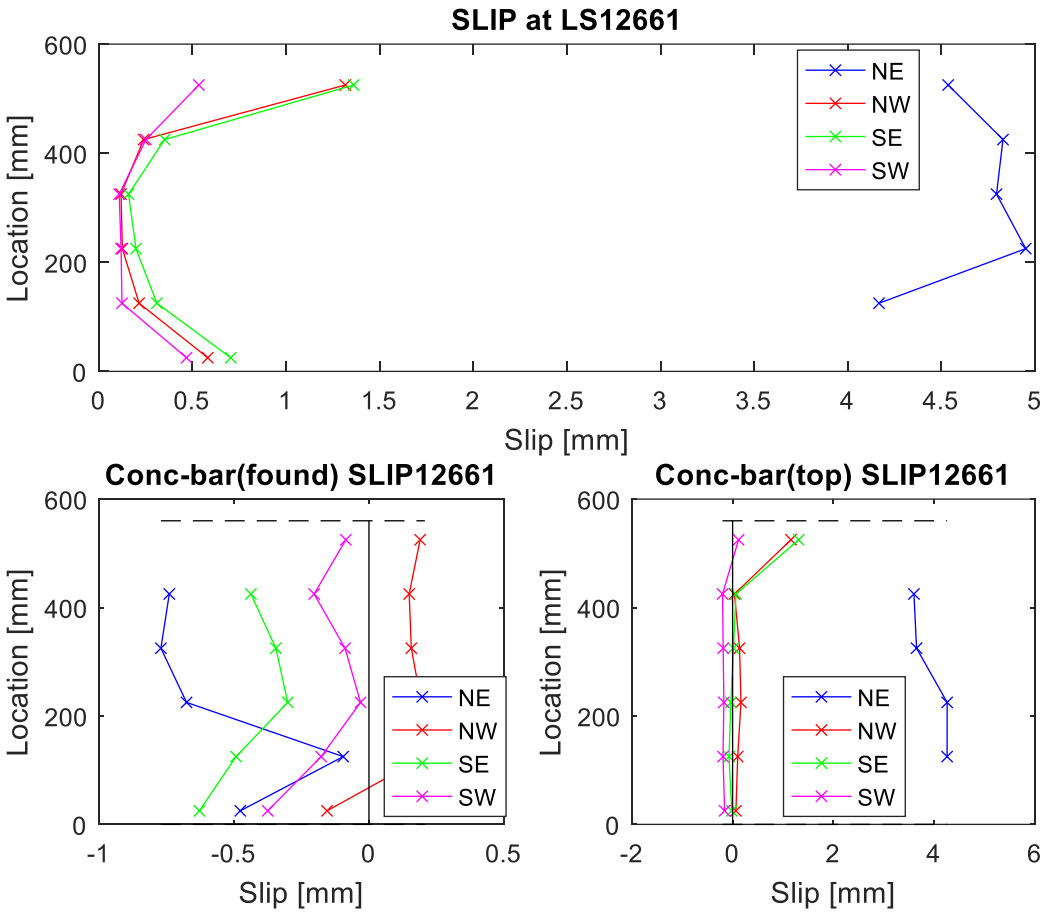

Figure 3.36: Slip LAP P3 after load step to 9 mm

At the end of the cycle to 9 mm LAP P3 failed. In figure 3.33 is possible to see biggest strains at the top of the splice in the strain map north of the specimen before failure. All the spliced bars anchored at the top reached the yielding strain in the top of the splice while just the bar anchored to the bottom at northwest have a bigger strain than the yielding strain at the bottom part of the splice.

As similar with LAP P2, also a slipping of the rebars at the NE splice can be seen in figure 3.34. The slipping between the longitudinal bars reached 1.3 mm at the top of the splice. Regarding the slipping between the bar and the surrounding concrete the biggest differences are at the bars anchored at the bottom where the bar at northeast have a bigger slipping than the remaining bars. The bars anchored at the top beam presented a uniform slip along the splice until the top, at the top the slip increased suddenly. This sudden increase can be explained by the yielding of the bars.

After failure, the damaged zone is evident in figure 3.35. The huge crack reported in sub-section 3.6 is supported by the strains on the top of the splice at the northeast side which feature a value of 0.04. The strains at the top of the splice in the bars at NW and SE anchored to the top are now two times bigger than at the peak strength featuring values higher than 1 %.

The slip between the rebars at northeast is perceptible in figure 3.36 with values that reached up to 5 mm. The slipping in the NE splice is supported by the figure representing the slipping between the bar anchored to the top and the concrete. Clearly, the bar anchored at the top at northeast slipped at failure presenting a slip more than ten times bigger than the slip at the peak strength.

By the other hand, no important slip is present in LAP P1 at the end of this cycle as depicted in figure 3.32. The differences of the strains along the specimen are clearer at the end of this cycle. In figure 3.31, the strain map at north show an evident different between the strains in and out of the splice zone.

3.7.4 Load Step to $\Delta = 21\ mm$

LAP P1

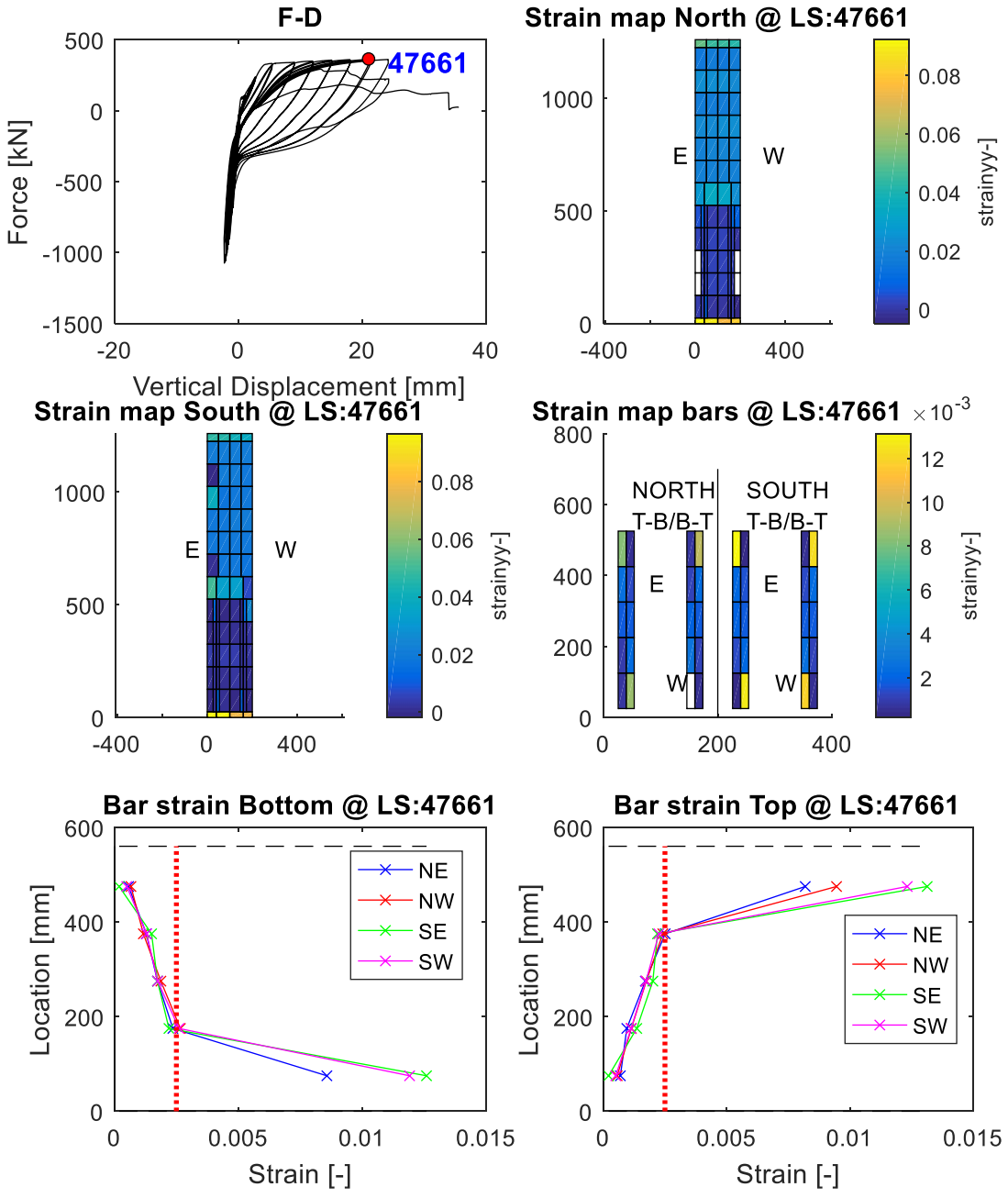

Figure 3.37: Strains of Lap P1 after load step to 21 mm

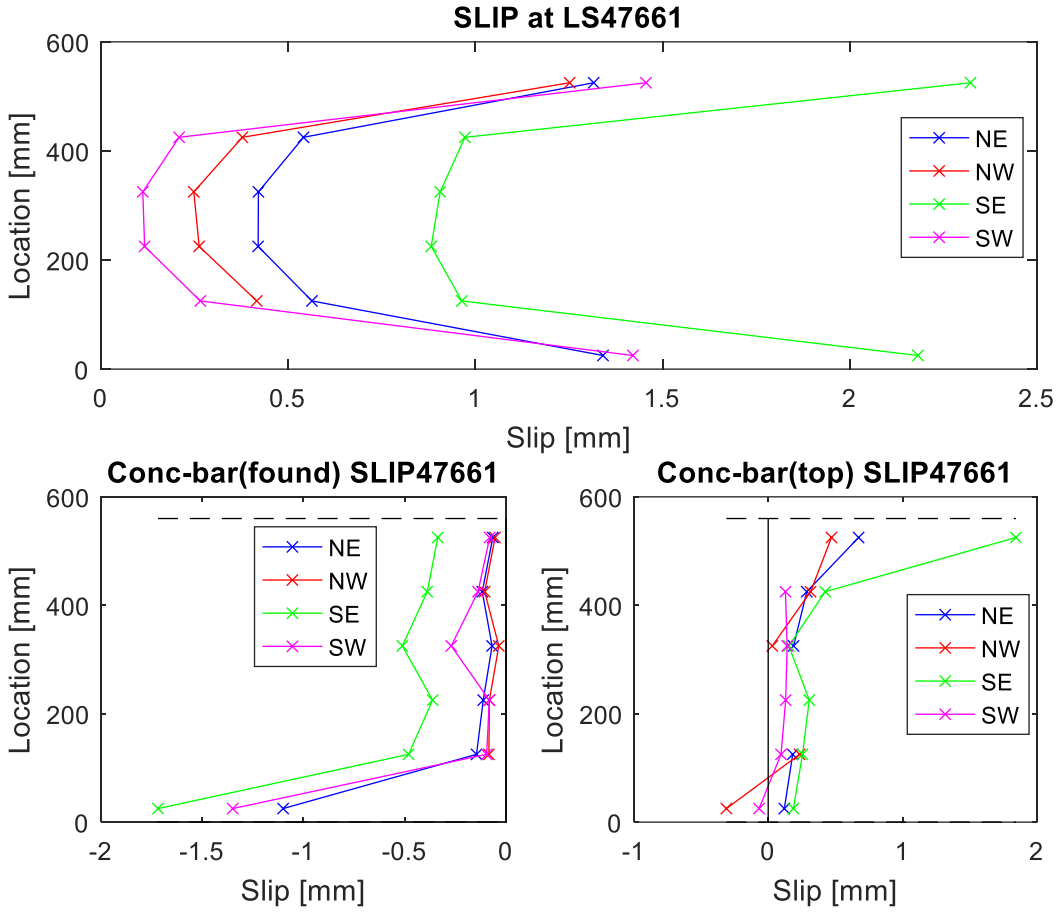

Figure 3.38: Slip of Lap P1 after load step to 21 mm

3.7.5 During second cycle to $\Delta = 24$ mm, LAP P1 failure

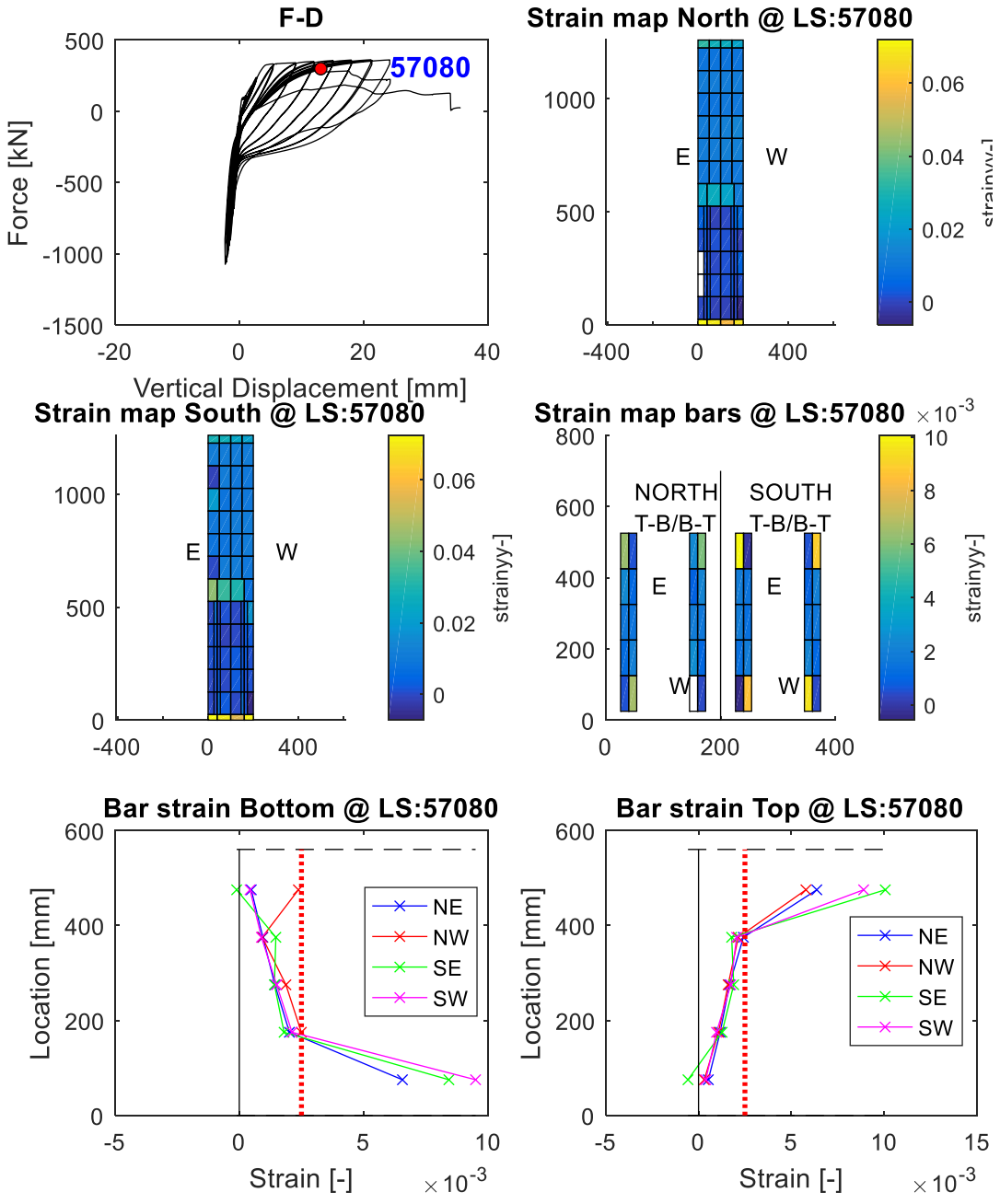

Figure 3.39: Strains of Lap P1 at failure

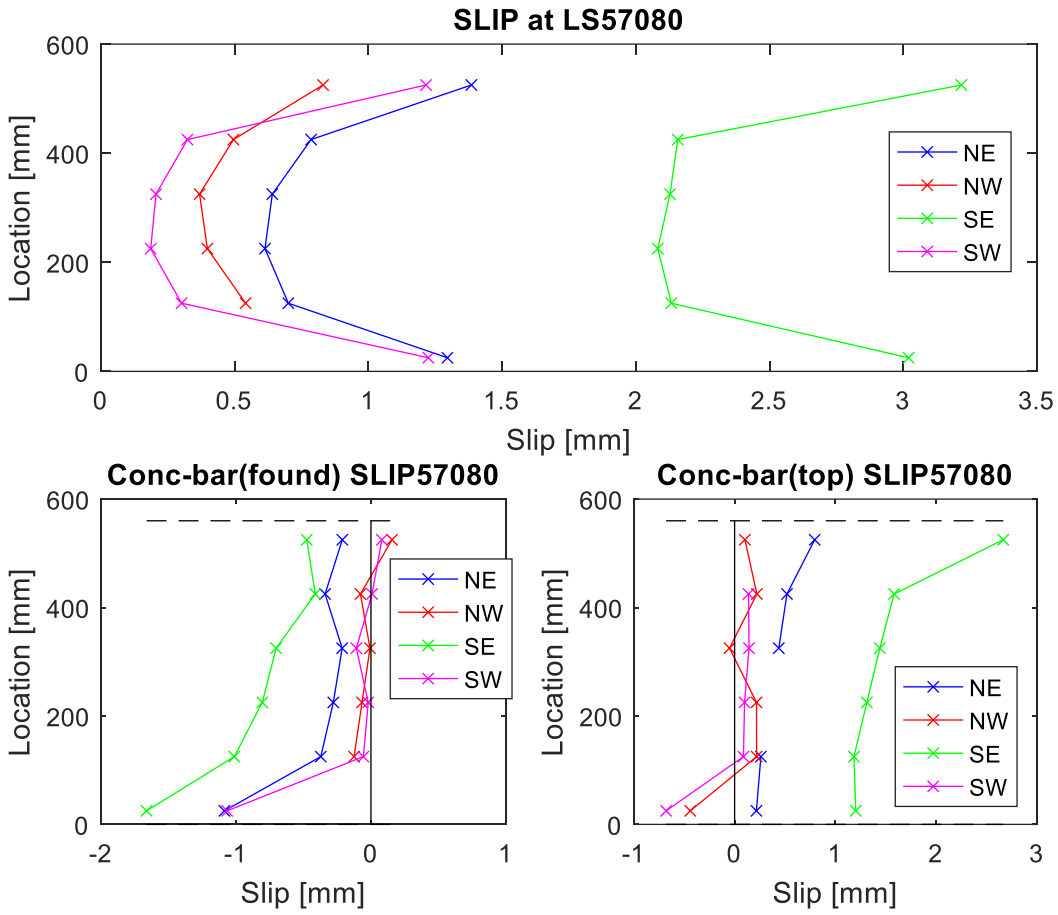

Figure 3.40: Slip of Lap P1 at failure

Figures 3.37 and 3.38 present the response of the specimen LAP P1 at the peak strength ($\Delta = 21$ mm), end of the cycle before failure (first cycle to $\Delta = 24$ mm) and at failure of the specimen (during second cycle to $\Delta = 24$ mm)

At the peak strength, the biggest strains are still at the top of the splice. The strains of the longitudinal reinforcement in the splice region are now bigger at the south of the specimen (see figure 3.37) and the strains at the extremities of the splices are now five times bigger than the yielding strain.

Figure 3.38 show some important slip in the splice at southeast of the specimen.

As presented in figure 3.40, the slip of the SE splice was evident at failure. The extremities of the rebars in the lap splice zone slipped approximately 3 mm on the SE splice while on the remaining splices the slip was just around 1.25 mm. The major slipping of the SE splice is also clear by the slipping between the bars and the surrounding concrete.

The highest strains were reached at the top of the splice with a bigger value at the Northeast side of the specimen. The strains in the reinforcement at the splice zone remained with the same behavior of the last cycle with a highest value for the bars at South of the specimen.

After, the stress and the bond stress along the longitudinal reinforcement in the splice zone are presented in figure 3.41.

LAP P1 at the end of the second load cycle to $\Delta = 24\ mm$

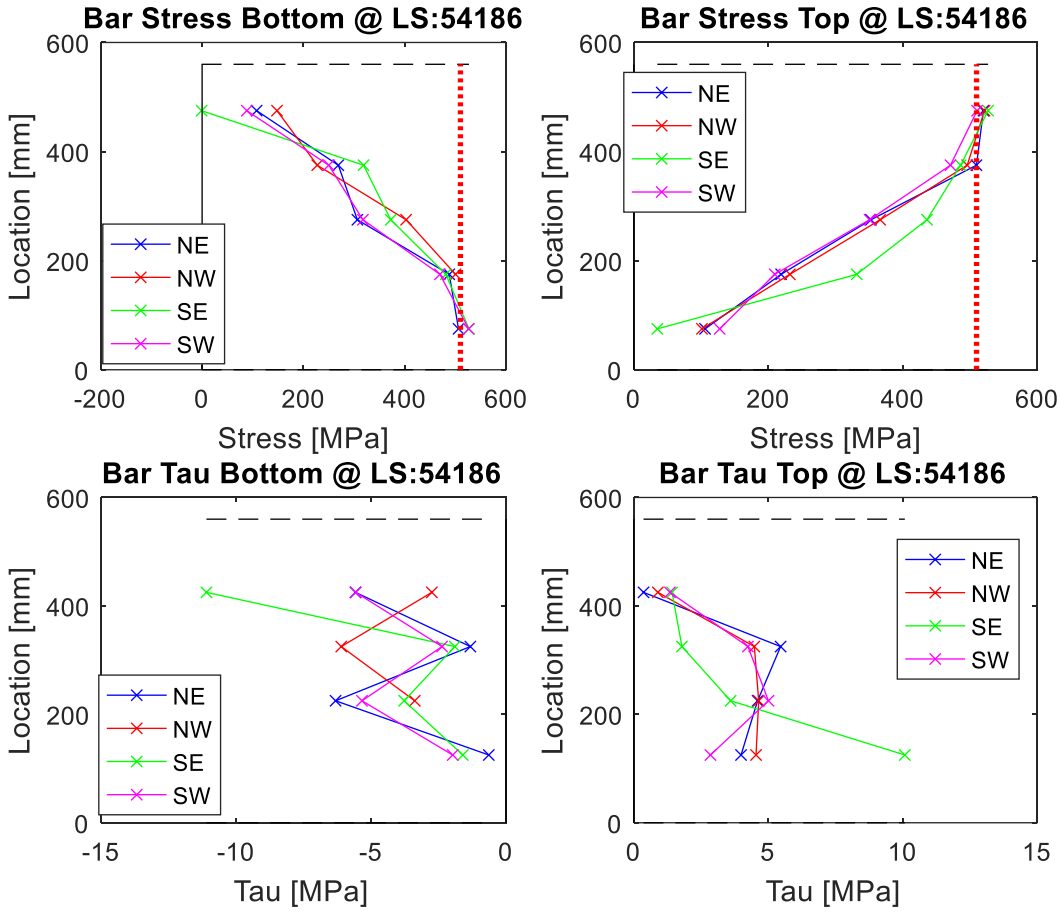

Figure 3.41: Bar Stress and Bond stress in lap splice region for LAP P1

As expected, the stress along the longitudinal reinforcement and the strains have an identical behavior before the yielding. In both longitudinal bars, anchored to the top and anchored to the bottom, the stress yielding was achieved until 200 mm of the peak stress end. After the yielding, the stress in the rebars is maintained constant.

Before addressing the bond stress in the lap splice zone, it should be noted that the former is directly dependent of the variation of stress along a certain length which means that if two stress values are rather different the bond stress can have an unrealistic value.

Reported by Shima et al. (1987), supported by a set of pull out tests, the bond stress along the rebar increases inversely proportional with the distance from the loaded end until achieved the yielding, i.e., the lower the distance to the loaded end, the greater the bond stress. When the bar yield, a brittle decrease happens. After the yielding the bond stress can decrease or be kept constant depending on the stress-strain relation of the steel.

In figure 3.41 it's presented the bond stress of the longitudinal reinforcement in the lap splice zone for LAP P1 at the end of the cycle in which the specimen failed. Since both specimens, LAP P2 and LAP P3, failed soon after the yielding their results of the bond stress were neglected because no relevant post-yielding behavior can be seen.

Although small discrepancies, in figure 3.41 is possible see the expected behavior predicted by Shima et al. (1987). Particularly in the figure that address the bond stress for the bars anchored to the top, it can be observed that the bond stress increased progressively along the lap splice length and when approaching the top end, that had already yield, the bond stress dropped to values close to zero in all the splices.

3.8 Summary of Results and Comparison with available models

The main observations with regards to the load and strain of the above described test are presented in table 3.4. It summarizes the maximum forces in compression and tension as well as the reinforcement strains and slip at the peak strength and at failure for each specimen. The average lap splice strains and the cycle at which the failure occurred are also depicted. The strains directly in the bars were measured with the rows of LEDs and the average lap splice strains at degradation were measured with the corresponding LVDTs

After, the constitutive models described in sub-section 2.5 to predict the splice strength and strain were applied to the tested specimens and its values are also presented in table 3.4.

Concerning the behavior of each specimen after and before failure, LAP-P2 and LAP-P3 showed small slip that increased suddenly during the cycle in which the failure occurred. The former specimens revealed a slip of 0.9 mm and 1.3 mm before failure and after a slippage of 4 mm and 5 mm occurred respectively in LAP P2 and LAP P3 reveling an increase of 344 %. By other hand, in specimen with the highest transversal reinforcement (LAP-P1) no important slipping was seen, displaying an increasing of 30 % after failure.

Regarding the strains, the test specimen with the highest transversal reinforcement exhibited a continuous increasing of strains being the specimen that developed the highest strains. The remaining specimens, showed strains with a value three times inferior than the value of strains obtained by the specimen LAP-P1.

Furthermore, the strains obtained by the two specimens with lower transversal reinforcement were rather inferior comparing with the strains obtained by the model of Tarquini et al. (2017). Both specimens revealed a strength superior to the yielding and therefore the stress-strain curve of the steel could be considered but the strain limit predicted by the former model was not achieved and both specimens failed at a rather small reinforcement strain. Such a difference can be justified due to the neglecting of the cyclic loading which is proved that will increase the degradation of the specimen. (table 3.5)

This difference in the results shows that a model to predict the strains of the longitudinal reinforcement in the lap splice zone is still missing in the literature. The accuracy of the results decreases with the decrease of the amount of transversal reinforcement.

Table 3.4:Summary of Results

		LAP-P1	LAP-P2	LAP-P3
F_t (kN)		368.1	323.1	326.1
F_c (kN)		1074	568	681.8
Peak Strength	**Top Bar Strain** %	*1.2*	*0.25*	*0.43*
	Bottom Bar Strain %	*1.2*	*0.25*	*0.3*
	Slip (mm)	*2.2*	*0.9*	*1.3*
Failure	**Top Bar Strain** %	*1.0*	*0.4*	*1.0*
	Bottom Bar Strain %	*1.0*	*0.3*	*0.9*
	Slip (mm)	*3*	*4*	*5*
Average Lap-splice Strain at degradation %		*1.4*	*0.36*	*0.47*
$\varepsilon_{u,ls}$ % **(Tarquini, et al., 2017)**		*0.85*	*0.50*	*0.59*
Failure at displacement cycle		2^{nd} 24 mm	1^{st} 6 mm	1^{st} 9 mm

Table 3.5: Comparison of Ultimate Strains with available models

	LAP-P1	LAP-P2	LAP-P3
Maximum Lap-splice Strain before failure %	*1.2*	*0.25*	*0.43*
$\varepsilon_{u,ls}$ % **(Tarquini, et al., 2017)**	*0.85*	*0.50*	*0.59*
Difference %	29.*2*	50	27.2

4 Conclusions and Outlook

Three specimens were tested under cyclic loading in the laboratory of the *École Polytechnique Fédérale de Lausanne*. The specimens represented the bottom corner region of a bridge pier where lap splices are usually placed. The conclusions and interesting findings taken from this experimental campaign are displayed below:

- The transversal reinforcement has an unquestionable influence in the lap splices behavior. Although a bigger transversal reinforcement increases both strength and displacement of a RC member, an increase in the transversal reinforcement it is even more important regarding the ductility capacity of the member.

- The amount of transversal reinforcement also play an important role in the failure of the specimen. For LAP-P1 the specimen with the highest reinforcement, the damage was mainly concentrate at the top extremity of the splice through a major horizontal crack. By other hand, the specimen with less transversal reinforcement failed through vertical splitting cracks along the entire splice length concentrating the damage inside the splice region.

- Despite the large amount of studies addressing the lap splice behavior there isn't still a reliable model that can predict the lap splice strain. The most recent model proposed by Tarquini et al. (2017) show still some important differences specially regarding the specimens with less transversal reinforcement.

- The proposed test setup showed results in line with the expected results having in mind the literature review presented in section 2. The outcome of this test setup shows that more studies should be made regarding specimens with the similar geometrical features. The viability of this test setup can then boost a further research regarding the lap splice behavior.

As said previously, this dissertation is included in currently existing research program developed in École *Polytechnique Fédérale de Lausanne* that aims to present a constitutive law that can predict the lap splice deformation capacity. It is clear that the very large topic of seismic assessment of lap splices cannot be completely conclusive with just three experimental tests. Further tests specimens will be tested during this remaining research program regarding different geometrical features that can be found in Swiss bridge piers.

The factors that will be tested in the following campaign are detailed as follows:

- The influence of the lap splice length. The influence of a bigger and a smaller lap splice should be considered since different splice lengths were proposed in the codes during the past years.

- The influence of the cyclic loading will be compared with experimental tests. Therefore, identical specimens should be tested under cyclic and monotonic loading.

- The real influence of the transversal reinforcement should be studied in more detail. Specimens with the same transversal reinforcing ratio but bigger spacing and specimens with similar spacing but different transversal reinforcement ratio should be tested.

- Since the transfer of forces between the bars and the concrete is made in part by the lugs of the rebars, the response between specimens with ribbed and smooth rebars is expected to be different. However, is not possible to find any experimental test the behavior of regarding lap splices in smooth rebars. Therefore, further studies should be made considering this feature.

- The difference in having lap splices in a RC member should be tested through a specimen featuring a continuous reinforcement. Thus, a benchmark of the specimens described in this dissertation should be tested.

5 References

1. Aaleti S, Brueggen BL, Johnson B, French CE, Sritharan S. Cyclic Response of Reinforced Concrete Walls with Different Anchorage Details: Experimental Investigation. Journal of Structural Engineering. 2013 Jul;139(7):1181–91.

2. Aboutaha RS, Engelhardt MD, Jirsa JO, Kreger ME. Retrofit of Concrete Columns with Inadequate Lap Splices by the Use of Rectangular Steel Jackets. Earthquake Spectra. 1996 Nov 1;12(4):693–714.

3. ACI-ASCE Committee 408, editor. Report on steel reinforcing bars under cyclic loads. Farmington Hills, MI: American Concrete Institute; 2012. 35 p.

4. Almeida JP, Prodan O, Tarquini D, Beyer K. Influence of Lap Splices on the Deformation Capacity of RC Walls. I: Database Assembly, Recent Experimental Data, and Findings for Model Development. Journal of Structural Engineering. 2017 Dec 1;143(12):04017156.

5. Almeida JP, Prodan O, Rosso A, Beyer K. Tests on Thin Reinforced Concrete Walls Subjected to In-Plane and Out-of-Plane Cyclic Loading. Earthquake Spectra. 2017 Feb;33(1):323–45.

6. Angeli G, Hannewald P, Beyer K. Behaviour of poorly detailed lap-splices under cyclic loading. Proceedings of the Vienna Congress on Recent Advances in Earthquake Engineering and Structural Dynamics 2013

7. Bimschas M. Displacement Based Seismic Assessment of Existing Bridges in Regions of Moderate Seismicity. PhD Thesis, ETH ZURICH 2010.

8. Birely A. Seismic Performance of Slender Reinforced Concrete Structural Walls.PhD Thesis, University of Washington. 2012.

9. Biskinis D, Fardis MN. Effect of Lap Splices on Flexural Resistance and Cyclic Deformation Capacity of RC Members. Beton- und Stahlbetonbau. 2007 Sep;102(S1):51–9.

10. Canbay E, Frosch RJ. Bond Strength of Lap-splices Bars. ACI Structural Journal; Farmington Hills Vol. 102, 2005.

11. ChaiI YH, Priestley MJN, Seible F. Seismic Retrofit of Circular Bridge Columns for Enhanced Flexural Performance. SJ. 1991 Sep 1;88(5):572–84.

12. Chinn J, Ferguson PM, Thompson JN. Lapped Splices in Reinforced Concrete Beams. JP. 1955 Oct 1;52(10):201–13.

13. EC2-1-1.Design of concrete structures-Part 1-1: General rules and rules for buildings. 2004.

14. Elnady MME. Seismic Rehabilitation of RC Structural Walls. [Thesis]. 2008

15. EN1998-1. Eurocode 8: Design of structures for earthquake resistance. 2004.

16. EN1998-2. Eurocode 8- Design of Structures for earthquake resistance- Part2: Bridges.

17. Ferguson PM, Briceno EA, Krishnaswamy CN. Tensible lap splices. Center for Highway Research, University of Texas at Austin; 1971.

18. Lukose PGK, White RN. Behavior of Reinforced Concrete Lapped Splices for Inelastic Cyclic Loading. Journal Proceedings. 1982 Sep 1;79(5).

19. Goto Y. Cracks Formed in Concrete Around Deformed Tension Bars. JP. 1971 Apr 1;68(4):244–51.

20. Hannewald P. Seismic Behavior of Poorly Detailed RC bridge Piers. PhD Thesis, EPFL. 2013.

21. Hannewald P, Bimschas M, Dazio A. Quasi-static cyclic tests on RC bridge piers with detailing deficiencies. IBK Bericht Nr. 352. 2013.

22. Hardisty JN, Villalobos E, Richter BP, Pujol S. Lap Splices in Unconfined Boundary Elements. CI. 2015 Jan 1;37(1):51–8.

23. Kilic SA, Sozen MA. Evaluation of Effect of August 17, 1999, Marmara Earthquake on Two Tall Reinforced Concrete Chimneys. SJ. 2003 May 1;100(3):357–64.

24. Kim S, Shiohara H. Dynamic Response Analysis of A Tall RC Chimney Damaged during 2007 Niigata-ken Chuetsu-Oki Earthquake.WCEE Lisboa. 2012.

25. Liu X, Zhan FB, Hong S, Niu B, Liu Y. A bibliometric study of earthquake research: 1900–2010. Scientometrics. 2012 Sep 1;92(3):747–65.

26. Lowes LN, Lehman DE, Birely AC, Kuchma DA, Marley KP, Hart CR. Earthquake response of slender planar concrete walls with modern detailing. Engineering Structures. 2012 Oct;43:31–47.

27. Lukose K, Gergely P, White RN. Behavior of Reinforced Concrete Lapped Splices for Inelastic Cyclic Loading. JP. 1982 Sep 1;79(5):355–65.

28. Mander JB, Priestley MJ, Park R. Theoretical stress-strain model for confined concrete. Journal of structural engineering. 1988;114(8):1804–1826.

29. Melek M, Wallace JW. Cyclic Behavior of Columns with Short Lap Splices. SJ. 2004 Nov 1;101(6):802–11.

30. Mergos PE, Beyer K. Loading protocols for European regions of low to moderate seismicity. Bulletin of Earthquake Engineering. 2014 Dec;12(6):2507–30.

31. Pam HJ, Ho JCM. Effects of Steel Lap Splice Locations on Strength and Ductility of Reinforced Concrete Columns. Advances in Structural Engineering. 2010 Feb 1;13(1):199–214.

32. Paterson J, Mitchell D. Seismic Retrofit of Shear Walls with Headed Bars and Carbon Fiber Wrap. Journal of Structural Engineering. 2003 May 1;129(5):606–14.

33. Paulay T. Lapped Splices in Earthquake-Resisting Columns. JP. 1982 Nov 1;79(6):458–69.

34. SeismoSoft, Seismostruct. A computer program for static and dynamic non-linear analysis of framed structures. Version 2016.

35. SeismoStruct. User Manual. 2016.

36. Sezen H, Whittaker AS, Elwood KJ, Mosalam KM. Performance of reinforced concrete buildings during the August 17, 1999 Kocaeli, Turkey earthquake, and seismic design and construction practise in Turkey. Engineering Structures. 2003 Jan 1;25(1):103–14.

37. Shima H, Chou L, Okamure H. 1987. Micro and Macro Models for Bond in Reinforced Concrete. Journal of the Faculty of Engineering, University of Tokio. 1987.

38. SIA.SIA261. Actions on structures.Building code, Swiss Society of Engineers and Architects. 2003.

39. SIA160, SIA. Building Code,Swiss Society of Engineers and Architects. 1970.

40. Sivakumar B, White RN, Gergely P. 1982. Behavior and Design of Reinforcement Concrete Column-Type Lapped splices Subjected to High-Intensity Cyclic Loading. Technical Report National Science Foundation.1982.

41. Sparling B, Rezansoff T. The effect of confinement on lap splices in reversed cyclic loading. Canadian Journal of Civil Engineering. 1986;13(6):681–692.

42. Tarquini D, Almeida JP, Beyer K. Influence of Lap Splices on the Deformation Capacity of RC Walls. II: Shell Element Simulation and Equivalent Uniaxial Model. Journal of Structural Engineering. 2017

43. Villalobos E, Escolano-Margarit D, Ramírez-Márquez AL, Pujol S. Seismic response of reinforced concrete walls with lap splices. Bulletin of Earthquake Engineering. 2017 May;15(5):2079–100.

44. Zuo J, Darwin D. Splice strength of conventional and high relative rib area bars in normal and high-strength concrete. 2000